FHWA/ NJ-99-026-7270

NONLINEAR REPONSE OF MSSS BRIDGES UNDER EARTHQUAKE GROUND MOTIONS: CASE STUDIES

Final Report

OCTOBER 1999

BY

M. ALA SAADEGHVAZIRI, and
ALIREZA YAZDANI-MOTLAGH

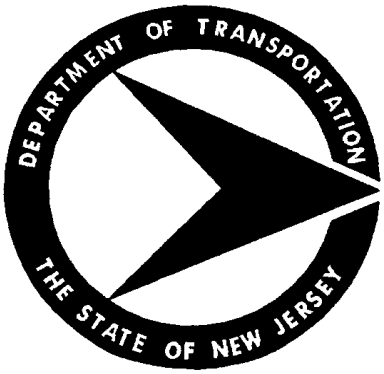

Prepared By
New Jersey Institute of Technology
Department of Civil and Environmental Engineering
In Cooperation With
New Jersey Department of Transportation
Division of Research and Technology,
U.S. Department of Transportation
Federal Highway Administration,
National Center for Industrial Productivity @ NJIT

1. Report No.	2. Government Accession No.	3. Recipient's Catalog No.
FHWA/NJ-99-026-7270		

4. Title and Subtitle	5. Report Date
NONLINEAR RESPONSE OF MSSS BRIDGES UNDER EARTHQUAKE GROUND MOTIONS: CASE STUDIES	October 1999
	6. Performing Organization Code NJIT / NCTIP
7. Author(s) M. Ala Saadeghvaziri, and Alireza Yazdani-Motlagh	**8. Performing Organization Report No.** FHWA/NJ-99-026-7270
9. Performing Organization Name and Address DEPARTMENT OF CIVIL AND ENVIRONMENTAL ENGINEERING NATIONAL CENTER FOR TRANSPORTATION AND INDUSTRIAL PRODUCTIVITY New Jersey Institute of Technology 323 Martin Luther King Blvd. Newark, NJ 07102	**10. Work Unit No. (TRAIS)** **11. Contract or Grant No.**
12. Sponsoring Agency Name and Address NEW JERSEY DEPARTMENT OF TRANSPORTATION	**13. Type of Report and Period Covered** Final Report July 1997 – August 1999 **14. Sponsoring Agency Code**

15. Supplementary Notes

16. Abstract

This report presents the results of the second phase of a comprehensive analytical study on the seismic response of highway bridges in New Jersey. Most bridges in New Jersey are multi-span simply supported (MSSS) where due to impact at the joints the seismic response is highly nonlinear. Therefore, detailed seismic analysis of essential bridges should employ nonlinear computer models that consider the important behavioral characteristics. Among these are; behavior of steel bearings, impact between adjacent spans and between the end-span and the abutment, soil-structure interaction, frictional characteristics following bearing failure, plastic hinges and/or shear failure at the columns, and combined effect of horizontal and transverse ground motion excitations. In light of these, the overall objective of this phase of the study was to evaluate the nonlinear seismic response of actual bridges with emphasis on soil-structure interaction and three-dimensional effect of ground motion. Furthermore, capacity / demand ratios for various components were determined based on FHWA's *seismic retrofitting manual for highway bridges.*

The results indicate that even under low intensity earthquakes high impact forces will be generated within an MSSS bridge. As a result the steel bearings, which are employed in most bridges in New Jersey, will most likely fail. However, if the failure is followed by stable Coulomb-Friction at the interface of the steel bearing and the steel girder or the interface of the bearing and concrete seat, it is not expected that the bridge will collapse. Actually, due to energy dissipation capacity of this mode of failure the response of the bridge will be constrained. Thus, the bridges investigated under this study can survive an earthquake with peak ground acceleration (PGA) of 0.18g, which is the maximum seismic coefficient for New Jersey based on AASHTO's Seismic Specifications. For a ground motion with PGA of 0.4g, the bridges considered will sustain shear failure of columns in addition to bearing failure. This in turn can cause collapse of the bridge. Soil-structure interaction and frictional coefficient at the failed bearings have significant effect on the response of MSSS bridges in the longitudinal direction. Considerations should be given to increasing seat lengths and strengthening concrete seat under the bearings to ensure stable behavior following bearing failure. Future research work may consider experimental work to support the analytical conclusions reported here, and further analytical work on development of pushover analysis methodology and nonlinear design spectrum for MSSS bridges.

17. Key Words	18. Distribution Statement
Seismic Design, Bridges, Seismic Retrofit, Multi-Span Simply Supported Bridges, Bearings, Soil-Structure Interaction	No Restrictions

19. Security Classification (of this report)	20. Security Classification (of this page)	21. No. of Pages	22. Price
None	None	140	Free

Table of Contents

1) INTRODUCTION: 1

2) DESCRIPTION OF BRIDGES: 4

3) MODELING OF SOIL-STRUCTURE INTERACTION (SSI): 20

4) STIFFNESS AND CAPACITY OF THE REINFORCED CONCRETE PIER COLUMNS 45

5) STIFFNESS AND CAPACITY OF THE BEARINGS 61

6) COMPUTER MODELS 65

7) RESULTS OF 2-D ANALYSES 79

8) RESULTS OF 3-D ANALYSES 116

9) CONCLUSIONS AND RECOMMENDATIONS 136

10) REFERENCES 139

SECTION 1

INTRODUCTION

1-1) General

Most bridges in New Jersey are multi-span simply supported (MSSS) where due to impact at the joints the seismic response is highly nonlinear. Therefore, although the response of each bent, or frame, in a MSSS bridge in any direction (longitudinal or transverse) is dominated by a single mode, the use of single mode spectral analysis is not expected to give an accurate estimate of the seismic forces. Detailed seismic analysis of essential bridges should employ nonlinear computer models that consider the important characteristics of MSSS bridges. Among these characteristics for MSSS bridges in New Jersey are; behavior of steel bearings, impact between adjacent spans and between the end-span and the abutment, soil-structure interaction, frictional characteristics following bearing failure, plastic hinges and/or shear failure at the columns, and combined effect of horizontal and transverse ground motion excitations.

During the first phase of this investigation using detailed finite element models the behavior of steel bearings were investigated. Furthermore, nonlinear models that can accurately account for impact within the bridge system were developed and verified. Time history analyses of MSSS bridge models were performed using 2-D models. Both longitudinal and transverse ground motions were considered. The results of the first phase of this study on the seismic response of bridges in New Jersey are reported elsewhere [1-4]. It should be emphasized that it was determined that failure of steel bearings will very likely occur even under low intensity ground motions. However, their replacement may not be necessarily warranted as long as the post-failure mode of response at the bearing is defined by Coulomb-friction. That is, upon failure of the connecting bolts (the weak link) of the steel bearings the girders will remain stable and their response is governed by sliding at the interface.

This report presents the results of the second phase of this research project.

1-2) Research objectives

The overall objective of this phase of the study was to evaluate the nonlinear seismic response of actual bridges with emphasis on soil-structure interaction and three-dimensional effect of ground excitation. Therefore, the research tasks were:

- Identify three typical bridges of various spans for detailed analyses as case studies,
- Identify/develop suitable methodologies to determine the properties (strength & stiffness) of boundary springs to model soil-structure interaction at the abutments and at the base of column piers
- Perform parametric study to investigate the nonlinear response of actual MSSS bridges in the longitudinal direction reported to be the most vulnerable direction for MSSS bridges under earthquake ground motion. Important parameters to consider were soil-structure interaction and frictional coefficient at failed bearings.
- Evaluate the combined effect of longitudinal and transverse earthquake excitations on the response of actual MSSS bridges using 3-D models,
- Determine the capacity / demand (C/D) ratios for various bridge components using FHWA's guidelines, and
- Recommend possible modifications to the design of new bridges and propose possible retrofit procedures for existing bridges.

1-3) Report organization

In section 2, detailed descriptions of all three bridges are presented. For these bridges the number of spans are equal to two, three and four. These are expected to represent the majority of bridges in New Jersey. Information provided in section 2 include material properties; weight of various components; and geometry and descriptions of decks, pier bents, abutments, footings, and columns.

The details of how to model the soil-structure interaction is provided in section 3. This includes footing stiffnesses, abutment wall stiffness, how to arrive at simplified equivalent stiffness in the longitudinal direction, and determination of abutment strength in the longitudinal direction. Furthermore, the procedures to determine the abutment transverse and vertical stiffnesses are also described.

In sections 4, using FHWA's guidelines and a special purpose computer program the stiffness and capacity of the reinforced concrete pier columns are obtained. Effective moment of inertia, moment capacity, shear capacity, plastic rotation capacity, and column interaction diagram are among RC column characteristics that are obtained in this section.

In section 5, stiffness and capacity of the bearings are determined.

In section 6, details of the computer models used for 2-D and 3-D analyses are provided. DRAIN-2DX and DRAIN-3DX were used for this purpose. The input earthquake records are also described in this section.

Sections 7 and 8 present the results of 2-D and 3-D analyses, respectively. Each section includes explanation of individual bridge response as well as overall behavioral characteristics that were observed. Furthermore, each section also includes a comparison between the nonlinear time history analysis and push-over analysis.

Finally, in section 9 the conclusions and recommendations of this research investigation are presented. This section draws upon the results of the first phase of this study too.

SECTION 2

DESCRIPTION OF BRIDGES

2-1) General

Three simple span and simply supported bridges, representative of typical bridges in New Jersey, are evaluated under this study. For these bridges the number of spans are equal to two, three and four. They have concrete slab on steel girder decks and reinforced concrete pier bents and abutments. The pier columns are all circular with spiral or circular lateral reinforcements and footings are rested on soil without any pile. The spread footings for each abutment, beneath two wing walls and one back wall, are continuous U-shaped foundations. Detailed descriptions of the bridges follow.

2-2) Name and Location

Bridge #1: Clements Bridge is a three span bridge located in Gloucester County, Deptford Township, on County Route 544 (Clements Bridge Road) over Route 55, Sec. 13a.

Bridge #2: Alexander Bridge is a two span bridge located in West Windsor Township, Mercer County on Route one.

Bridge #3: Bridge-5 is a four span bridge located in Morris County, Parsippany-Troy Hills Township, Eastbound Littleton Road Relocation over Interstate Route 80, Sec. 3g-2

2-3) Material Properties

Clements Bridge

Concrete	f'_c=3000 psi	
Reinforcing bars	ASTM A615 Grade 60	(fy=60 ksi)
Steel	ASTM A36 – 75	(fy=36 ksi)

Alexander Bridge

Concrete	f'c=4000 psi	(class A, for upper structure)	
	f'c=3000 psi	(class B, for foundations)	
Reinforcing bars	ASTM A615	Grade 60	(fy=60 ksi)
Steel	ASTM A709	Grade 36	(fy=36 ksi)

Bridge-5

Concrete	f'c=3000	
Reinforcing bars	Grade 40	(fy=40 ksi)
Steel	ASTM A36	(fy=36 ksi)

2-4) Decks and Pier Bents

The bridge decks are composite concrete slab on steel girders and pier bents consist of reinforced concrete circular columns and one or two cap beams (depending on the existence of any separation in the bridge width). The cross section of deck steel girders varies along the length. For each bridge a typical girder with a pertinent concrete slab is shown in Figure 2-1. The cross-sectional properties of the deck are obtained by multiplying the properties of this unit by the number of girders in the deck (N_G).

Clements Bridge

This bridge has three spans in lengths of 140′, 95′and 140′. The width of the bridge is made of two separated symmetric half-decks. Each half-deck has 6 girders 89″ apart supporting a 9.5″-thick concrete slab. Separate pier bents beneath each half-deck consist of two 4’-diameter circular columns and a cap beam (Figure 2-2a). The deck steel girder

dimensions in the mid-span and adjacent to the end-span segments are presented in Table 2-1.

Alexander Bridge

This bridge has two equal spans in length of 97′-4″. Each deck has 15 girders 95.5″ apart, supporting a 8.75″-thick concrete slab. The deck cross section has two separate parts, namely parts 1A and 1B (Figure 2-2b). Correspondingly, the pier bent consists of two parts with a total of ten 3′-diameter circular columns. The girder dimensions in the mid-span and adjacent to the end-span segments are presented in Table 2-1b.

Bridge-5

This bridge has four spans in lengths of 42’, 130’, 120’ and 88’ (lengths obtained from indirect measurements over available bridge drawings). Each deck has 7 girders 86″ apart, supporting an 8″-thick concrete slab. Each column bent consists of five 3.5′-diameter circular columns and a cap beam (Figure 2-2c). Since the details of steel girders were not available, estimated values based on other two bridges were used.

2-5) Abutments and Footings

Each abutment has a continuous U-shaped foundation under its wing walls and back wall. Figure 2-3 shows the dimensions of the abutment footings. Also Figure 2-4 and Table 2-2 present the geometrical information (dimensions and area) of the abutment walls cross sections. All bridges have continuous rectangular spread footing at each pier bent. The dimensions for pier footings are shown in Table 2-3.

2-6) Columns

All bridges have circular columns with spiral or circular lateral reinforcements. The level of concrete confinement varies for each bridge. The lowest confinement belongs to the Clements Bridge with #3 circular hoops at 12” spacing. On the other hand Alexander Bridge and Bridge-5 both have well confinement details for their pier columns, which consist of spiral reinforcement at small pitch (3.5” to 2.25”). Table 2-4 shows the cross sectional properties and reinforcements in the pier columns for all three bridges.

2-7) Bearings and Edge Distances

A typical fixed bearing is shown in Figure 2-5, which consists of a parted metal casing with each part welded to the top and bottom steel plates. The top steel plate is connected to the deck steel girder by connection bolts and the bottom steel plate is connected to the concrete support by anchor bolts. For roller bearings, except the casings which have a special configuration for allowing free movement to the supported deck in longitudinal direction, the details are similar to the fixed bearings. Table 2-5 shows the fixed bearings dimensions and connection bolts and welding.

In case of the shear failure at fixed bearings or excessive movement over roller bearings, one of the important parameters in preventing the deck from falling off of its support is the edge distance “e” (Figure 2-6). This distance can be compared to the deck relative movement to its support and if this relative movement is greater than the edge distance then there is a possibility of falling off the deck. Table 2-6 presents the edge distances of the studied bridges at pier bents and abutments. Edge distances are measured from the corner of bearing casings to the edge of the support in the bridge longitudinal direction.

2-8) Estimated Weights for Different Bridge Components

Table 2-7 shows the estimated weight for various structural components for all three bridges. The deck dead weight was increased by 10% to account for additional attached elements and the simplified geometry assumption in the weight calculations.

Table 2-1 Cross-section of composite decks at mid-span and supports

Bridge Name	Span No.	Girder cross section		n	Composite equivalent sec. Area in^2	N_G
		Support	**Mid-span**			
Clements (half-deck)	**1 & 3**	20" * 7/8" 60" * 5/8" 18" * 1.375" sum=79.75 in^2	20" * 1.5" 60" * 5/8" 24" * 2.5" sum = 127.5 in^2	8.824 FHWA	L_s = 2*28 ft L_m = 84 ft 1777 in^2	6
	2	16" * .75" 48" * 0.5" 18" * 1.375" sum = 60.75 in^2	16" * 1.125" 48" * 0.5" 18" * 2" sum = 78 in^2		L_s = 2*27 ft L_m = 41 ft 1443.4 in^2	
Alexander	**1 & 2**	20* 7/8 42 * 7/16 24 * 1.375	20*1.5 42* 7/16 24*2	7.642	L_s = 2* 18 ft L_m = 60 ft 1486.1 in^2	15
Bridge-5	**1**	Details are missing and cross sectional properties were estimated indirectly.			970	7
	2				1700	
	3				1700	
	4				1400	

Notes:

1) For Clements Bridge due to symmetry, properties of half of the deck are presented.
2) A girder cross section includes top flange, web, and bottom flange plates and is given in the form of length*thickness.
3) n is the ratio of steel to concrete modulus of elasticity
4) N_G is number of girders in deck cross section

Table 2-2 Dimensions and cross sectional areas of abutment walls

Bridge Name	Abut. #	Wing Wall Cross Section			Abutment wall Cross Section			
		H_w (ft)	t_w (ft)	A_w (ft^2)	H_m (ft)	t_m (ft)	c (ft)	A_m (ft^2)
Clements	**1**	14.1	2.0	51.5 54.0	14.1	2.0	7.5	64.6
	2	20.8	2.0	85.0	20.6	2.25	7.5	95.4
Alexander	**1**	15.9	3.0	79.4 99.4	17.0	3.0	5.9	89.5
	2	16.3 12.8	3.0	80.8 65.2	13.9	3.0	5.7	78.3
Bridge-5	**1**	13.1	2.5	58.4 57.4	13.1	2.5	7.5	49.9
	2	16.2	2.5	67.8 66.2	16.2	2.5	6.7	68.1

Note: For notations used in the table refer to Figure 2-4.

Table 2-3 Pier footing dimensions

Bridge Name	Footing for	Length (ft)	Width (ft)	Thickness
Clements (Half the width)	Pier#1	47.5	14	3’-3”
	Pier#2	47	18	3’
Alexander (Whole width)	Pier#1	115	14	3’
Bridge-5	Piers #1,#2 & #3	71	8	3’

Table 2-4 Pier column reinforcement

Bridge Name	Type No.	D (ft)	Longitudinal steel	Transverse steel
Clements	1	4	20-#9 A_b=1.0 in^2 ρ=.011	#3 @1' A_b=.11 in^2 d_b=.375 in circular hoop
Alexander	1	3	16-#10 A_b=1.27 ρ=.02	#5 @ 3.5" A_b=.31 in^2 D=.625 in spiral
Bridge-5	1	3.5	9-#11 A_b=1.56 ρ=.01	#4 @ 2.25" A_b=.20 in^2 D=.5 in spiral
	2	3.5	13-#11 A_b=1.56 ρ=.015	#4 @ 2.25" A_b=.20 in^2 D=.5 in spiral
	3	3.5	15-#11 A_b=1.56 ρ=.017	#4 @ 2.25" A_b=.20 in^2 D=.5 in spiral
	4	3.5	20-#11 A_b=1.56 ρ=.023	#4 @ 2.25" A_b=.20 in^2 D=.5 in spiral

Table 2-5 Fixed bearing dimensions

Bridge Name	Bearing Type No	L (in)	b (in)	h_1 (in)	h_2 (in)
Clements	**1**	18	5	10	3.75
	2	18	5	5	3.75
Alexander	**1**	20	5	4.5	4.0
Bridge-5	**1**	11	5	4.0	4.0
	2	17	5	4.0	4.0
	3	19	5	4.0	4.0

Note: For notations used in the table refer to Figure 2-5.

Table 2-6 Fixed bearing edge distances

Bridge Name	**Location of support**	**α** (Deg)	**c (in)**	**e (in)**
Clements	**Abutments**	33	7	8
	Piers	33	7	10
Alexander	**Abutments**	3	5	7
	Piers	3	5	7
Bridge-5	**Abutments**	45.4	5.7	9.3
	Piers	45.4	#1 5.7 #2 8.5 #3 7.8	9.3 9.5 10.2

Notes:

1) $c=(L / 2) * \sin(\alpha) * + (b / 2)* \cos(\alpha)$
2) For notations used in the table refer to Figure 2-6.

Table 2-7 Weight of various bridge components

Bridge Name	Element	Weight (kips)	Unit Weight (kips/ft)
Clements (whole width)	Deck #1 and #3	2763.0	19.7
	Deck #2	1677.0	17.7
	Columns of Pier #1 (4 columns)	140.8	1.6
	Columns of Pier #2 (4 columns)	179.5	2.1
	Cap Beam (2 segments)	292.6	3.4
	Abutment #1	1360.0	15.8
	Abutment #2	2400.0	27.9
Alexander	Deck #1 and #2	2110.3	21.7
	Columns of the Pier (10 col.)	188.9	1.7
	Cap Beam	258.3	2.3
	Abutment #1	1850.0	16.6
	Abutment #2	1500.0	13.4
Bridge-5	Deck #1	440	10.5
	Deck #2	1500	11.5
	Deck #3	1380	11.5
	Deck #4	910	10.3
	Columns of Pier #1 (5 columns)	110	2.3
	Columns of Pier #2 (5 columns)	115	2.4
	Columns of Pier #3 (5 columns)	90	1.9
	Cap Beam	181	3.7
	Abutment #1	1100	22.7
	Abutment #2	1230	25.4

Notes:
1) For Bridge-5, deck weights are based on the estimated values.
2) For decks unit weight is per span length and for other components is per bridge width.

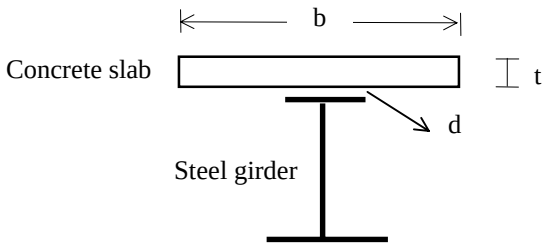

Bridge Name	b (inch)	t (inch)	d (inch)
Clements	89.0	9.5	3
Alexander	95.5	8.75	1.625
Bridge-5	86.0	8.0	No Info.

Figure 2-1 Typical girder with pertinent concrete slab dimensions

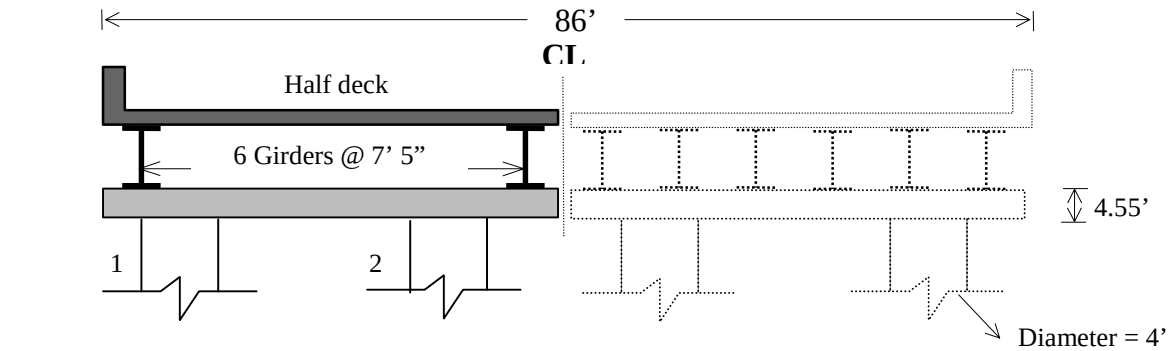

a) Clements Bridge

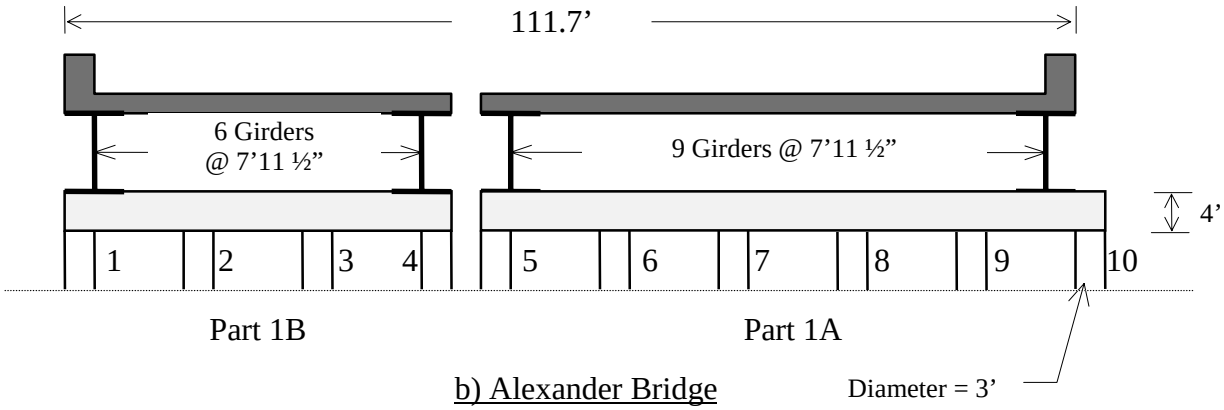

b) Alexander Bridge

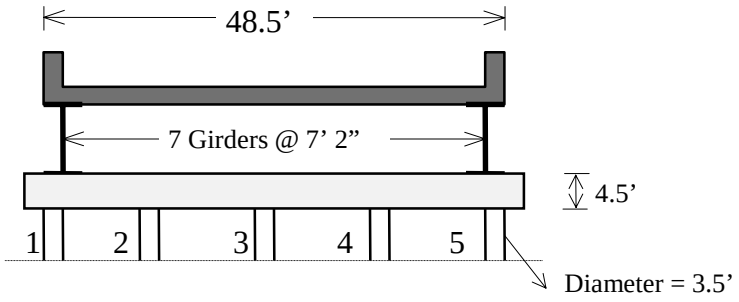

c) Bridge-5

Figure 2-2 Cross sections of the bridge decks

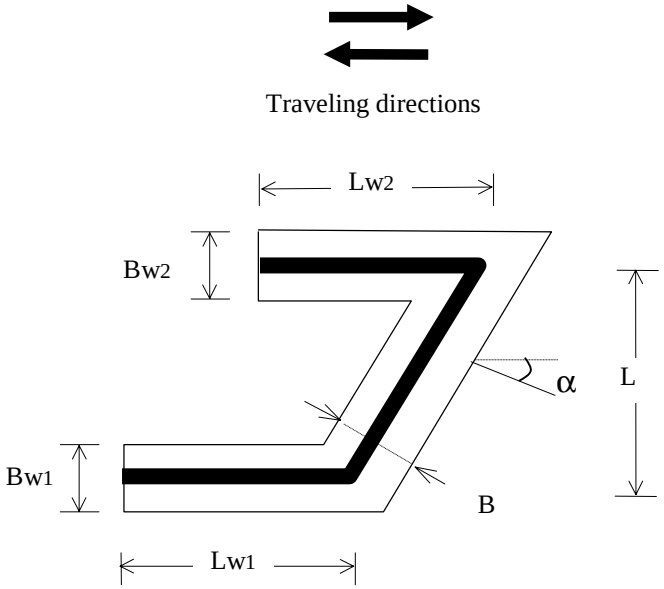

Bridge Name	Left Abutment (#1)						Right Abutment (#2)						α
	L	**B**	**Lw1**	**Bw1**	**Lw2**	**Bw2**	**L**	**B**	**Lw1**	**Bw1**	**Lw2**	**Bw2**	
Clements	86	13.3	23	13.8	23	12.5	86	16.3	36.5	17.8	36	17.8	33^o
Alexander	111.7	13	12.7	17	11	14.5	111.7	13	6.0	13.0	9.3	14.5	3^o
Bridge-5	55	7	31.5	9	25.8	9	46.7	8.5	30.5	11	23	11	45^o

Figure 2-3 Abutment footings

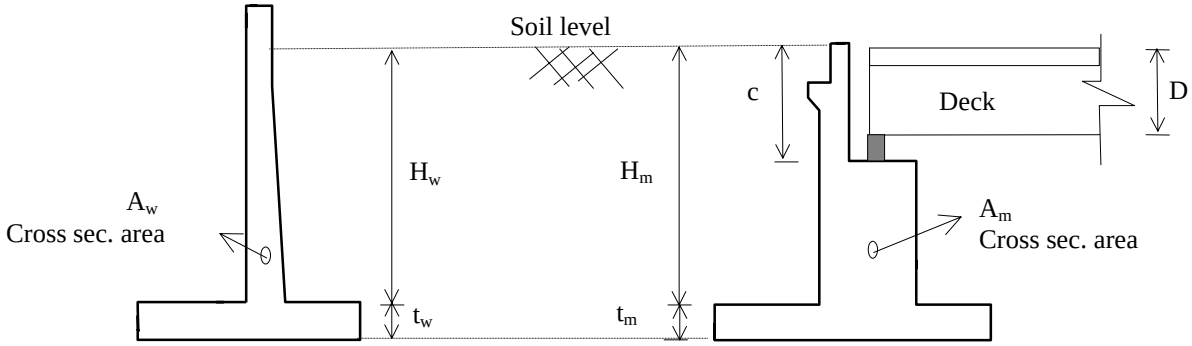

a) Typical wing wall section

b) Typical main wall section

Figure 2-4 Cross sections of abutment walls

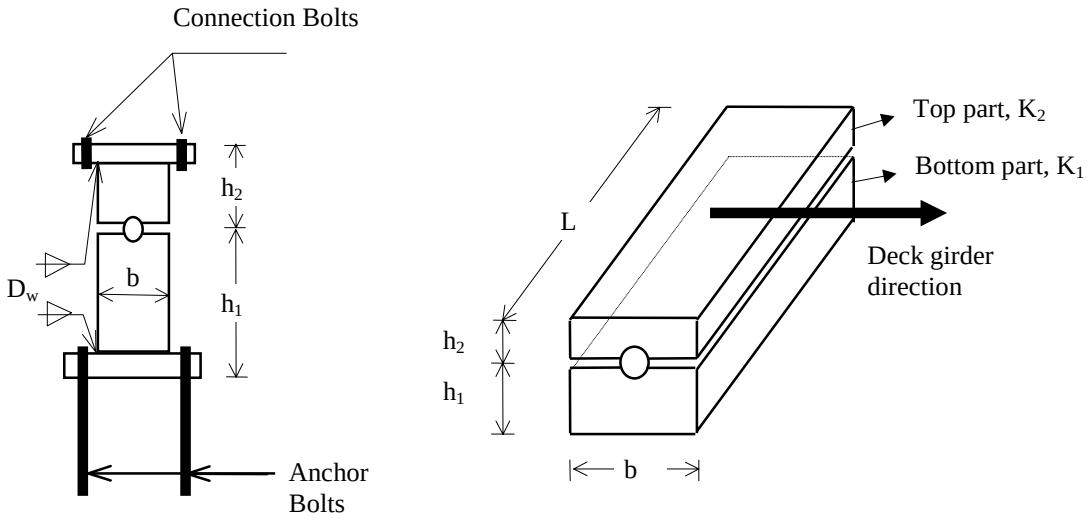

Figure 2-5 Fixed bearing general shape and components

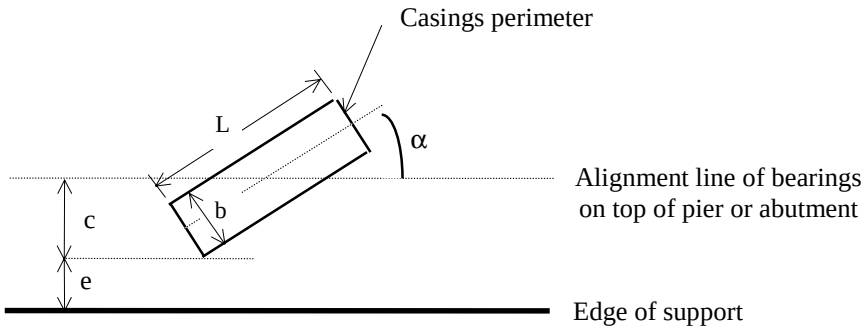

Figure 2-6 Edge distance of bearings

SECTION 3

MODELING OF SOIL-STRUCTURE INTERACTION (SSI)

3-1) General

The importance of including the flexibility and strength of supports at the abutments and piers in dynamic analysis of highway bridges is well recognized by various agencies such AASHTO [6] and CALTRANS (California Department of Transportation) [7]. In designing new bridges using these specifications, either an iterative process is used to estimate the stiffness and displacement at the abutments or simplified rules are employed to determine the stiffness and strength of the boundary springs. Such procedures are overly simplified and do not take into account the properties of soil and all physical dimension of the substructure. In a study conducted on the US 101/Painter Street Overpass [8] the "actual" abutment capacity and stiffness determined from analyses of earthquake records are compared to "design" values provided by CALTRANS and AASHTO. It is reported that the actual strength and stiffness values are affected by soil-structure interaction and are time variant, "decreasing significantly as the abutment deformation increases." It is concluded that the CATRANS procedure results in a good estimate of the stiffness and capacity of the abutment in the transverse direction. However, in the longitudinal direction the CATRANS procedure overestimates the capacity and stiffness by a factor of two. This indicates that the assumed ultimate passive capacity of 7.7 ksf by CATRANS may be too high. It is also concluded that the AASHTO-83/ATC-6 procedure results in large estimate of the abutment stiffness in both directions. Other researchers have also conducted extensive investigations to determine the stiffness and strength of boundary springs to represent the abutments in an analytical model used in time history analysis. Such studies are based on scientific knowledge of the properties of soil and more detailed consideration of the geometrical properties of the abutment. Most notable among these studies are works by Siddharthan, El-Gamal, and Maragakis [9], and Wilson and Tan [10]. Here, the procedures given by FHWA's *Seismic Design of Highway Bridge Foundations* [5] and Wilson and Tan [10] are used to determine the parameters of the boundary springs at the abutments and at the base of the

column piers. An important aspect of soil-structure interaction is foundation damping which is a complex problem. Radiation damping associated with wave propagation between the masses of the superstructure and foundation-soil is one form of energy dissipation due to soil-structure interaction. Material nonlinearity in the foundation-soil is another form of damping. In this study the latter form of energy dissipation is explicitly modeled, while the radiation damping is implicitly accounted for through equivalent viscous damping. Descriptions of the procedure used to obtain soil spring properties are as follows.

3-2) Footing Stiffness

FHWA's procedure [5] for rigid footing foundation on a semi-infinite elastic half-space is used to determine translational and rotational stiffnesses for abutment and pier foundations. It is reported that for most highway bridges in evaluating the stiffness characteristics of footings the dynamic effects can be ignored. The static stiffness can be determined using the following procedure:

General Form of Stiffness matrix:

The 6 X 6 stiffness matrix for a circular rigid footing along with the directions of translational degrees of freedom is shown in Figure 3-1. The vertical translation and torsional rotation degrees of freedom are uncoupled from the other degrees of freedom. The two components of translations in the horizontal plane are coupled with the rotational degrees of freedom in this plane resulting in off-diagonal terms. However, the values of these off-diagonal terms are small, especially for a typical highway bridge where the footings are shallow.

Stiffness Coefficients:

The following general equation is recommended by FHWA for stiffness matrix, K, of an embedded footing:

$$K = \alpha * \beta * K_0$$

Where K_0 is the stiffness matrix of an equivalent circular footing bonded to the surface of an elastic half-space, α is the shape correction factor for the foundation, and β is the foundation embedment factor.

The stiffness coefficients for various degrees of freedom of matrix K_0 can be determined using the following relationships:

$$K_{11} = K_{22} = 8GR / (2-\nu)$$
$$K_{33} = 4GR / (1-\nu)$$
$$K_{44} = K_{55} = 8GR^3 / 3(1-\nu)$$
$$K_{66} = 16GR^3 / 3$$

Where K_{11} and K_{22} are for horizontal translations, K_{33} is for vertical translation, K_{44} and K_{55} are for rocking rotations and K_{66} is for torsional rotation. G and ν are the shear modulus and Poisson's ratio for the elastic half-space, respectively. R is the radius for circular footings.

The application of these equations to rectangular footings involves two steps. First the radius of an equivalent circular footing must be determined as shown in Figure 3-2. The next step requires determination of the shape factor, α, which depends on aspect ratio (Length, L / Width, B) and mode of displacement. FHWA [5] provides graphical relationships for this factor which is in the range of 1.0 to 1.2 for typical L/B values between 1.0 and 4. The typical value for α, based on the geometry of the studied bridges, is around 1.1. Similarly, the embedment factor, β, for various modes of displacements is given in a graphical format. The embedment factor depends on the embedment ratio,

which for the typical situation encountered in highway bridges is equal to the ratio of footing depth (D) to footing radius (R). For D/R in the range of 0.0 to 2.5, for translational degrees of freedom the value of β is in the range of 1.0 to 2.75, and for torsional and rotational modes it varies from 1.0 to as high as 8. For the bridges considered in this study, the value of β is around 1.1 for translational degrees of freedom and about 1.4 for rotational/torsional degrees of freedom.

In the studied bridges, abutment footings are U-shaped, continuous and skewed. In order to use the FHWA's procedure, the U shaped and skewed footings are idealized into equivalent rectangular segments and then the above procedure is applied to each of them. Tables 3-1 to 3-6 present the footings' calculated stiffnesses.

In the FHWA procedure the flexibility of the footings was not considered in calculating the stiffness coefficients. This leads particularly to unreasonable rotational stiffnesses for long rectangular footings (as in pier footings). To include footing flexibility in rotational stiffnesses, a separate model of foundation with a uniform distribution of vertical springs and short-side-rotation springs is considered. In these models, half of the uncracked cross sectional moment of inertia and torsional constant are assigned for the footings. Table 3-7 presents the bridge footing stiffnesses that also include the obtained rotational stiffnesses by this method (shaded cells in the figure) and Figure 3-3 shows the local axis of the footings in which these stiffnesses are presented. For the pier columns translational and rotational soil springs are placed at the base of the columns and their load-deformation behavior is assumed to be linear and elastic.

3-1) Abutment Wall Stiffness

In the previous section development of stiffness coefficients for soil-foundation system were discussed. In this section the stiffness of the system consisting of the abutment wall and backfill soil will be evaluated. In the next section the procedure to combine all abutment foundation and wall stiffnesses into a simple longitudinal spring is discussed.

In abutment stiffness calculation, it is assumed that the abutment wall is always in contact with back fill soil and always contributes to overall abutment stiffness. In determination of the stiffness of the abutment wall-backfill system, the FHWA's procedure considers the nature of pressure/displacement distribution when the wall is displaced (pushed) into the backfill by longitudinal seismic forces from the bridge deck [5]. Employing the appropriate pressure diagrams for translational and rotational cases, the resultant stiffnesses for longitudinal translational and rotational (tilting) modes can be obtained using the following equations.

For translational stiffness (longitudinal):

$$K_w = 0.425 * E_s * B$$

For rotational stiffness:

$$K_{Rw} = 0.072 * E_s * B * H^2$$

Where

E_s = Young's modulus of soil = $2*(1+\nu_{soil})* G_s$, $\nu_{soil} = 0.4$

G_s = shear modulus of soil.

B = width of the abutment wall.

H = height of the wall.

These two springs is located at 0.37 of the height of the wall as shown in Figure 3-4. Table 3-8 presents the calculated abutment wall stiffnesses for the studied bridges.

3-2) Equivalent Abutment Spring in Bridge Longitudinal Direction

Figure 3-5 shows schematic diagrams of various foundation springs at an abutment including the final simplified model. In arriving at the final simple model, it is assumed that the abutment deforms as a rigid body and translational stiffness of the system at the location of impact between the abutment and bridge deck is determined. It should be

noted that experimental investigation [17] has shown that the abutment movement is indeed rigid body movement.

As shown in Figure 3-5b, the rotational and translational stiffness springs from various components (abutment footings and the back wall) are moved to the center of stiffness located at height x above the base of the footing. The resultant translational stiffness is equal to the simple algebraic sum of all translational stiffnesses, that is:

$$K_T = K_{f1} + K_{f2} + K_w$$

Where K_{f1} is the stiffness for the backwall footing, K_{f2} is the stiffness for the wing wall footings (sum of the two), and K_w is the stiffness of the backwall. The resultant rotational stiffness is equal to:

$$K_R = K_{rw} + K_{r1} + K_{r2} + K_W*(0.37H_w + t_f - x)^2 + (K_{f1} + K_{f2})*x^2$$

Where K_{rw} is rotational stiffness for the backwall, K_{r1} rotational stiffness for the backwall footing, K_{r2} rotational stiffness for the wing wall footings (sum of the two), H_w is height of the backwall, and t_f is the depth of the footing, x is the center of stiffness from the base of the footing and is equal to:

$$x = (K_W / K_T) * (0.37H_w + t_{f)}$$

Continuing on the assumption of rigid body movement of the abutment, the model of Figure 3-5b is simplified further into an equivalent translational stiffness, K_h, equal to:

$$K_h = (K_R * K_T) / (K_T* h^2 + K_R)$$

As an example, using the above procedure the final value of translational springs at the abutments for Clements Bridge (one of the three case studies) are 1875G k/in and 1930G k/in, where G the shear modulus of soil is in ksi. For a typical value of G = 4 ksi the

abutment longitudinal stiffness is 7,600 k/in. For the same bridge, CALTRANS' simplified procedure, which only depends on the width of the bridge in this case, will result in a value of 17,200 k/in. The factor of two difference is consistent with the results reported by Goel and Chopra [8].

Similarly, the mobilized abutment mass is lumped at the point of impact between the deck and abutment forming a simple spring-mass system as shown in Figure 3-5c. Note that the point of impact is assumed to be at the centroid of the deck. Table 3-9 presents the calculated stiffnesses for the bridge abutments.

3-3) Abutment Transverse and Vertical Stiffnesses

Transverse and vertical translational springs were calculated based on the methodology presented by John C. Wilson [10]. Note that FHWA does not provide any guidelines with regard to transverse and vertical directions. The Wilson method is used because it is more compatible with FHWA's procedure as it relates to consideration of soil properties in calculating these stiffnesses. Based on Wilson's method transverse and vertical stiffnesses are dependent on soil embankment dimensions and soil elastic and shear modulus. Following are the equations that were used for this purpose.

Transverse stiffness of the soil embankment for unit length:

$$k_t = 2SG \Big/ Ln\left| 1 + 2S\frac{H}{W} \right|$$

Vertical stiffness of the soil embankment for unit length:

$$k_{vt} = 2SE \Big/ Ln\left| 1 + 2S\frac{H}{W} \right|$$

Where

E = Elastic modulus of the embankment soil

G = Shear modulus of the embankment soil

S = Side slope of the embankment soil

W = Wedge top width of the embankment soil

H = Height of the embankment soil

The length (L) for the embankment soils were assumed equal to the abutment's wing wall length. Figure 3-6 shows the dimensions of an embankment used in calculating transverse and vertical stiffnesses as shown in Table 3-10.

3-4) Abutment Strength

It is assumed that abutment behavior in transverse and vertical directions is elastic. A nonlinear load-deformation characteristic is employed for the translational springs that model abutment in the longitudinal direction. The nonlinearity includes yielding of the spring as well as an unequal strength under compressive and tensile loads on the abutments.

Under the longitudinal compressive load, the established Mononobe-Okabe pseudostatic approach for passive force is employed to determine the yield strength in compression. Under the assumptions of full mobilization of soil strength, cohesionless back-fill soil, and lack of liquefaction, the suggested formula for compressive yield force, C_y, is [5]:

$$C_y = (½) * \gamma * H^2 * (1 - K_v) * K_{PE} * B$$

Where

$$K_{PE} = \frac{\cos^2(\phi - \theta + \beta)}{\cos\theta * \cos^2\beta * \cos(\delta - \beta + \theta) * \left| 1 - \sqrt{\frac{\sin(\phi - \delta) * \sin(\phi - \theta + i)}{\cos(\delta - \beta + \theta) * \cos(i - \beta)}} \right|^2}$$

H = Height of backfill soil (here, from bottom of back wall footing)

B = Abutment width

γ = Unit weight of soil

ϕ = Angle of friction of soil

θ = Arc tan [k_h / (1 - k_v)]

δ = Angle of friction between soil and abutment, assumed equal to (ϕ / 2)

k_h = Horizontal acceleration coefficient, for New Jersey this is 0.18

k_v = Vertical acceleration coefficient.

i = Backfill slope angle.

β = Slope of backfill soil.

Table 3-11 presents K_{PE} values for different soil angle of frictions and Table 3-12 shows the calculated Cy for different bridges.

Tensile yield strength at the abutment, T_y, is assumed to be equal to frictional sliding capacity. That is:

$$T_y = N * \tan \delta$$

Where δ is the frictional angle between abutment footing and foundation soil, and it is assumed to be equal to ϕ/2. N is the total normal force at the interface, which is equal to the sum of the supported dead load plus the entire abutment weight (including wing walls, back wall, footings and soil over the footings) and listed in Table 3-13.

3-5) Damaged Backwall

The actual geometry of abutment backwall consists of two segments. One portion, which is narrower, is the back of the seat normally slightly longer than the depth of the superstructure and referred to as the backwall. The second segment, which extends from the seat to the top of the footing, is called the breast wall. It is quite possible for inertia forces in the longitudinal direction to cause shear failure of the abutment at the juncture

of these two segments, normally called backwall failure (Figure 3-7). It is even recommended in seismic design to use this mode of damage as a fuse, since fixing the upper portion of the abutment is much easier. As a parametric study in this investigation, special attention is devoted to this possible mode of failure. For damaged backwall situation the stiffness of the abutment in the longitudinal direction is determined based on mobilizing only an amount of soil equal to the depth of the superstructure (Table 3-14). Two different load transfer mechanisms control the capacity of a section at the juncture of the backwall and breast wall, namely: i) shear resistance provided by the concrete, and ii) shear friction, which is a post failure behavior and follows the first mode. The strength of the latter mode is actually larger and it is used. In accordance with AASHTO LRFD [11] the following equation can be used to determine the nominal shear capacity, V_n:

$$V_n = \mu * A_{vf} * F_y$$

Where μ is the friction coefficient between two sliding surfaces and here is assumed equal to one for concrete placed against hardened concrete, A_{vf} is the sum of areas of vertical rebars at the juncture, and F_y is the yield strength of the rebars. Table 3-15 presents the calculated values for the bridges.

If time history analysis indicates that this shear capacity is exceeded, the model is modified such that the backwall stiffness and compressive strength are determined using only the height of the back wall (i.e. total abutment height minus breast wall height). The strength of the abutment in tension is also reduced since only the weight of the back wall is used in calculating the frictional resistance when the abutment is under tensile load.

Table 3-1 Clements Bridge soil spring stiffnesses for pier footings

Bridge Name	Footing of	2L (ft)	2B (ft)	Stiffness component	R (ft)	K_0	α	K
Clements (half-width)	**Pier #1**	47.5	14	**Vertical**	14.55	1,163.9*G	1.11	1,291.9*G
				Horizontal -X		872.9*G	1.16	1,012.6*G
				Horizontal -Y			1.04	907.8*G
				Rocking-X	19.97	61,209,000*G	1.13	69,166,000*G
				Rocking-Y	10.84	9,794,000*G		11,067,000*G
	Pier #2	47	18	**Vertical**	16.41	1,313*G	1.07	1,404.9*G
				Horizontal -X		984.6*G	1.11	1,092.9*G
				Horizontal -Y			1.03	1,014.1*G
				Rocking-X	21.10	72,166,000*G	1.09	78,661,000*G
				Rocking-Y	13.06	17,104,000*G		18,643,000*G

Table 3-2 Clements Bridge soil spring stiffnesses for abutment footings.

Bridge Name	Footing of	2L (ft)	2B (ft)	Stiffness component	R (ft)	K
Clements (whole-width)	**Abutment #1 Back wall**	86	13.25	**Vertical**	19.05	1,523*G
				Horizontal -X		1,143*G
				Horizontal -Y		
				Rocking-X	30.75	223,327,000*G
				Rocking-Y	12.07	13,506,000*G
	Abutment #1 Wing wall	23	13.1	**Vertical**	9.79	783.5*G
				Horizontal -X		587.6*G
				Horizontal -Y		
				Rocking-X	11.40	11,389,000*G
				Rocking-Y	8.61	4,896,000*G
	Abutment #2 Back wall	86	16.25	**Vertical**	21.09	1,687*G
				Horizontal -X		1,265*G
				Horizontal -Y		
				Rocking-X	32.36	260,267,000*G
				Rocking-Y	14.07	21,377,000*G
	Abutment #2 Wing wall	36	17.75	**Vertical**	14.26	1,141*G
				Horizontal -X		855.7*G
				Horizontal -Y		
				Rocking-X	17.22	39,196,000*G
				Rocking-Y	12.09	13,570,000*G

Notes:

1) For wing walls that have different footing dimensions, the average dimensions were used for calculating equivalent soil spring constants.
2) For U-shaped abutment footings no shape correction factor (α) is used.
3) For definition of the coordinates in which stiffnesses are calculated refer to Figure 3-2.

Table 3-3 Alexander Bridge soil spring stiffnesses for pier footings

Bridge Name	Footing of	2L (ft)	2B (ft)	Stiffness component	R (ft)	K_0	α	K
Alexander	Pier #1	115	14	Vertical	22.64	1881.0G	1.25	2263.8G
				Horizontal -X		1358.3G	1.25	1697.9G
				Horizontal -Y			1.15	1562.0G
				Rocking-X	38.77	447,532,000G	1.45	648,921,000G
				Rocking-Y	13.53	19,009,000G	1.3	24,711,700G

Table 3-4 Alexander Bridge soil spring stiffnesses for abutment footings

Bridge Name	Footing of	2L (ft)	2B (ft)	Stiffness component	R (ft)	K
Alexander	Abutment #1 Back wall	111.7	13	Vertical	21.50	1719.9G
				Horizontal -X		1290.G
				Horizontal -Y		
				Rocking-X	37.24	396,634,000G
				Rocking-Y	12.70	15,742,000G
	Abutment #1 Wing wall	11.85	15.75	Vertical	7.71	616.6G
				Horizontal -X		462.5G
				Horizontal -Y		
				Rocking-X	7.26	2,941,000G
				Rocking-Y	8.37	4,506,000G
	Abutment #2 Back wall	111.7	13	Vertical	21.50	1719.9G
				Horizontal -X		1290.G
				Horizontal -y		
				Rocking-X	37.24	396,634,000G
				Rocking-Y	12.70	15,742,000G
	Abutment #2 Wing wall	7.67	13.75	Vertical	5.79	463.5G
				Horizontal -X		347.6G
				Horizontal -Y		
				Rocking-X	5.07	998,000G
				Rocking-Y	6.78	2,396,000G

Notes:

1) For wing walls that have different footing dimensions, the average dimensions were used for calculating equivalent soil spring constants.
2) For U-shaped abutment footings no shape correction factor (α) is used.
3) For definition of the coordinates in which stiffnesses are calculated refer to Figure 3-2.

Table 3-5 Bridge-5 soil spring stiffnesses for pier footings

Bridge Name	Footing of	2L (ft)	2B (ft)	Stiffness component	R (ft)	K_0	α	K
Bridge-5	Piers #1,2,3	71	8	Vertical	13.45	1075.7G	1.35	1452G
				Horizontal -X		806.77G	1.25	1008G
				Horizontal -Y			1.2	968G
				Rocking-X	23.48	99,381,752G	1.5	149,073,000G
				Rocking-Y	7.88	3,758,842G	1.35	5,074,000G

Table 3-6 Bridge-5 soil spring stiffnesses for abutment footings

Bridge Name	Footing of	2L (ft)	2B (ft)	Stiffness component	R (ft)	K
Bridge-5	Abutment #1 south Back wall	55	7	Vertical	11.070	885.6G
				Horizontal -X		664.2G
				Horizontal -Y		
				Rocking-X	18.749	50,617,000G
				Rocking-Y	6.689	2,298,000G
	Abutment #1 south Wing wall	28.65	9	Vertical	9.060	724.8G
				Horizontal -X		543.6G
				Horizontal -Y		
				Rocking-X	12.242	14,089,000G
				Rocking-Y	6.861	2,481,000G
	Abutment #2 North Back wall	46.7	8.5	Vertical	11.241	899.3G
				Horizontal -X		674.4G
				Horizontal -Y		
				Rocking-X	17.409	40,521,000G
				Rocking-Y	7.427	3,147,000G
	Abutment #2 North Wing wall	26.75	11	Vertical	9.678	774.2G
				Horizontal -X		580.7G
				Horizontal -Y		
				Rocking-X	12.226	14,034,000G
				Rocking-Y	7.840	3,701,000G

Notes:

1) For wing walls that have different footing dimensions, the average dimensions were used for calculating equivalent soil spring constants.
2) For U-shaped abutment footings no shape correction factor (α) is used.
3) For definition of the coordinates in which stiffnesses are calculated refer to Figure 3-2.

Table 3-7 Soil spring stiffnesses at the base of pier columns considering pier footing flexibility.

a) Clements Bridge

Pier	Translational (kips/inch)			Rotational (kips-in/rad)	
	Kx	**Ky**	**Kz**	**Kr(x-x)**	**Kr(y-y)**
Left (#1)	506G	454G	646G	G=0.4 ksi $5.8*10^6$ G=4.0 ksi $23*10^6$ G=40 ksi $51*10^6$	G=0.4 ksi $3.6*10^6$ G=4.0 ksi $19*10^6$ G=40 ksi $82*10^6$
Right(#2)	546G	507G	702G	G=0.4 ksi $6.1*10^6$ G=4.0 ksi $24*10^6$ G=40 ksi $54*10^6$	G=0.4 ksi $5.7*10^6$ G=4.0 ksi $29*10^6$ G=40 ksi $125*10^6$

b) Bridge-5

Pier	Translational (kips/inch)			Rotational (kips-in/rad)	
	Kx	**Ky**	**Kz**	**Kr(x-x)**	**Kr(y-y)**
1,2 &3	202*G	194*G	290*G	G=0.4 ksi $5.3*10^6$ G=4.0 ksi $30*10^6$ G=40 ksi $46*10^6$	$1.0*10^6$

Notes:

1) Shaded areas mark the stiffness values which the flexibility of pier footings is considered in their calculations.
2) For Bridge-5, Kr(x-x) is calculated at the second pier column base. This value is considered as an average and typical value.
3) Since no 3-D model is developed for Alexander Bridge, stiffness values presented in Table 3-3 are sufficient.
4) For definition of the coordinates in which stiffnesses are calculated refer to Figure 3-3.
5) G is in ksi.

Table 3-8 Abutment wall stiffnesses

Bridge Name	Abutment No.	H (ft)	B (ft)	K_W (kips/in)	K_{RW} (kips-in / rad)
Clements	**1**	14	86	1228G	5,872,000G
	2	21	86	1228G	13,212,000G
Alexander	**1**	17	111.7	1595G	11,246,000G
	2	13.9	111.7	1595G	7,518,000G
Bridge-5	**1 south**	13.1	55	785G	13,805,000G
	2 north	16.2	46.7	667G	12,308,000G

Notes:
1) B is the width of the abutment wall
2) For notations used in the table refer to Figure 3-4.

Table 3-9 Equivalent spring stiffnesses of the abutment-soil system

Bridge Name	**Abut. #**	**K_T (kips/in)**	**K_R (kips-in/rad)**	**Hw (ft)**	**tf (ft)**	**c (ft)**	**t_d (in)**	**e (ft)**	**x (ft)**	**h (in)**	**K_h kips/in**
Clements (Whole-width)	**1**	(1228+1143+2 *587.6)*G =3546*G	48,146,105	14.05	2.0	7.5	74.8	4.4	2.5	110	1875*G
	2	(1228+1265+ 2*855.7)*G = 4204*G	124,750,450	20.8	2	7.5	74.8	4.4	2.8	187	1930*G
Alexander	**1**	(1595+1290+2 *462.5)G =3810G	44,394,068G	17	3	5.9	54.6	3.6	3.9	150	1300*G
	2	(1595+1290+2 *347.6)G =3580G	33,701,190G	13.9	3	5.7	54.6	3.4	3.6	118.8	1432*G
Bridge-5	**1 south**	(785+664.2+ 2*543.6)G =2536G	48,494,142G	13.1	2.5	7.5	~70	4.6	2.3	104.4	1615*G
	2 north	(667+674.4+ 2*580.7)G =2503G	48,605,901G	16.2	2.5	6.7	~70	3.8	2.3	151.2	1150*G

Notes:

1) In Caltrans method the abutment longitudinal stiffness for Clements Bridge is equal to 200(k/in)/ft * B = 200*86 = 17200 k/in
2) In Caltrans method the abutment longitudinal stiffness for Alexander Bridge is equal to 200(k/in)/ft * B = 200*111.7' = 22,340 k/in
3) In Caltrans method the abutment longitudinal stiffness for Bridge-5 is equal to 200(k/in)/ft * B_{ave} ~ 200*50 = 10,000 k/in
3) For notations used in the table refer to Figure 3-5.

Table 3-10 Abutment spring stiffnesses in transverse and vertical directions

Bridge Name	Abutment	Transverse (kips/inch)	Vertical (kips/inch)
Clements (whole width)	Left (#1)	883.5G	2473.7G
	Right (#2)	1382.8G	3871.8G
Bridge-5	South (#1)	422*G	1183*G
	North (#2)	426*G	1191*G

Table 3-11 K_{PE} coefficient for different soil frictional angle (ϕ).

ϕ (Deg)	K_{PE}
20	1.554
30	2.096
35	2.440
40	2.859
45	3.384
50	4.071

Note:
In this study it is assumed that for soils with G=0.4 and 4 ksi, ϕ is equal to 20^o and for soils with G=40 ksi, ϕ is equal to 45^o.

Table 3-12 Compression yield capacity (C_y) of the abutments in longitudinal direction

Bridge Name	Abutment No.	Height (ft)	Width B (ft)	C_y (kips)
Clements (whole width)	**1**	14+2 = 16	86	$1321*K_{PE}$
	2	20.8+2 = 22.8	86	$2682*K_{PE}$
Alexander	**1**	20	111.7	$2681*K_{PE}$
	2	16.9	111.7	$1914*K_{PE}$
Bridge-5	**1 south**	15.6	55	$803*K_{PE}$
	2 north	18.7	46.7	$980*K_{PE}$

Table 3-13 Total normal weight (N) on the abutment footings

Bridge Name	Abutment No.	P_D (kips)	W_m (kips)	W_w (kips)	W_s (kips)	N (kips)
Clements (whole width)	**1**	1381.4	992.8	363.8	1014	3752
	2	1381.4	1466.8	924.4	3212	6985
Alexander	**1**	1055.2	1498.7	335	715.3	3604
	2	1055.2	1312	183.2	385.2	2936
Bridge-5	**1**	3400	578.2	509.9	831	5319
	2	4900	678.9	536.4	1144	7259

Notes:
1) P_D is the dead load of superstructure carried by abutment.
2) W_m is the weight of abutment main wall and it's footing.
3) W_w is the weight of abutment wing-walls and their footings.
4) W_s is the weight of soil over the abutment footings.

Table 3-14 Back-wall geometry and its soil spring properties

Bridge Name	L (ft)	c (ft)	t_w (ft)	Weight (kips)	Stiffness K_s (kips/in)	Compression Yield Limit C_y (kips)
Clements	102.5	7.5	1.5	173	1228.1*G	290.25*K_{PE}
Alexander	111.8	5.9 5.7	1.5	148 143	1595.1G	225.46*K_{PE} average
Bridge-5	77.3 66.5	7.5 6.7	1.5	130.4 100.2	785.4G 666.9G	156*K_{PE} average

Table 3-15 Shear friction capacity (Vn) of the abutment back-wall cross section

Bridge Name	Rebar I			Rebar II			A_{vf} in^2	F_y ksi	V_n kips
	Size	No.	Area	Size	No.	Area			
Clements	5	131	131*.31	4	76	76*.2	55.81	60	3349
Alexander	5@12	112	112*.31	5@12	112	112*.31	69.44	60	4166
Bridge-5	6@12	~70	70*.44	6@12	~70	70*.44	61.6	40	2464

Note:
Locations for bars (I and II) and the critical section where the shear capacity is calculated are presented in Figure 3-8.

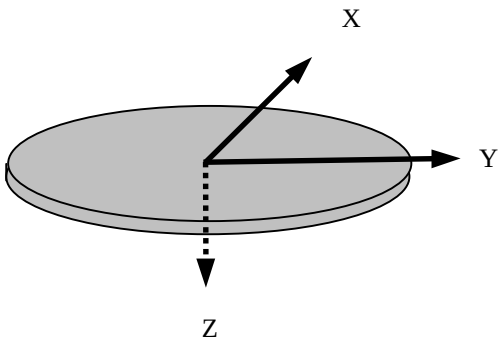

$$
\begin{array}{c}
\begin{matrix} \delta_X & \delta_Y & \delta_Z & \theta_X & \theta_Y & \theta_Z \end{matrix} \\
\begin{bmatrix}
K_{11} & 0 & 0 & 0 & -K_{15} & 0 \\
0 & K_{22} & 0 & K_{24} & 0 & 0 \\
0 & 0 & K_{33} & 0 & 0 & 0 \\
0 & K_{42} & 0 & K_{44} & 0 & 0 \\
-K_{51} & 0 & 0 & 0 & K_{55} & 0 \\
0 & 0 & 0 & 0 & 0 & K_{66}
\end{bmatrix}
\end{array}
$$

Figure 3-1 Stiffness matrix of an equivalent circular footing (K_o)

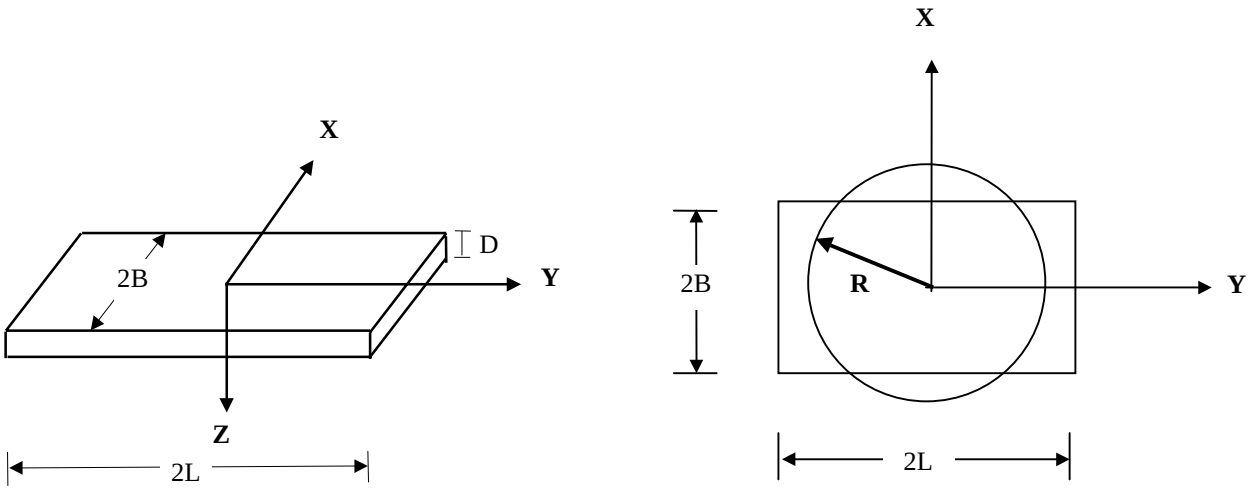

Translation:

$$R = \sqrt{(4BL)/\pi}$$

Rotation:

$$R = \left[(2B) * (2L)^3 / 3\pi\right]^{\frac{1}{4}} \qquad \text{(X-axis Rocking)}$$

$$R = \left[(2B)^3 * (2L) / 3\pi\right]^{\frac{1}{4}} \qquad \text{(Y-axis Rocking)}$$

$$R = \left[(4BL) * \left(4B^2 + 4L^2\right) / 6\pi\right]^{\frac{1}{4}} \qquad \text{(Z-axis Torsion)}$$

Figure 3-2 Equivalent radius for rectangular footings.

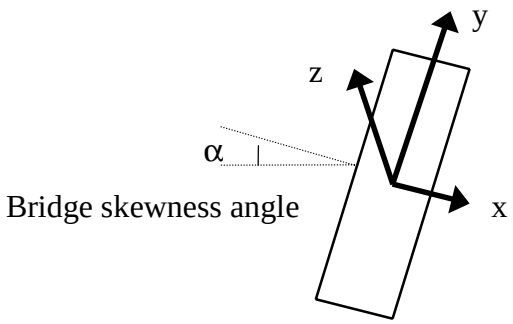

Figure 3-3 Footings Local axes

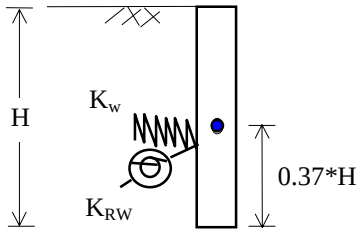

Fig.3-4 Abutment back wall and equivalent soil springs.

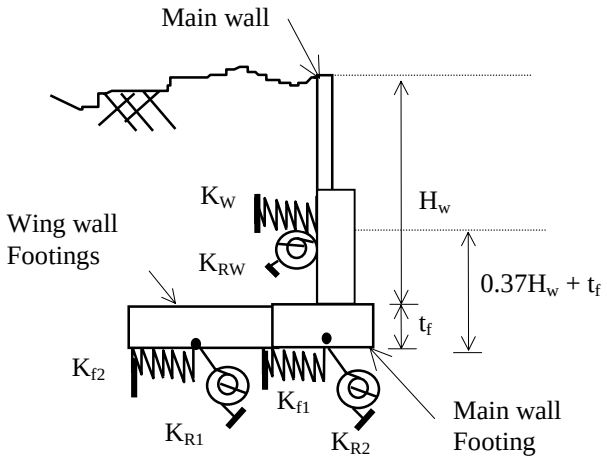

a) Abutment main wall and footings soil springs (Step1)

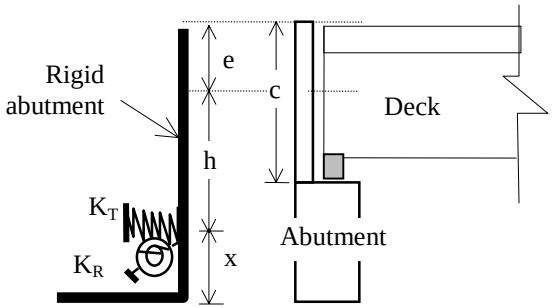

b) Equivalent spring set at the center of stiffness (Step2)

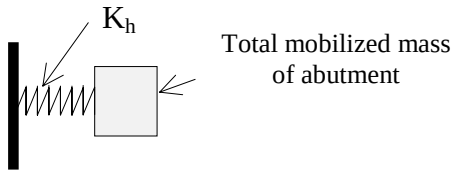

c) Simplified abutment model (Step3)

K_{f1} = Equivalent horizontal spring stiffness for main wall footing. K_{f2} =Equivalent horizontal spring stiffness for wing wall footings.
K_W = Equivalent horizontal spring stiffness for main wall. K_{R1} =Equivalent rotational spring stiffness for back wall footing.
K_{R2} = Equivalent rotational spring stiffness for wing wall footings. K_{RW} =Equivalent rotational spring stiffness for back wall.
$K_R = K_{RW}+K_{R1}+K_{R2}+K_W*(0.37H_w+t_f - x)^2+(K_{f1}+K_{f2})*x^2$ $K_T=K_{f1}+K_{f2}+K_w$
$x =(K_W / K_{tot})*(0.37H_w+t_f)$ locates the center of stiffness. $h =(H_w+t_f)-x–e$
e = Distance from top of the back wall to the application point of the resultant impact force, which assumed to be equal to {c-(Deck-Thickness)/2}.
K_h = Equivalent translational stiffness at distance " e " below top of the abutment back wall = $(K_R*K_T)/(K_T*h^2+K_R)$

Figure 3-5 Graphical illustration of determination of equivalent abutment model

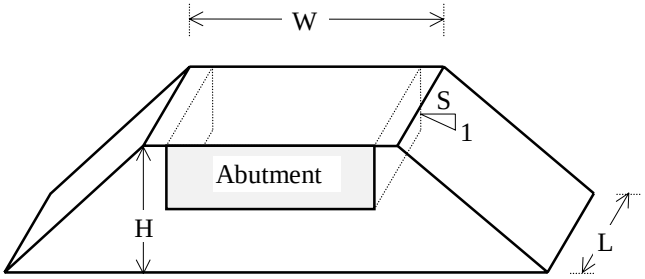

Figure 3-6 Abutment embankment dimensions used in calculating transverse and vertical stiffnesses

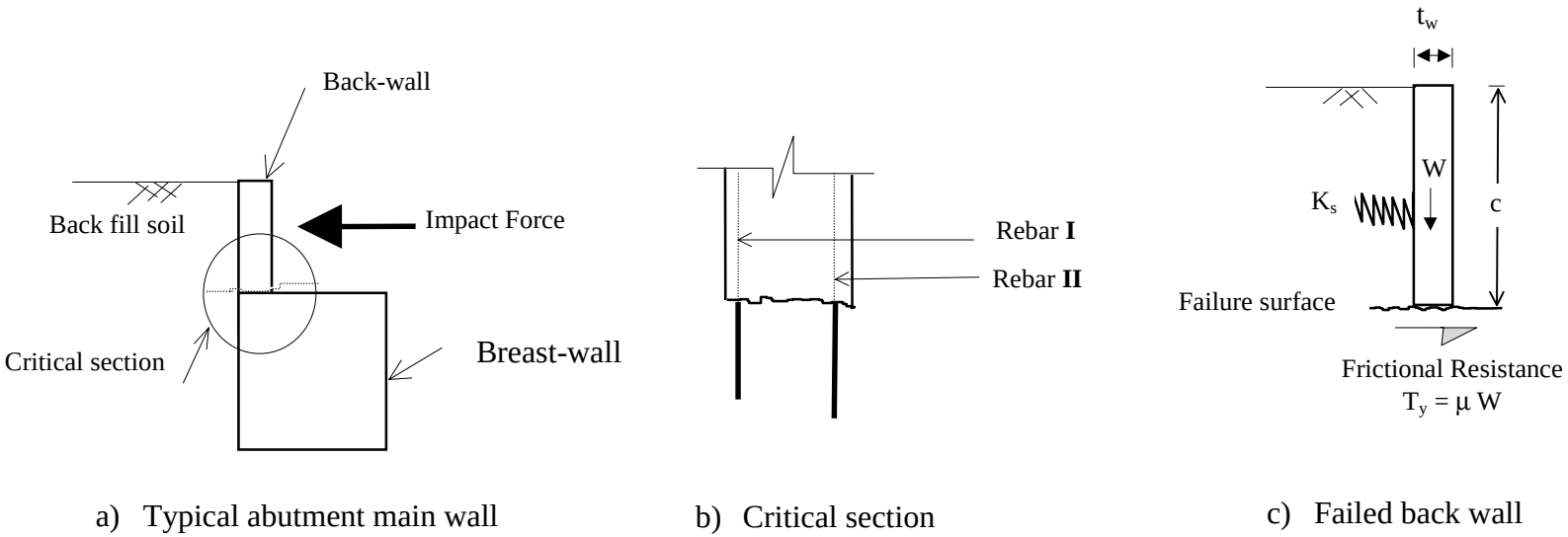

a) Typical abutment main wall

b) Critical section

c) Failed back wall

T_y = Abutment back wall frictional resistance force, assumed equal to μ*W with μ = 1
K_s = Back fill equivalent translational spring stiffness =0.425 E_s B
W = L*c*t_w*$\gamma_{concrete}$, $\gamma_{concrete}$ = 0.15 kips/ft^3
E_s = Soil modulus of elasticity = 2(1+ν)*G, (ν=0.4)
L = B / cos α, α is the angle between deck centerline and an axis perpendicular to the abutments back wall. B is the width of abutment.

Figure 3-7 Typical abutment wall and damaged backwall

SECTION 4

STIFFNESS AND CAPACITY OF THE REINFORCED CONCRETE PIER COLUMNS

4-1) General

All three bridges analyzed under this study have round columns. The confinement effect is considered in the evaluation of column curvature ductility and plastic rotation capacity using FHWA's guidelines [12]. The effects of column curvature ductility and lateral reinforcement on shear capacity are also considered. The exact moment-curvature relationship and moment-axial load interaction for column cross-sections are determined. This is achieved by dividing the cross-section into a number of fibers and satisfying compatibility and equilibrium by commonly used stress-strain relationships for concrete and steel materials. The column is then modeled using elasto-plastic beam elements with initial stiffness equal to effective moment of inertia determined using FHWA's guidelines [12]. The plastic moment capacity is determined by fitting the bilinear model to the actual moment-curvature relationship. The actual moment-curvature relationship along with the equations given by FHWA for plastic hinge rotation and plastic hinge length is used to determine the plastic hinge capacity. Following are the descriptions of the procedures used in calculating stiffness, strength and ductility of the concrete pier columns.

It should be noted that due to lack of field strength testing of the concrete, no increase in concrete strength due to aging is considered and on the other hand, no strength reduction factors were applied for capacity calculations.

4-2) Effective Moment of Inertia

The stiffness of pier columns depends on several factors such as the material properties, the longitudinal reinforcement ratio, the axial load level, and the distribution of cracking along the height of the column. Stiffness calculations can be made by assigning an effective moment of inertia to the column based on these factors as suggested by FHWA [12]. Tables 4-1 and 4-2 show the calculated values for the three bridges.

4-3) Shear Capacity

Shear strength equations for reinforced concrete columns in existing codes such as ACI 318-89 and AASHTO tend to give a poor estimate of actual strength. They are conservative at low flexural ductility levels, and unconservative at high ductilities. An exception is in cases where no contribution from concrete in section shear capacity is considered and transverse reinforcement provides all the shear resistance. A shear strength calculation considering the curvature ductility level at the column cross section is introduced by FHWA [12]. For circular sections the corresponding FHWA equation is as follows:

$$V_n = V_c + V_s + V_p = v_c * A_e + (\pi/2) * A_v * F_y * D'/s * \cot g(\theta) + 0.2 * P$$

Where

V_c is the shear carried by concrete shear-resisting mechanisms (aggregate interlock, compression zone shear transfer, dowel action) and is equal to:

1) $3.5\sqrt{f'_c}$ (psi), for low ductility demand level ($\mu_\phi \leq 2$).

2) $1.2\sqrt{f'_c}$ (psi), for high ductility level ($\mu_\phi \geq 4$).

μ_ϕ is curvature ductility and is equal to $\phi_u / \phi_y = 1 + \phi_p / \phi_y$

V_s is the shear carried by truss mechanisms, and V_p is the shear carried by axial compression, which here was ignored.

θ is the angle between the column axis and the diagonal concrete compression strut, taken as 45^o in the ACI approach. In the case of light transverse reinforcement in the form of

stirrups, a value of 30^o could be used [12]. Here θ conservatively is taken to be equal to 45^0.

A_e is the effective shear area which may be taken as $0.8*A_g$ for circular columns.

D' is the diameter of the circular hoop or spiral.

A_v is the area of the circular hoop or spiral.

F_y is the yield limit of lateral confining steel.

4-4) Plastic Rotation Capacity

Plastic rotation capacity can be calculated by assuming a plastic hinge length (L_p), over which a constant curvature ($\phi_u - \phi_y$) is maintained:

$$\theta_p = L_p * (\phi_u - \phi_y)$$

Where

ϕ_y is the yield curvature corresponding to the first yielding at the longitudinal reinforcing bars. ϕ_u is the ultimate curvature obtained by the column M-ϕ diagram.

L_p is the plastic hinge length and based on the FHWA [12] for pier columns without pile footings is equal to:

$$L_p = 0.08\ Z\ +\ \chi * d_b$$

Where Z is the distance of critical section to the point of contraflexure, d_b is the diameter of longitudinal reinforcement and χ is a coefficient equal to 6 and 9 for grade 40 and 60 rebars, respectively. The first term (0.08 Z) is calibrated to experimental and theoretical results for typical curvature distributions of an element with linear moment variation. The second term ($\chi * d_b$) accounts for the increase in plastic rotation length resulting from strain penetration of the longitudinal reinforcement into the concrete beyond the critical section.

Table 4-4 shows the calculated values for different bridges.

4-5) M-ϕ and M-P Diagrams

The M-ϕ and M-P diagrams are generated by a computer program which divides the column cross section into the steel and concrete fibers with corresponding stress-strain curves. The stress-strain curves assumed for concrete and steel are shown in Figure 4-1.

In this program plane sections are assumed to remain plane after deformation and the effect of increased compressive strength of confined concrete and cover crushing at large strains were ignored. The ultimate curvature on the M-ϕ diagrams is achieved when concrete strain reaches the ultimate compressive strain or the moment decreases to 85% of the moment capacity of the section, which ever happens first.

For flexural strength calculation, the ultimate compressive strain of 0.005 is assumed for unconfined concrete [12]. For confined concrete, the following equation based on the energy-balance concept is used to calculate the ultimate compressive strain [12]:

$$\varepsilon_{cu} = 0.004 + \left(1.4 * \rho_s * f_{yh} * \varepsilon_{sm}\right) \Big/ f'_{cc}$$

Where

ρ_s is the effective volumetric ratio of the confining steel

f_{yh} is the lateral confining steel yield stress

ε_{sm} is the strain at peak stress for confining reinforcement and is equal to 0.15 and 0.12 for grade 40 and 60 reinforcements, respectively.

f'_{cc} is the compressive strength of confined concrete. This can be determined by an energy-balance method or in an approximate way is equal to $1.5*f'_c$ for low-to-moderate confinement ratios. Here, the Mander's method [14] was used for calculating f'_{cc} and the brief description follows.

Ultimate Compressive Stress for Confined Concrete (f'_{cc})

A stress-strain curve was proposed by Mander [14] for confined concrete under uniaxial compressive loading. The concrete section may contain any general type of confining steel either spiral or circular hoops or rectangular hoops with or without supplementary cross-ties.

The ultimate compressive strain of a confined concrete section, defined as the strain at which first hoop fracture occurs, is determined by tracing the work done on the confined concrete and longitudinal steel in compression. In this energy-balance approach, when the external work exceeds the available strain energy for the transverse steel, the ultimate compressive stress has been reached.

As a result of the above approach, the following formula is obtained for the ultimate compressive stress of the confined concrete:

$$f_{cc}' = f_{co}'\left(-1.254 + 2.254 * \sqrt{1 + 7.49\, f_l'/f_{co}'} - 2\, f_l'/f_{co}'\right)$$

Where

$f'_l = k_e * f_l$, effective lateral confining stress on the concrete

$f_l = 0.5 * \rho_s * f_{yh}$, lateral confining pressure on concrete

k_e = confinement effectiveness coefficient = $(1-s'/2d_S) / (1-\rho_{CC})$ for circular spirals

= $(1-s'/2d_S)^2 / (1-\rho_{CC})$ for circular hoops

d_S = diameter of the confined concrete core, measured from the lateral bar centers

s' = clear vertical spacing between lateral confining bars

ρ_{cc} = ratio of the longitudinal reinforcement area to the confined core area

ρ_s = ratio of the confining steel volume to the volume of the confined concrete core.

f_{yh} = yield strength of the transverse reinforcement

f'_{co} = compressive strength of the unconfined concrete

Table 4-5 shows the ultimate confined concrete strains for different bridges. Figures 4-2 to 4-7 show the M-P and M-ϕ diagrams for different bridge columns with a brief description for each pier column.

Table 4-1 Pier columns material and dead axial load (P_D)

Bridge Name	Concrete f'_c (psi)	Reinforcement f_y (psi)	P_D (kips)	$P_D / (f'_c * A_c)$
Clements	3,000	60,000	668	0.12
Alexander	4,000	60,000	256	0.06
Bridge-5	3,000	40,000	294 average	.071

Table 4-2 Pier columns reinforcement and cross sectional information

Bridge Name	Type No.	D (ft)	Longitudinal steel	Transverse steel	I_g (in^4)	A_c (in^2)	$I_{effective}$ (in^4)
Clements	1	4	20-#9 A_b=1.0 in^2 ρ=.011	#3 @1' A_b=.11 in^2 d_b=.375 in circular hoop	260576.3	1809.56	$0.38I_g$ = 99019
Alexander	1	3	16-#10 A_b=1.27 ρ=.02	#5 @ 3.5" A_b=.31 in^2 D=.625 in spiral	82,448.0	1017.88	$0.43I_g$
Bridge-5	1	3.5	9-#11 A_b=1.56 ρ=.01	#4 @ 2.25" A_b=.20 in^2 D=.5 in spiral	152,745	1385.4	0.33 I_g
	2	3.5	13-#11 A_b=1.56 ρ=.015	#4 @ 2.25" A_b=.20 in^2 D=.5 in spiral	152,745	1385.4	0.39 I_g
	3	3.5	15-#11 A_b=1.56 ρ=.017	#4 @ 2.25" A_b=.20 in^2 D=.5 in spiral	152,745	1385.4	0.41 I_g
	4	3.5	20-#11 A_b=1.56 ρ=.023	#4 @ 2.25" A_b=.20 in^2 D=.5 in spiral	152,745	1385.4	0.48 I_g

Table 4-3 The shear and flexural strength of pier columns

Bridge Name	**D'** **(inch)**	**V_c** **(kips)**	**V_s** **(kips)** $\theta = 45^0$	**Shear strength** **(kips)**	**Flexural strength under dead load axial force (P_D)**	
					P_D **(kips)**	**M_n** **(kips-in)**
Clements	43.625	$\mu_\theta \le 2$ *277.5* $\mu_\theta \ge 4$ *95.1*	37.7	$\mu_\theta \le 2$ 315 $\mu_\theta \ge 4$ 133	668	31151
Alexander	31.375	$\mu_\theta \le 2$ *180.2* $\mu_\theta \ge 4$ *61.8*	261.9	$\mu_\theta \le 2$ 442 $\mu_\theta \ge 4$ 323.7	256	18787
Bridge-5	37.5	$\mu_\theta \le 2$ *212.4* $\mu_\theta \ge 4$ *72.8*	209.4	$\mu_\theta \le 2$ 421.8 $\mu_\theta \ge 4$ 282.2	1) 294 2) 347 3) 252 4) 283	1) 13788 2) 17881 3) 18513 4) 23128

Note:
μ_θ is the curvature ductility demand.

Table 4-4 Pier columns plastic rotation capacities

Bridge Name	**Pier #**	**Z (in)**	**Column Diameter (ft)**	**Longitudinal Rebar**		L_p **(in)**	ϕ_y **(rad/in)**	ϕ_u **(rad/in)**	θ_p **(rad)**
				#	d_b				
Clements	**1**	272	4	9	1.128”	31.9	0.00008	0.00055	0.015
	2	334	4	9	1.128”	36.8	0.00008	0.00055	0.0173
Alexander	**1**	214	3	10	1.27”	28.6	0.0001	0.0045	0.126
Bridge-5	**1&2**	~288	3.5	11	1.41”	31.5	0.00006	0.0040	0.124
	3	204	3.5	11	1.41”	24.8	0.00006	0.0040	0.098

Table 4-5 Ultimate compressive stress and strain for confined concrete in pier columns

Bridge Name	f’cc confined maximum compression strength	ε_{cu} Concrete maximum compressive strain
Clements	$1.044*f'_c \sim f'_c$	.005 (no confinement)
Alexander	$1.45*f'_c$	0.0236
Bridge-5	$1.355*f'_c$	0.0236

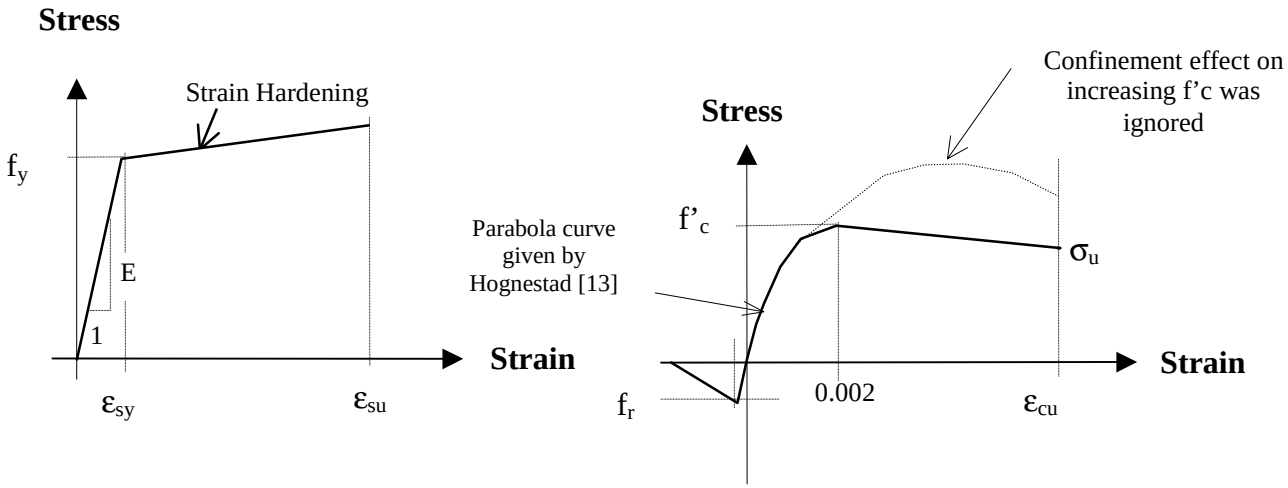

a) Steel stress-strain curve

b) Concrete stress-strain curve

Figure 4-1 Stress-strain curves for steel and concrete

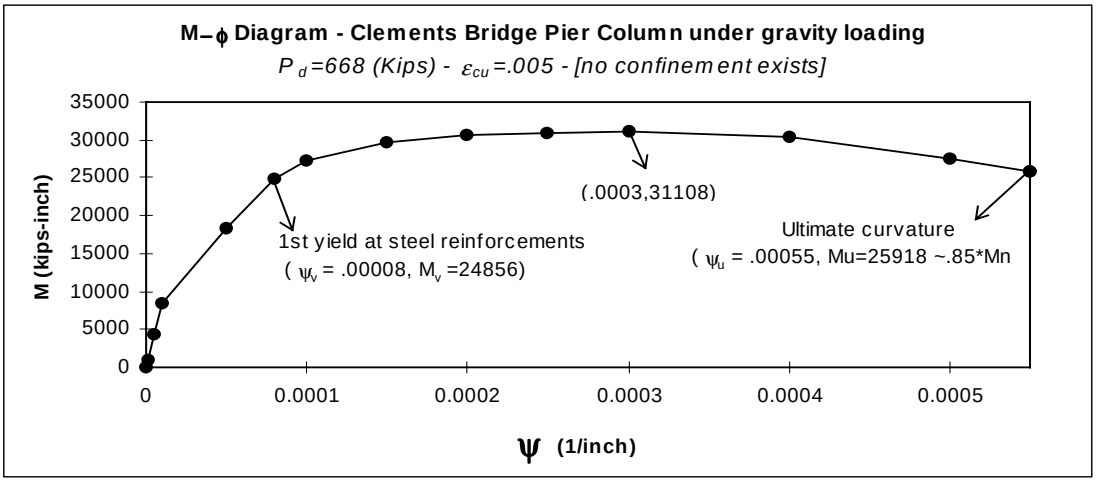

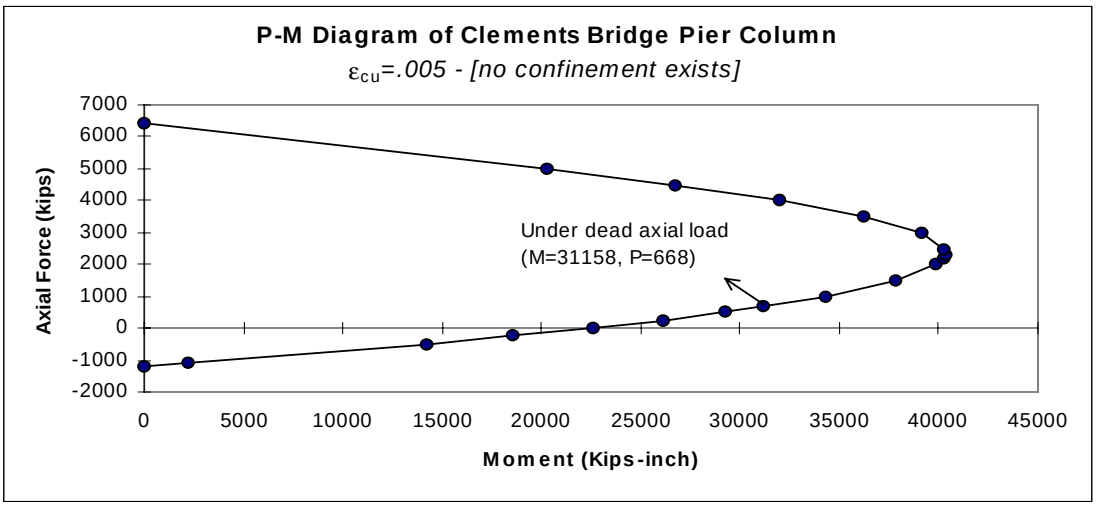

CLEMENTS BRIDGE PIER COLUMNS IN BRIEF

circular column D = 4' & 20 #9 Longitudinal steel reinfocement
#3 @ 12" circular lateral reinforcement
f'c=3000 psi concrete
fy = 60000 psi steel reinforcement
Steel Strain Hardening = 0%

	$\mu_\psi < 2$	$\mu_\psi > 4$
Vc =	277.5 kips	95.1 kips
Vs =	37.7 kips	37.7 kips
Vn =	315	133

Mn = 31151 (kips-inch) Flextural capacity under gravity loading (P=668 kips)
Columns hight L (min.) = 272"
V-flextural (max.) = Mn / L(min.) = 31151 / 272 = 114.5 kips

Figure 4-2 Capacity of Clements Bridge pier column

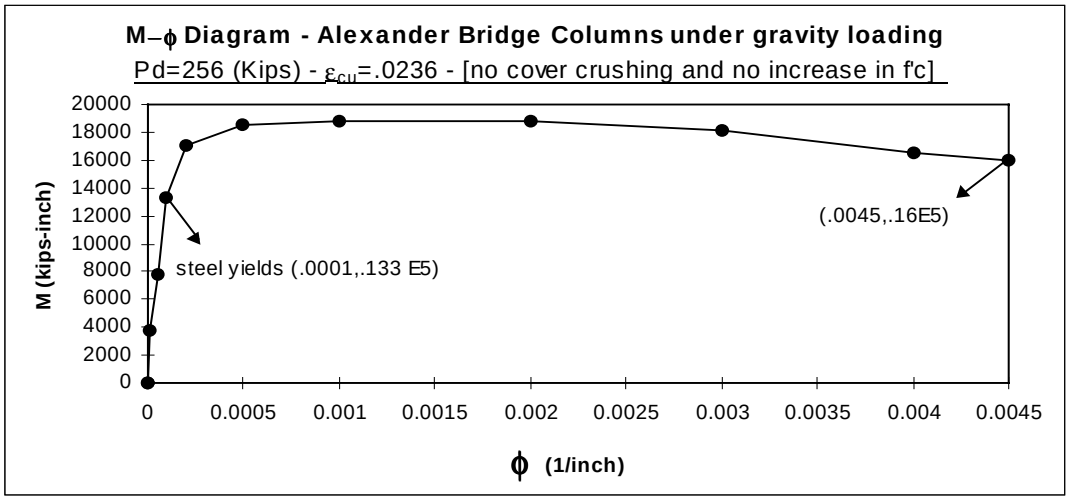

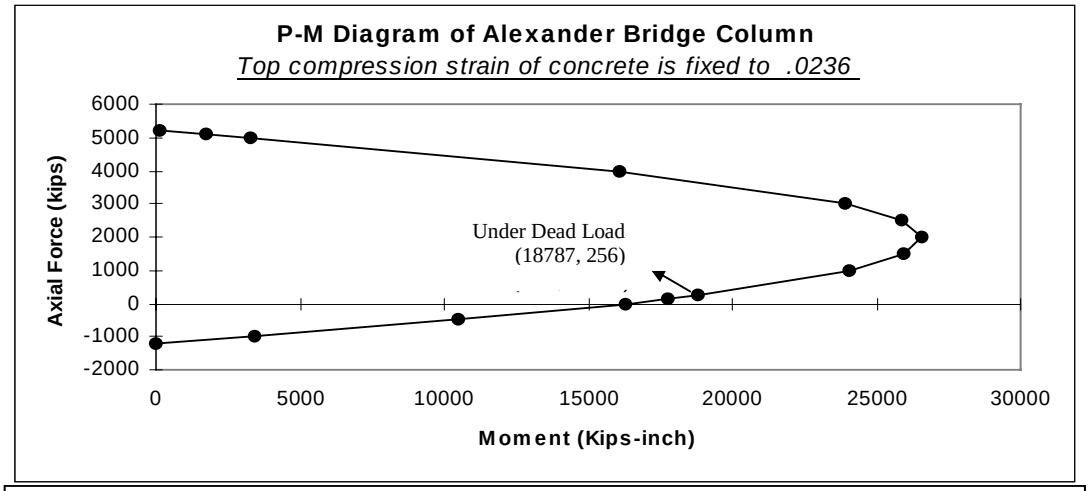

ALEXANDER BRIDGE PIER COLUMNS IN BRIEF

circular column D = 3' & 16#10 Longitudinal steel reinfocement
#5 @ 3.5" spiral lateral reinforcement
f'c=4000 psi concrete
fy = 60000 psi steel reinforcement
Steel Strain Hardening = 0%

	$\mu\theta < 2$	$\mu\theta > 4$
Vc =	180.2 kips	61.8 kips
Vs =	261.9	261.9
Vn =	442.1	323.7

Mn = 18787 (kips-inch) Flextural capacity under gravity loading (P=256 kips)
Columns hight L ~ 262"
V-flextural = Mn / L = 18787 / 262 = 71.7 kips

Figure 4-3 Capacity of Alexander Bridge pier column

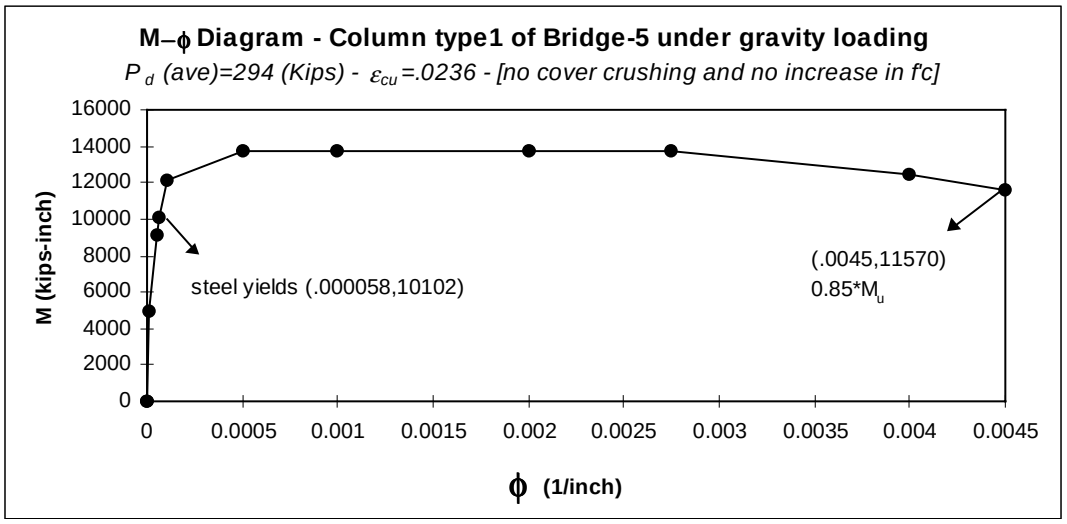

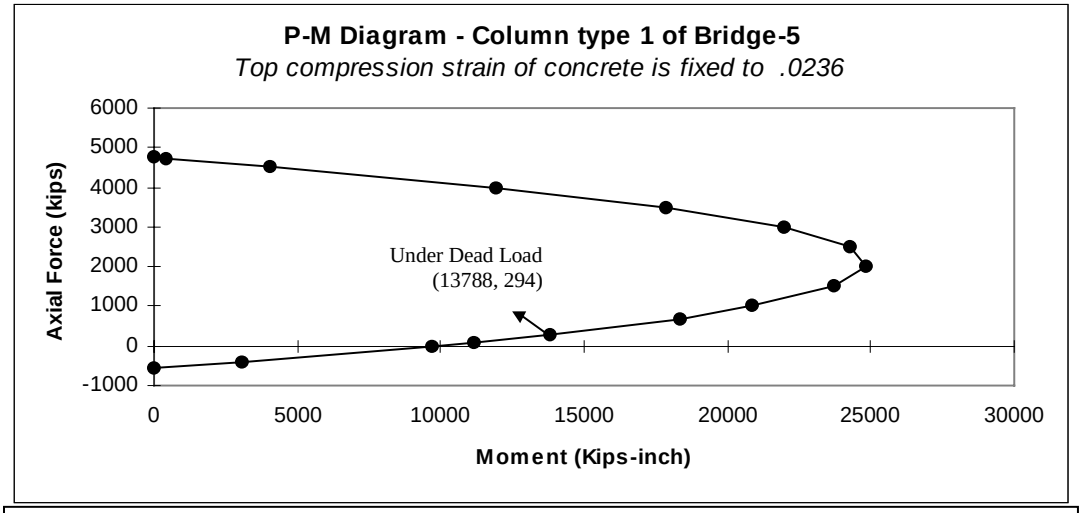

COLUMN TYPE 1 OF BRIDGE-5 IN BRIEF

circular column D = 3.5' & 9 #11 Longitudinal steel reinfocement
#4 @ 2.25" spiral lateral reinforcement
f'c=3000 psi concrete
fy = 40000 psi steel reinforcement
Steel Strain Hardening = 0%

	$\mu\theta < 2$	$\mu\theta > 4$
Vc =	212.4 kips	72.8 kips
Vs =	209.4 kips	209.4 kips
Vn =	421.8	282.2

Mn = 13788(kips-inch) Flextural capacity under gravity loading { Pd (ave) = 294 kips }
Minimum columns hight L =204" @pier 3 *this col. type exists in all piers* .
V-flextural (maximum) = Mn / L = 13788 / 204 = 67.7 kips

Figure 4-4 Capacity of column type-1 from Bridge-5

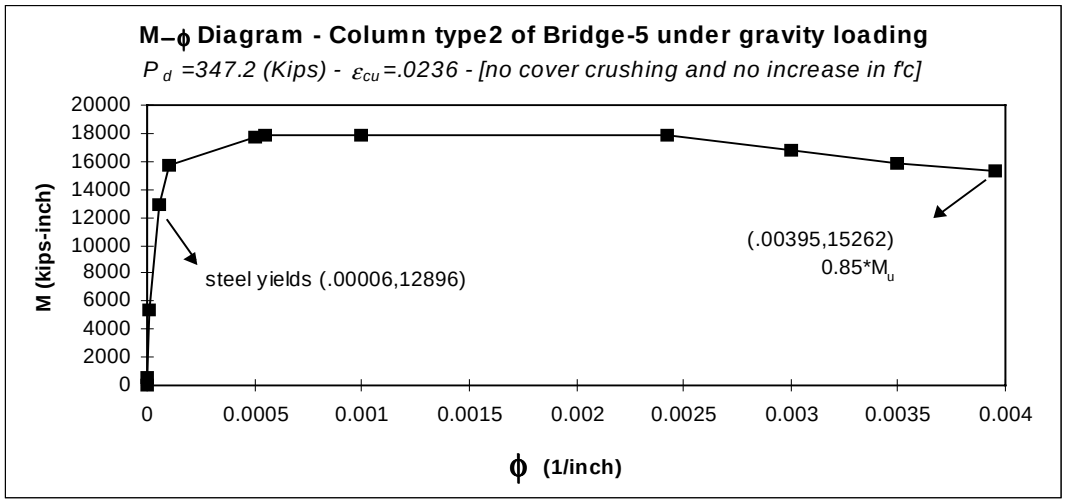

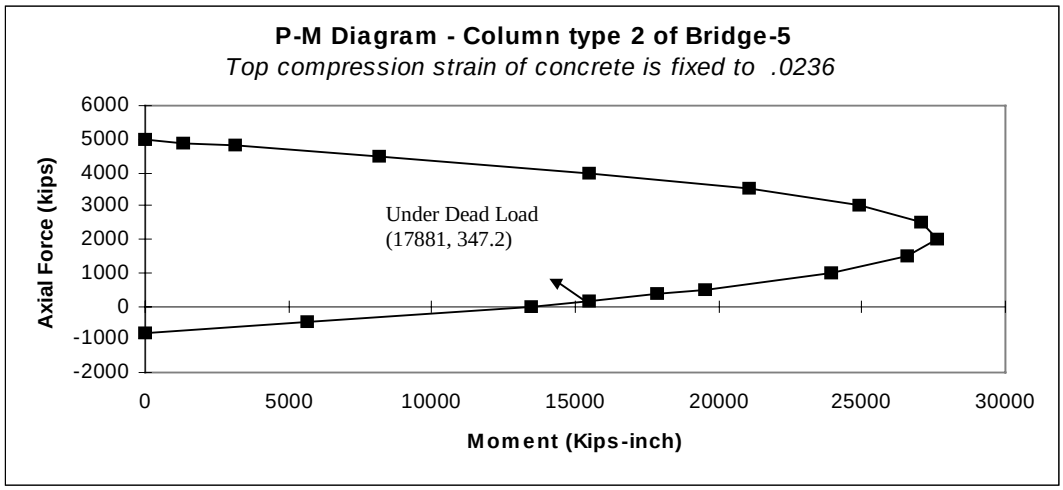

COLUMN TYPE 2 OF BRIDGE-5 IN BRIEF

circular column D = 3.5' & 13#11 Longitudinal steel reinfocement
#4 @ 2.25" spiral lateral reinforcement
f'c=3000 psi concrete
fy = 40000 psi steel reinforcement
Steel Strain Hardening = 0%

	$\mu\theta < 2$	$\mu\theta > 4$
Vc =	212.4 kips	72.8 kips
Vs =	209.4 kips	209.4 kips
Vn =	421.8	282.2

Mn = 17881 (kips-inch) Flextural capacity under gravity loading { Pd = 347.2 kips }
Columns hight L ~242" @pier 2
V-flextural (maximum) = Mn / L = 17881 / 242 = 73.9 kips

Figure 4-5 Capacity of column type-2 from Bridge-5

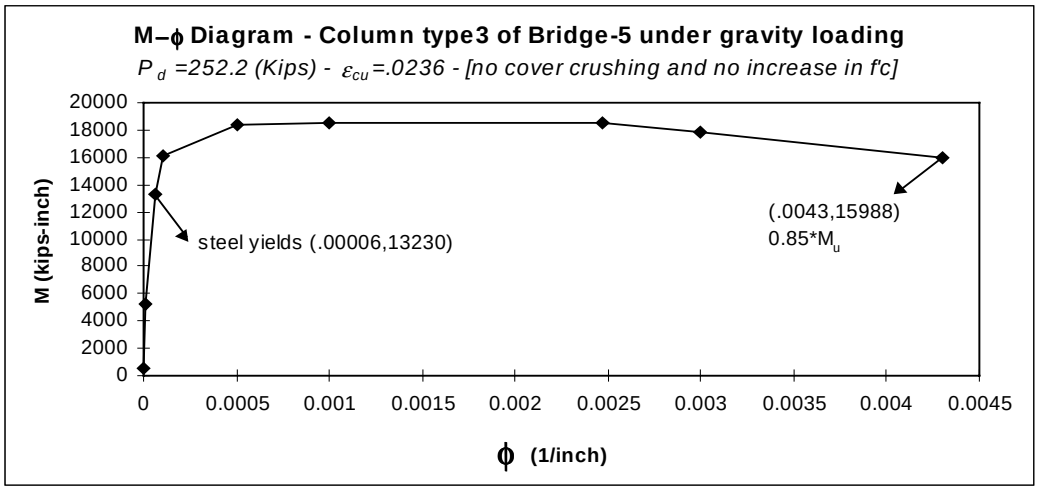

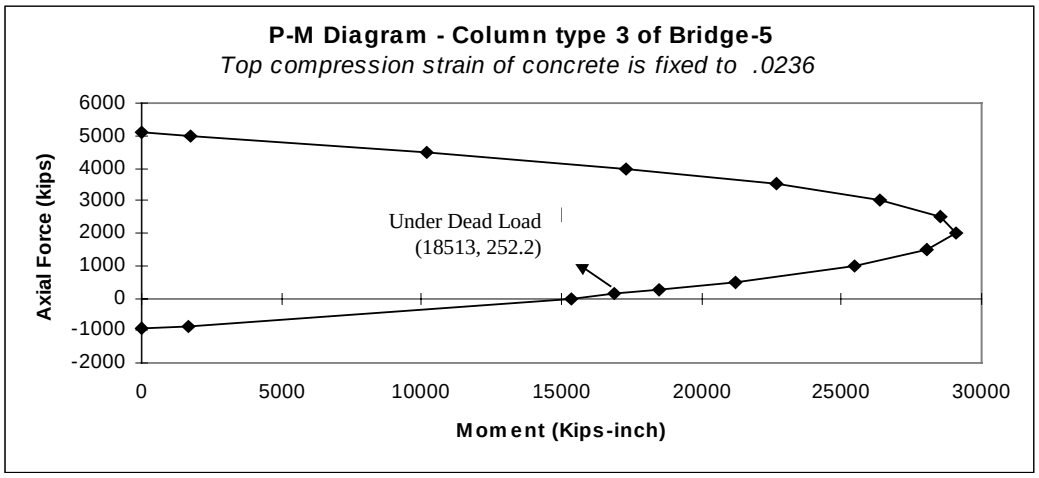

COLUMN TYPE 3 OF BRIDGE-5 IN BRIEF

circular column D = 3.5' & 15#11 Longitudinal steel reinfocement
#4 @ 2.25" spiral lateral reinforcement
f'c=3000 psi concrete
fy = 40000 psi steel reinforcement
Steel Strain Hardening = 0%

	$\mu\theta < 2$	$\mu\theta > 4$
Vc =	212.4 kips	72.8 kips
Vs =	209.4 kips	209.4 kips
Vn =	421.8	282.2

Mn = 18513 (kips-inch) Flextural capacity under gravity loading { Pd = 347.2 kips }
Columns hight L = 234" @pier 1
V-flextural (maximum) = Mn / L = 18513 / 234 = 79.1 kips

Figure 4-6 Capacity of column type-3 from Bridge-5

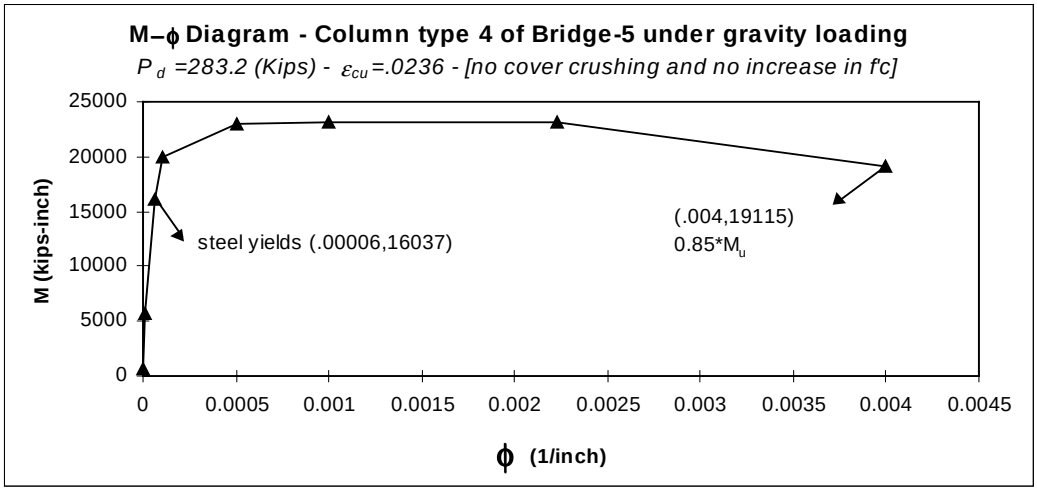

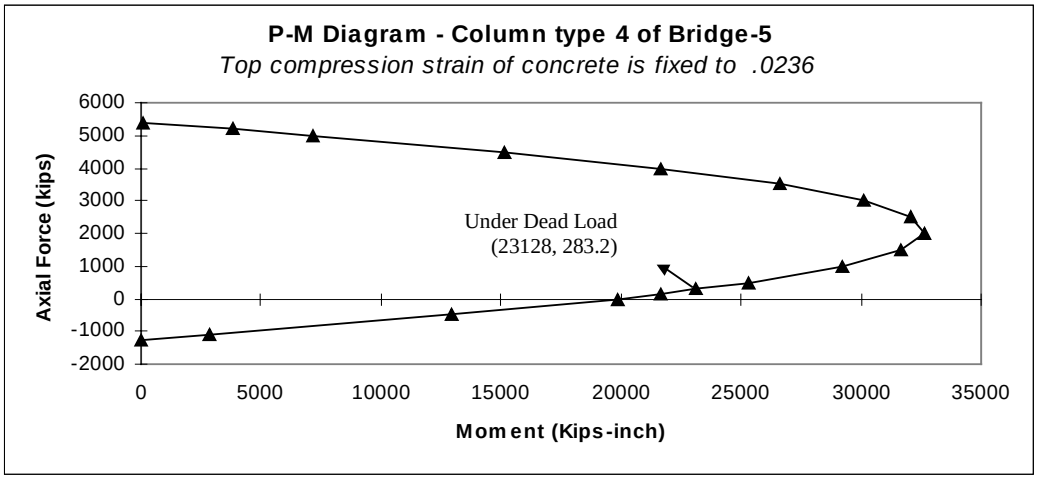

COLUMN TYPE 4 OF BRIDGE-5 IN BRIEF

circular column D = 3.5' & 20#11 Longitudinal steel reinfocement
#4 @ 2.25" spiral lateral reinforcement
f'c=3000 psi concrete
fy = 40000 psi steel reinforcement
Steel Strain Hardening = 0%

	$\mu\theta < 2$	$\mu\theta > 4$
Vc =	212.4 kips	72.8 kips
Vs =	209.4 kips	209.4 kips
Vn =	421.8	282.2

Mn = 23128 (kips-inch) Flextural capacity under gravity loading { Pd = 283.2 kips }
Columns hight L = 204"
V-flextural (maximum) = Mn / L = 23128 / 204 = 113 kips

Figure 4-7 Capacity of column type-4 from Bridge-5

SECTION 5

STIFFNESS AND CAPACITY OF THE BEARINGS

5-1) General

Steel bearings are used to transfer the vertical and horizontal forces from the superstructure to the substructure. Typically four 22-mm (7/8") diameter A325 steel bolts are used to connect the bearing to the girder, and two 38-mm (21/2") diameter A615 anchor bolts are used to connect the bearings to the abutments and cap beams. These elements are the weak links in the load transfer through the bearing from the superstructure to the substructure, and impact forces can easily exceed their shear capacity. Therefore, the post-failure behavior of the bearings (Coulomb Friction) is also investigated and is modeled by using a bilinear force-deformation relationship with yield strength equal to coefficient of friction times the normal force per bearing due to gravity (Figure 5-1). The coefficient of friction is taken to be in the range of 0.2 to 0.6 as a parameter. Parametric studies [1] have shown that the bridge response is not sensitive to the bearing stiffness. In this study for the modeling of frictional behavior at failed bearings, relatively large values are assigned to bearing stiffnesses in computer simulations.

5-2) Shear Strength of Welding and Bearing Bolts

Shear strength of the welding and bearing bolts are determined based on AASHTO-LRFD [11] specifications and are as follows.

Shear Strength of Welding

$$R_W = 0.707*D_W*L_W*f_W \qquad \textit{(pure shear on welds)}$$

f_w is the resistance strength for the fillet-welded connection subjected to shear and is equal to $0.6*F_{exx}$, of which F_{exx} is the tensile strength of the weld or welded material,

whichever is less. D_w is fillet weld size and L_w is fillet weld length. Calculated welding strengths are presented in Table 5-1.

Shear Strength of Bolts

$$R_n = F_v * A_b * Ns = (0.4 * F_{ub}) * A_b * N_s \qquad \textit{(Threads are included in the shear plane)}$$

A_b is the area of the bolt corresponding to the nominal diameter. N_s is the number of shear planes per bolt (here equal to one). F_v is shear strength of bolts which based on AASHTO-LRFD is equal to $0.4 * F_{ub}$, which F_{ub} is specified minimum tensile strength of the bolt as shown in Table 5-2. Calculated shear strengths are presented in Table 5-3. As seen from this table, the bearing capacity is in the range of 100-115 kips.

Table 5-1 Shear capacity of the welds at bearings

Bridge Name	D_W (in)	L_W (in)	F_{exx} (ksi)	f_W (ksi)	Ultimate shear capacity (kips)
Clements	3/8	2*(5 + 18) = 46	Steel A36, F_u=58	0.6*58=34.8	424
Alexander	3/8	2*(5 + 20) = 50	Steel A36, F_u=58	0.6*58=34.8	461
Bridge-5	3/8	2*(5 + 11) = 32 (min)	Steel A36, F_u=58	0.6*58=34.8	295 (min)

Note:
Whenever F_{exx} is not specified, it is taken equal to ultimate tensile strength of connected steel material (F_u).

Table 5-2 Minimum tensile strength for ASTM A325 bolt

Bolt Type	F_{ub} (ksi)
AASHTO M164, ASTM A325	120 for diameters 0.5" through 1.0" 105 for diameters 1.125" through 1.5"

Table 5-3 Shear capacity of connection bolts at bearings

Bridge Name	Connection to girder (Bolts)				Connection to concrete base (Anchor bolts)			
	Bolts & Steel type	Area (in^2)	f_v (ksi)	Shear Strength (kips)	Anchor bolts & Steel type	Area	f_v (ksi)	Shear Strength (kips)
Clements	4* ϕ7/8" A325	4*.601 = 2.405	48	2.405*48= 115	2* ϕ1/2" A615 G60	2*1.767 =3.53	.4*F_u =.4*90	127
Alexander	4* ϕ7/8" A325	4*.601 = 2.405	48	2.405*48= 115	2* ϕ1/2" A615 G60	2*1.767 =3.53	.4*F_u =.4*90	127
Bridge-5	4* ϕ7/8" A325	4*.601 = 2.405	48	2.405*48= 115	2* ϕ1/2" G40	2*1.767 =3.53	.4*F_u =.4*70	99

Note:
The material of anchor bolts was assumed similar to the reinforcement.

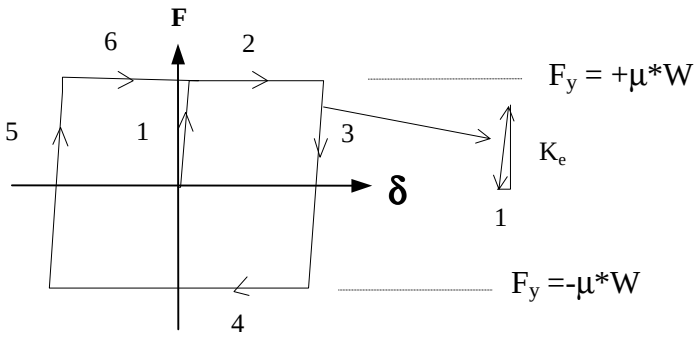

Figure 5-1 Bearings frictional hysteresis model

SECTION 6
COMPUTER MODELS

6-1) General

The bridges are analyzed using DRAIN-2DX [15] and DRAIN-3DX [16] computer programs, where beam-column elements are used to model the columns and simple connection elements are employed in modeling bearings and soil-structure springs. The link elements are use to model the gap and impact between adjacent spans and between an end-span and the abutment.

In this study a 5% damping is considered in the bridge models. This is consistent with AASHTO's response spectra and it is a commonly used value in time history analyses. This level of damping can be looked upon as radiation damping at the foundations. Since, there is no other source of viscous damping due to high rigidity of the deck cross-section. Note that, as mentioned before, energy dissipation due to nonlinear phenomena such as plasticity in the columns and friction at the bearings are modeled explicitly. It is assumed that the abutment back-wall is always in contact with the back-fill soil and contributes to the abutment stiffness. Abutment geometry, cap beam and deck widths are modeled with relatively rigid elements.

Several parameters are investigated for each bridge. These are types of soils (shear modulus of 400 psi, 4000 psi and 40,000 psi), backwall condition (intact and broken), bearing performance (intact and failed with two different coefficient of frictions equal to 0.2 and 0.6). Three earthquake records along with their orthogonal components, as described in section 6-3, are considered for the analyses. Following are the description of the 2-D and 3-D models of the bridges.

6-2) 2-D Models

Drain-2DX [15] was employed for modeling bridges in the longitudinal direction. For multi span simply supported (MSSS) bridges it is reported that longitudinal seismic response is more important [18]. Figures 6-1 to 6-3 show the analytical models and loadings for the bridge models. Table 6-1 presents the summary of soil spring stiffnesses at abutments and pier column bases for the studied bridges. For Clements Bridge because of symmetry with regard to center of the deck only half of the bridge was modeled. For Alexander Bridge, although unsymmetric, the dynamic characteristics of the segments are similar, and they are lumped together. Two-dimensional models are not able to represent the bridge skewness, for which one of the consequences is having a negligible axial force variation at pier columns from earthquake analyses. Cap beams and deck elements are assumed to remain elastic. A rigid-end-zone equal to the height of a bridge cap beam was placed at the top of pier columns. Rayleigh's damping proportional to both stiffness and mass matrices is used. The coefficients of proportionality are determined so that the damping matrix will correspond to 5% damping in the first and second modes. Under Peak Ground Acceleration (PGA) of 0.18g for each bridge, fifteen basic models as shown in Table 6-2 were analyzed under three different earthquake records (Parkfield, El-Centro and Nahanni). This results in a total of 135 computer runs. Additionally, for further investigation cases with PGA of 0.4g were also analyzed.

Following is a brief description of the DRAIN-2DX element types used to model bridges in longitudinal direction [15].

Beam-Column Element (Type 02)

This is a one-dimensional element that can be oriented arbitrarily in XY plane. Nonlinear behavior is limited to the concentric plastic hinges at the element ends. Plastic hinges are capable of considering P-M interaction curves for steel and reinforced concrete column sections. This element was used for modeling decks, piers and cap beams.

Simple Connection Element (Type 04)

This is a zero-length element that connects two coincident nodes. It has either rotational or translational stiffness. Element behavior is nonlinear with the ability to have elastic or inelastic unloading with or without gap. Complex behaviors can be obtained by placing two or more elements in parallel positions. Bearings, abutment back-fill soils (with inelastic unloading) and soil springs at the pier column footings were modeled by this element.

Link Element (Type 09)

The link element is a uniaxial element with finite length and arbitrary orientation. An element can be specified to act in tension (tension force and extension are positive) or in compression (compression force and shortening are positive). A tension element has finite stiffness in tension and goes slack in compression. A compression element has finite stiffness in compression and a gap opens in tension. This element was used between decks and also between an end-span and abutment for modeling the impact.

6-3) 3-D Models

DRAIN-3DX [16] is used for 3-D nonlinear time history analysis. Figures 6-4 and 6-5 show the analytical 3-D models for Clements Bridge and Bridge-5, respectively. Because of the lack of symmetry with regard to deck center (Figure 2-2b), a 3-D model of Alexander Bridge would require modeling two bridges along side each other with link elements in between and common abutments. Therefore, due to time limitations the 3-D analysis of this bridge was not performed. For Clements Bridge, similar to 2-D model, due to symmetry only half of the bridge is modeled. For major mode shapes in the three translational directions (i.e., longitudinal, transverse and vertical) corresponding mass proportional damping was assigned to the bridge models. For cap beams half of the gross moment of inertia (Ig) and torsional constant (J) are used to account for concrete cracking. However, for the composite decks due to the presence of steel girders, 75% of Ig for transverse bending and 75% of the torsional constant (J) are used. In vertical direction due to low amplitude response the gross moment of inertia is assumed for the composite deck sections. For major mode shapes 5% damping proportional to the mass

matrix is assumed (i.e., 5% damping for dominant modes in longitudinal, transverse and vertical directions).

A brief description of different element types that used in the 3-D models follows.

Fiber Hinge Beam-Column Element (Type 08)

This is an inelastic element for modeling steel, reinforced concrete or composite beam-columns. Three hinge types, namely P-M hinges, shear hinges, and connection hinges are available with this element type. Due to the aspect ratio of the bridge columns flexural mode is dominant, therefore only P-M plastic hinges were used. These are placed at the ends of the pier columns. The fiber arrangements and its property at each P-M hinge were defined such that the ultimate strength of the cross section is properly represented.

Elastic Beam-Column Element (Type 17)

This is a linear elastic beam-column element. This element is used to model decks, cap beams and abutments.

Simple connection element (type 04) and Compression/Tension link element (type 09)

This is the same as that described under 2-D model section.

As a part of the parametric study the following parameters and earthquake records were considered:

a) Post failure frictional coefficient μ was assumed to be equal to 0.2, 0.6 and infinity (i.e., no failure of the bearings)
b) Soil shear modulus was assumed to be equal to 0.4, 4 and 40 ksi.
c) Two earthquake records, Parkfield and El Centro, along with their orthogonal components were considered. These earthquake records are described in the following section.

d) Two alternative sets for each set of earthquake records are considered. Alternate 1 (alt-1) has component-1 in longitudinal direction and component-2 in transverse direction of the bridge, and Alternate 2 (alt-2) has reverse component arrangement.
e) Except for several specific cases, the strength and stiffens of the whole abutments are used.

6-4) Input Earthquake Motions

Two peak ground accelerations of 0.18g and 0.4g are considered. The former is the maximum acceleration coefficient in New Jersey per AASHTO. The latter is for higher seismicity regions such as California or can be considered as an event with a longer return period in New Jersey.

Two horizontal earthquake components were considered simultaneously to excite the 3-D models of the bridges in longitudinal and transverse directions. For each set of components two possible alternatives are considered. Alternative 1 (alt-1) refers to the earthquake record when component-1 is in the longitudinal direction and component-2 in the transverse direction of the bridge. Alternative 2 (alt-2) is the reverse of this. For 2-D models only the first component of the earthquake records, which is the strongest one of two, was considered. The following are earthquake records which after being scaled to PGA of 0.18g or 0.4g are used in analyzing the bridges:

Parkfield, California earthquake June 27, 1966

Component-1

N65E

Cholame, Shandon, California array N0. 2

PGA = -479.64 cm/sec^2 at 3.74 sec

Component-2

N05W

Cholame, Shandon, California array N0. 5

PGA = -347.82 cm/sec^2 at 7.40 sec

Imperial Valley earthquake May 18, 1940

Component-1

S00E

El Centro site Imperial Valley irrigation district

PGA = 341.70 cm/sec^2 at 2.12 sec

Component-2

S90W

El Centro site Imperial Valley irrigation district

PGA = 210.14 cm/sec^2 at 11.44 sec

Nahanni aftershock, Dec 23, 1985, Canada *(only used for 2-D models)*

Component-1

Site-2, Slide Mountain, Component 240

PGA=534.4 cm/sec^2

In the time history analyses only the first 10 seconds of the above records are used. Figure 6-6 presents the response spectrum of Parkfield and El Centro records (scaled to 0.18g) and AASHTO response spectrum for PGA of 0.18 and site coefficient (S) equal to 1.2. This site coefficient (S=1.2) is an average value based on the AASHTO specifications.

Table 6-1 Soil spring stiffness coefficients in 2-D computer models.

Clements Bridge

Abutments		**Piers**			
No. 1	**No. 2**	**No. 1**		**No. 2**	
Ka_1 (kips/in)	Ka_2 (kips/in)	Kh_1 (kips/in)	Kr_1 (kips-in/rad)	Kh_2 (kips/in)	Kr_2 (kips-in/rad)
½ *1,875*G Top portion: ½*1,228*G	½ *1,930*G Top portion: ½*1,228*G	1,012.6 *G	11,067,000*G	1,092.9 *G	18,643,000*G

Alexander Bridge

Abutments		**Pier**	
No. 1	**No. 2**		
Ka_1 (kips/in)	Ka_2 (kips/in)	Kh (kips/in)	Kr (kips-in/rad)
1,300*G Top portion: 1,595*G	1,432*G Top portion: 1,595*G	1,698*G	24,711,700*G

Bridge-5

Abutments		**Piers #1, #2 and #3**	
No. 1	**No. 2**		
Ka_1 (kips/in)	Ka_2 (kips/in)	Kh (kips/in)	Kr (kips-in/rad)
1,615*G Top portion: 785.4*G	1,150*G Top portion: 666.9*G	1,000*G	9,944,484*G

Note: G is in ksi.

Table 6-2 Different 2-D models with associated modeling parameters

Model No.	Description
1	At bearings μ=0.6, G-soil=.4 ksi, Damaged abutment
2	At bearings μ=0.6, G-soil=.4 ksi
3	At bearings μ=0.6, G-soil=4 ksi
4	At bearings μ=0.6, G-soil=40 ksi
5	At bearings μ=0.6, G-soil=40 ksi, Damaged abutment
6	At bearings μ=0.2, G-soil=.4 ksi, Damaged abutment
7	At bearings μ=0.2, G-soil=.4 ksi
8	At bearings μ=0.2, G-soil=4 ksi
9	At bearings μ=0.2, G-soil=40 ksi
10	At bearings μ=0.2, G-soil=40 ksi, Damaged abutment
11	Elastic bearings, G-soil=.4 ksi, Damaged abutment
12	Elastic bearings, G-soil=.4 ksi
13	Elastic bearings, G-soil=4 ksi
14	Elastic bearings, G-soil=40 ksi
15	Elastic bearings, G-soil=40 ksi, Damaged abutment

Notes:

1) μ is the coefficient of friction at failed bearings.
2) G-soil is soil shear modulus.
3) Damaged-abutment model is a case of shear failure at the juncture of back-wall and breast-wall (see Figure 3-7).

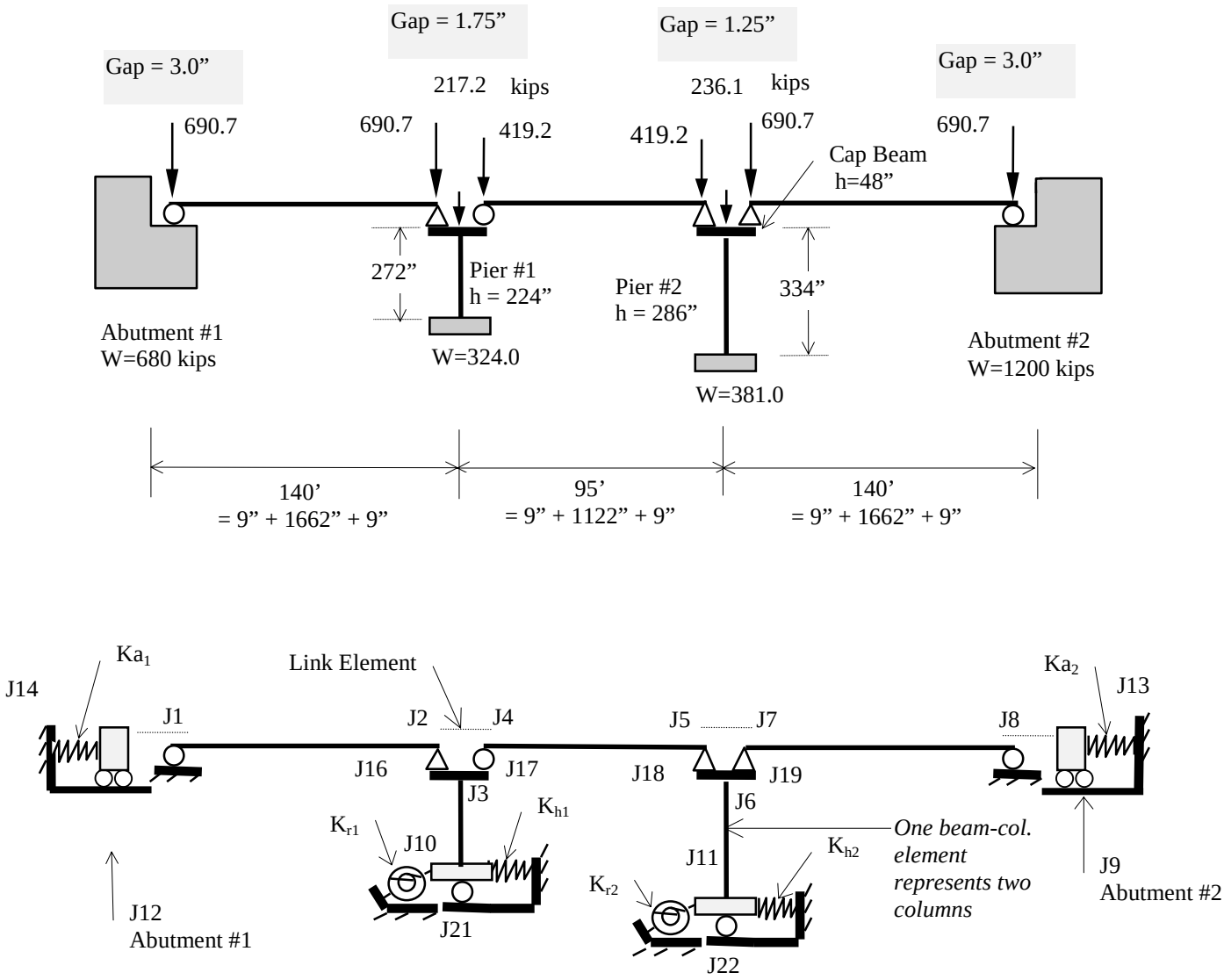

Figure 6-1 2-D computer model of Clements Bridge

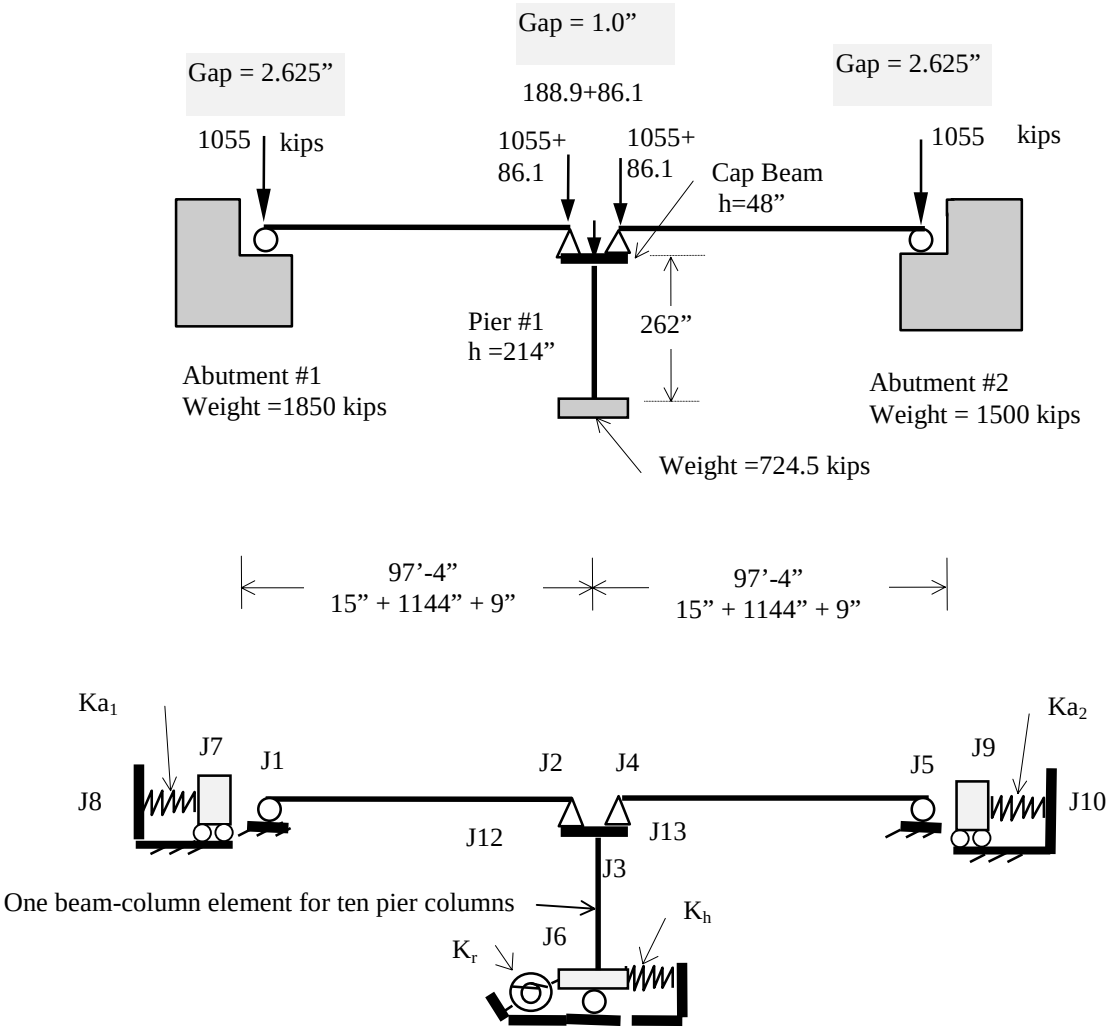

Figure 6-2 2-D computer model of Alexander Bridge

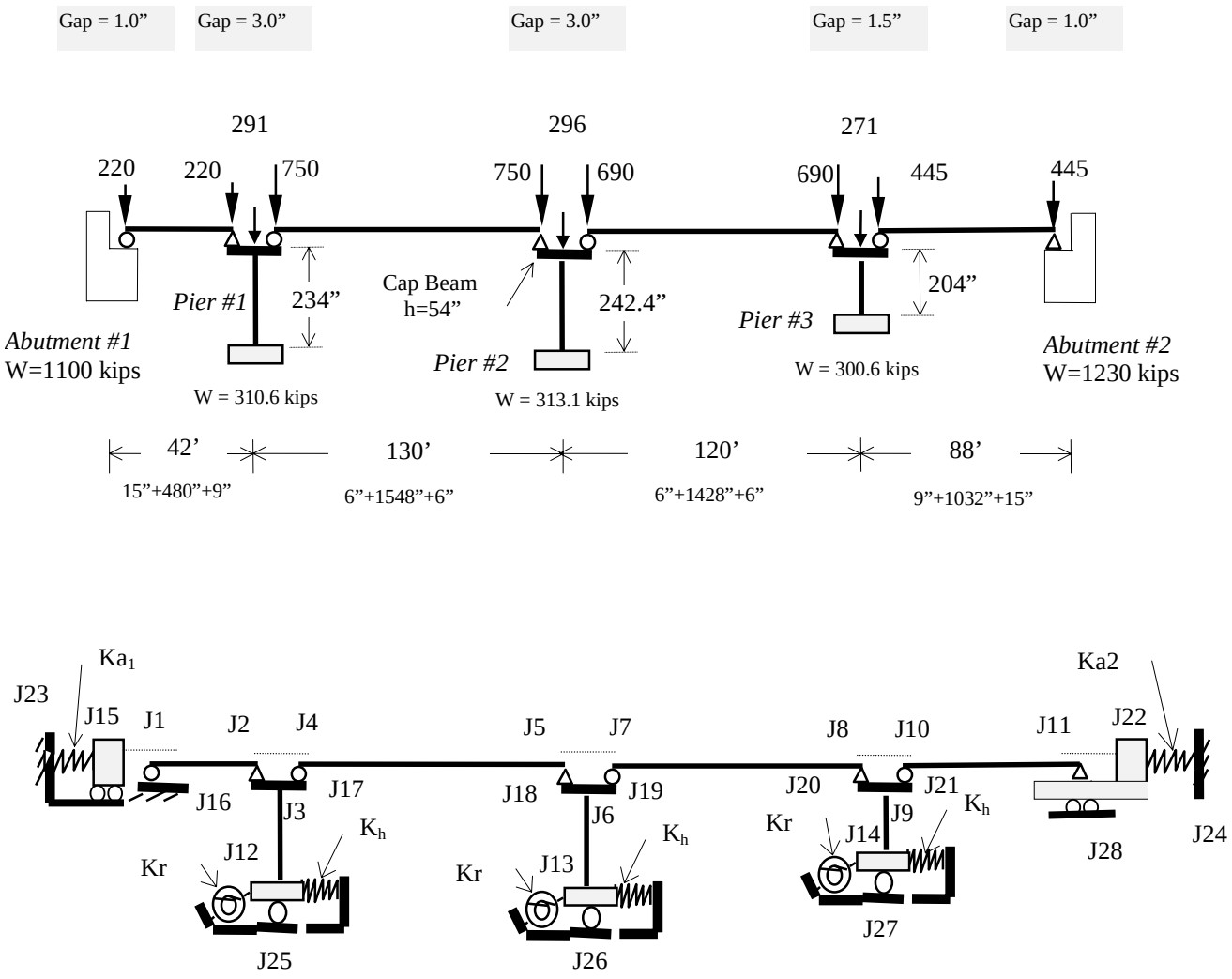

At each pier, five beam-column elements were used.
For col. type #1 the minimum flexural yield moment under the min. axial load at pier #3 is used as the yield limit at all pier locations.

Figure 6-3 The 2-D computer model of the Bridge-5

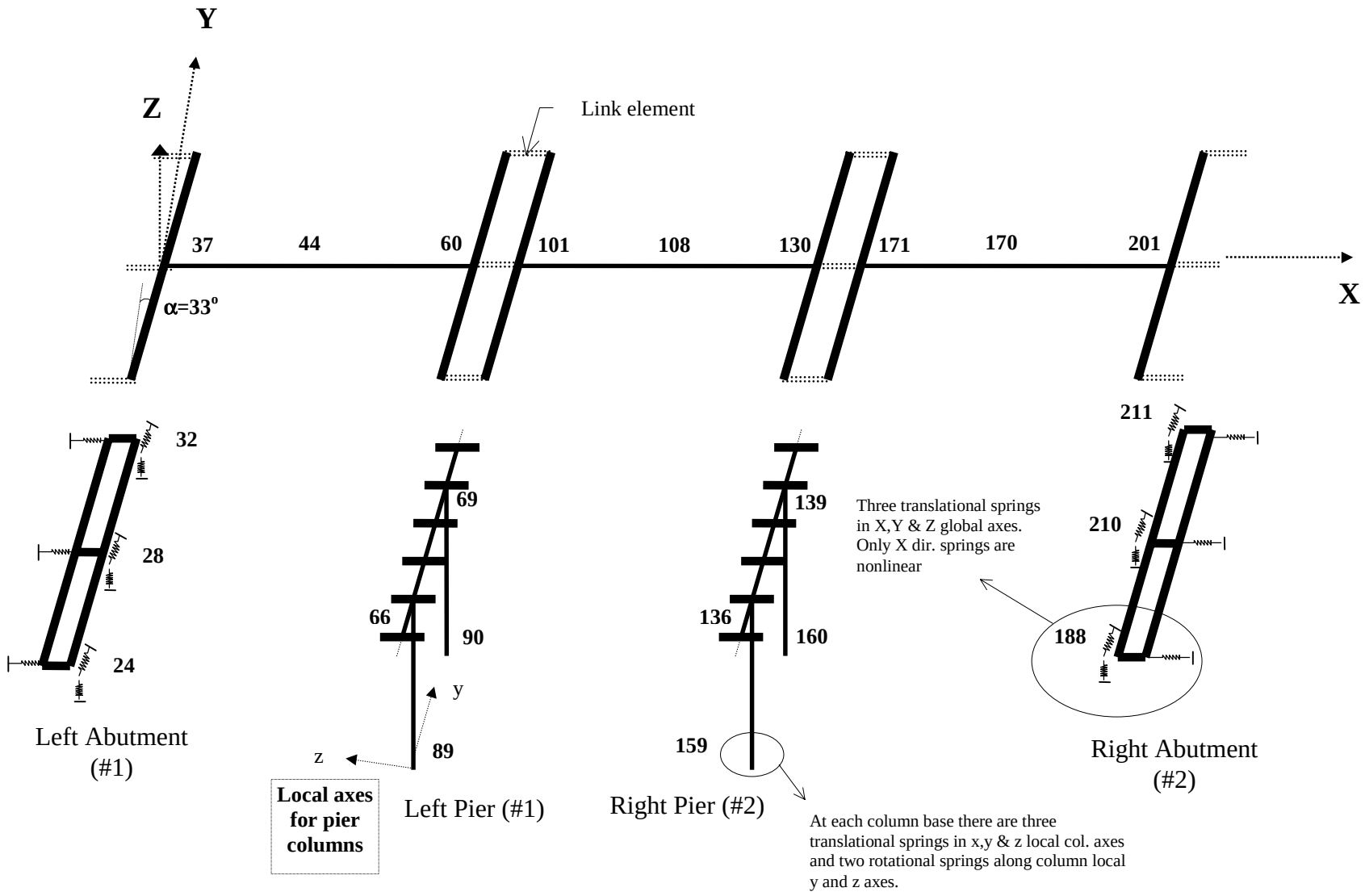

Figure 6-4 Clements Bridge 3-D model

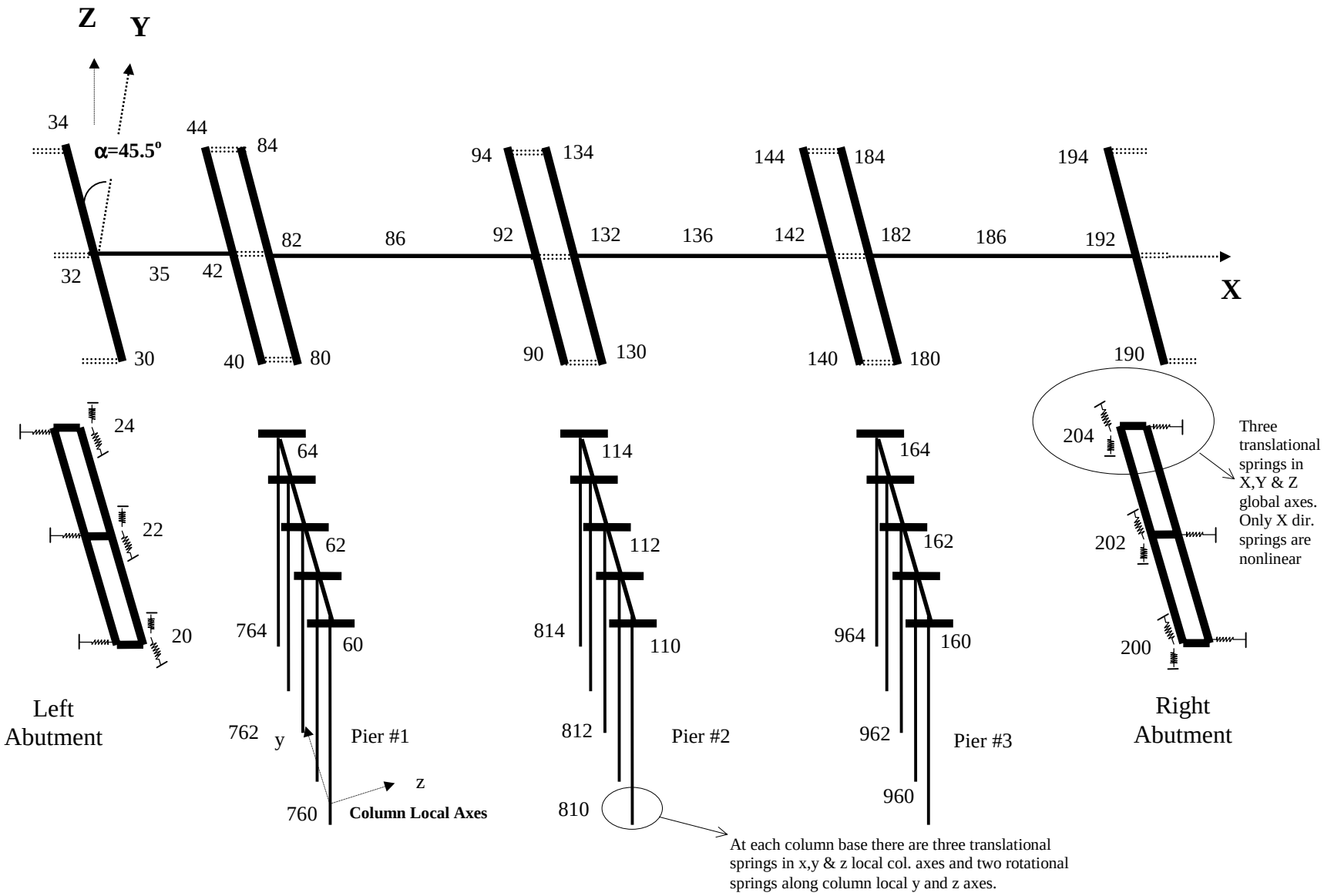

Figure 6-5 Bridge-5 3-D model

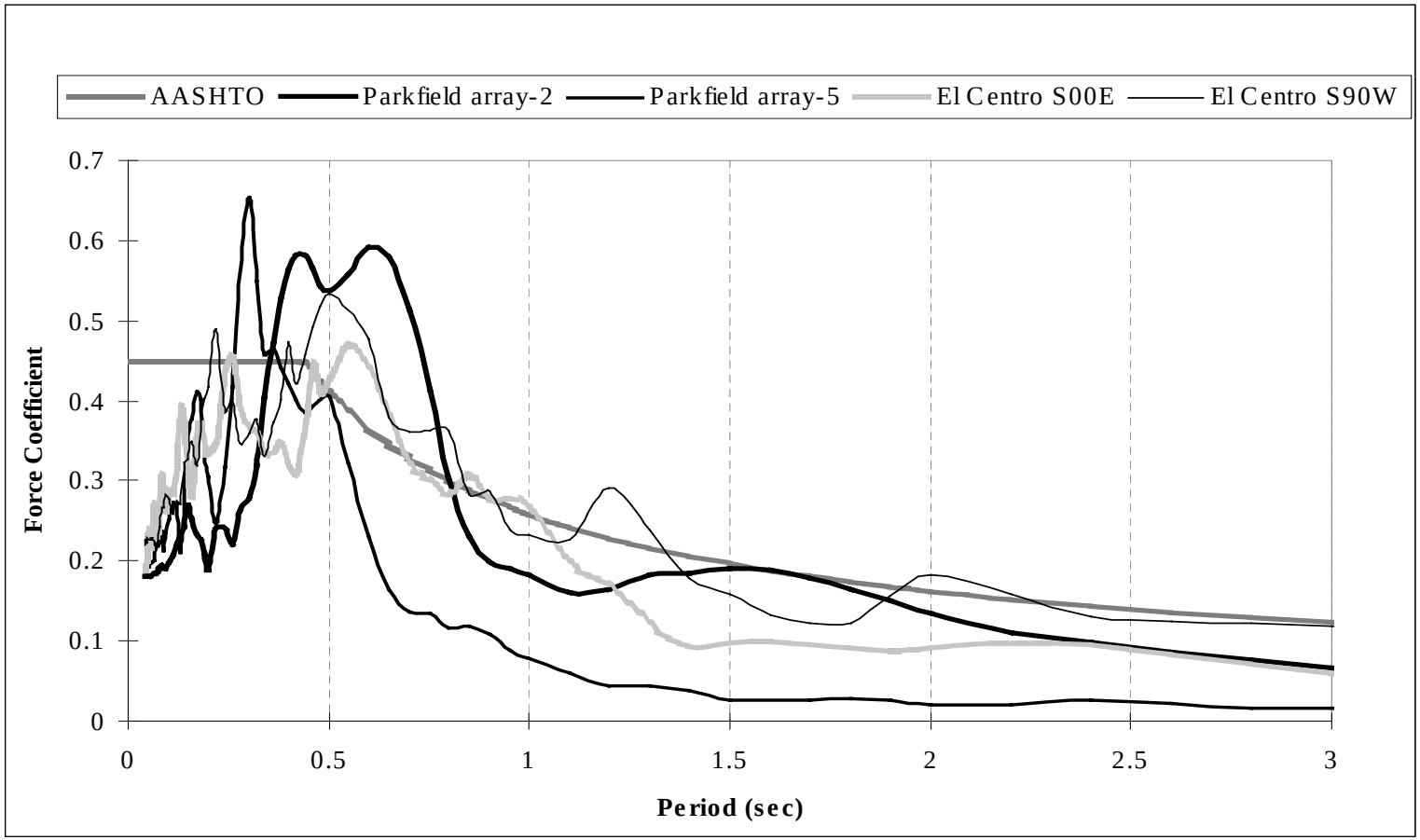

Figure 6-6 Response spectrum graphs (PGA=0.18g).

SECTION 7
RESULTS OF 2-D ANALYSES

7-1) General

In this section the results of the nonlinear time history analyses are presented. Primarily the PGA of 0.18g was considered in the bridge analyses and the effects of the higher PGA of 0.4g are investigated only for the Clements Bridge which had the poorest seismic response under 0.18g PGA. Also a nonlinear static analysis based on the AASHTO specifications is performed for the Clements Bridge and its nonlinear response characteristics, which can be generalized for other bridges, are explained by a simplified graphical approach. It should be noted that this method is commonly known as pushover analysis and is described first in the next sub-section.

7-2) Push-Over Analysis

Although push-over analysis was not among the initial objectives of this study, it is instructive to compare the relationship between the pseudostatic response and demand based on design guidelines. A graphically useful method for such comparison is to plot the push-over load-deformation behavior of the bridge along with AASHTO's response spectrum together. For the 2-D models this is done only for Clements Bridge, which has the poorest seismic response. This is shown in Figure 7-1 with AASHTO's response spectra for seismic coefficient equal to 0.18g and 0.4g and site coefficient (S) equal to 1.2 as an average value. It is assumed that stiffness is equal to load divided by displacement and then using the weight of the bridge the response spectrum is transferred from period vs. acceleration space to displacement vs. load. Thus, on this diagram, lines radiating from the origin will show systems with different periods (e.g., x-axis is a system with infinite period and y-axis a system with zero period). The load-deformation for the bridge is obtained by applying an increasing force at the level of the deck in the longitudinal direction. The load-deformation relationship, in general, is highly nonlinear and originally of a stiffening nature as the gaps close and other elements of the bridge system get involved. As seen from these curves, the stiffness and strength of the foundations

significantly influence the load-deformation behavior of the system. It appears that the abutment strength would have more effect on the seismic response of the system than the abutment stiffness and also more than the soil-structure interaction at the base of the columns. Shown in this figure is also the bridge response using CALTRANS approximate approach, where the maximum strength is based on the maximum soil strength of 7.7 ksf and stiffness is equal to 200 k/in per unit width of the deck.

Based on CALTRANS approach the displacement of the Clements Bridge in the longitudinal direction is limited due to high stiffness and strength at the abutment. Actually, using this method there is not much difference in the longitudinal deck displacement between the two seismic coefficients (0.18 and 0.4). There will be yielding in only one of the columns, in this case in the right pier columns since the push over analysis was initiated by pushing the span next to the right abutment towards the left abutment. Note that the maximum displacement is limited by the sum of the gap openings at the left pier and the left abutment plus deformation in the left abutment. In this example the maximum displacement is 4.75" plus the slight elastic deformation in the abutment. The abutment deformation is small due to high stiffness, and this is the reason for a minimal difference between seismic coefficient of 0.18 and 0.4. As seen from Figure 7-2, at this level of deformation (i.e., about 5") the plastic rotation in the columns of pier #2 (right pier) is well below the plastic rotation capacity.

Comparison of the design spectra to the load-deformation curves for the bridge where the soil-structure interaction is considered using the procedures outlined before, indicate that the bridge response will involve a significant nonlinear response at the abutments. As it can be seen from Figure 7-1, there is a significant difference between the effect of the two levels of motion. Similarly, bridges that may have failure in their abutment backwall will need a much large hystersis energy capacity and ductility demand at various components. Since the spectra are for 5% damping and linear system, the actual displacement demand can not be determined using the curves of Figure 7-1. This will require a time history analysis, which is described in the next section.

7-3) Results of the Nonlinear 2-D Time History Analyses

In this report first general observations for all three bridges under 0.18g PGA are described and along with that, the results of selected cases of Clements Bridge under 0.4g PGA are also presented. Then the response of each bridge is individually described.

General response of MSSS bridges

Among the three earthquake records used, almost always the Nahanni record caused the lowest response in all three bridges regardless of PGA and soil-structure interaction. Although, a similar conclusion can not be made about the other two records (both from California Earthquakes) responses were higher more often for the Parkfield record. This can be seen in Figures 7-3, 7-4 and 7-5, which show different responses of bridges under these earthquake records.

For an input motion with PGA of 0.18g the overall seismic response in the longitudinal direction is marginal with the lowest capacity / demand ratio (aside from bearing performance) of 1.04 for the seat length for Clements Bridge. Except for fixed bearings, other components of the bridges have enough capacity to withstand the demands under earthquakes with PGAs of 0.18g.

The level of impact force depends on the soil-type and abutment condition (intact vs. damaged backwall). When the abutment is assumed intact the impact forces are increasing as the soil stiffness decreases. In the case of damaged backwall the trend is reversed. For the same soil type there is less impact force in a damaged backwall case compared to an undamaged (or intact) abutment. These variations have to do with the relative value of the abutment stiffness with respect to its mobilized mass. Depending on these two parameters the amplitude of abutment response will change resulting in a different interaction with the bridge deck indicating the importance of modeling soil-structure interaction. The higher the input ground motion the more significant is the effect of soil-structure and abutments interaction on the response of the bridge.

Impact forces between two adjacent spans or between an end-span and the abutment are large enough to cause damage to the bridge in the form of bearing failure. Upon failure of the bearings the coefficient of friction has also an effect on the level of impact forces, where a higher coefficient of friction causes larger impact forces. This is probably due to the fact that under a lower coefficient of friction there is more energy dissipation through friction. Thus, the equal displacement concept does not necessarily hold.

Figure 7-6 shows various time histories of Clements Bridge for the Parkfield record with 0.4g peak ground acceleration. The time histories are for deck sliding at the right abutment for Clements Bridge for various SSI models. Note that the shear modulus, G, of 4 ksi is assumed to be, in an average sense, representative of typical fill and embankment soils used for bridges in New Jersey. Furthermore, the case of 0.4 ksi shear modulus is taken as the extreme lower end of the spectrum, and may not represent actual cases. The compressive strength of abutments with this type of soil is assumed equal to that for G = 4 ksi (proportional to frictional angle of 20 degree). However, the stiffnesses are different. This will enable comparison of results with respect to both strength and stiffness.

As it can be seen from Figure 7-6, for the case of the damaged backwall, deck displacement exceeds the seat length. The maximum horizontal deck displacements of Clements Bridge for different SSI models are given in Table 7-1. A lower strength for the case of damaged backwall, as it will be discussed later, is the main cause of higher deck displacements for all three soil types. However, comparison of two cases of G = 0.4 ksi and 4 ksi indicates that abutment stiffness also has an important effect (e.g., 7.3” vs. 9.7” or 33 percent increase) on the seismic response. Bridge displacement in the longitudinal direction is limited by abutment deformation and stiffer soils tend to act more like the fixed abutment.

The only difference between two cases of undamaged backwall and reduced compressive strength is in their strength. For the latter case the strength is reduced to that for a damaged abutment with G = 4 ksi. Comparison of these two curves indicates that

abutment strength has a more dominant effect on the response. Time histories of plastic rotation at the base of the columns in both Piers 1 and 2 of Clements Bridge are shown in Figure 7-7. Again, SSI plays a significant role on the ductility demand at the base of the columns. However, the trend is not directly proportional to soil property. Note that consideration of soil type and its interaction with the bridge includes boundary springs and masses at the base of the piers too. In general, bridges supported on softer soil will have larger displacements, mostly due to deformation of the abutment. For the same bridge deck displacement, flexibility at the base of the columns for softer soils will mean lower plastic rotation. Increasing the soil stiffness, one expects, should further increase the plastic rotation demand. But, as the results show, the plastic rotation demand at the base of the columns may even be less for stiffer soils (Table 7-2). This is due to a limiting effect of abutment for stiffer soils because of its higher strength and stiffness. This nonlinear effect on the substructures interaction with the superstructure causes the highest plastic rotation demands in the columns for moderately stiff soils and not in the stiffest soil. Once again demonstrating the need for explicit consideration to SSI. It should be mentioned that for lower PGAs where abutments are not significantly involved, the plastic rotation is higher for stiffer soils as expected.

The complete list of the maximum responses under PGA of 0.18g at critical locations are presented in the appendix I, but in the following sections a brief description of the analyses results for each bridge under PGA of 0.18g is given.

2-D Response of Clements Bridge Under PGA of 0.18g

The maximum displacements, plastic rotations and shear forces at selected locations are presented in Tables 7-3, 7-4, and 7-5, respectively. Table 7-6 presents minimum Capacity/Demand (C/D) ratios for different bridge components. As it is seen, the most critical C/D ratio belongs to the deck relative displacement over abutment #2, which for the softest considered soil (G = 0.4 ksi) under the Parkfield earthquake reaches a value of 1.04. Under the Parkfield earthquake the deck sliding C/D ratios for different models are also presented in Table 7-7 and as seen, this ratio ranges from 1.04 to 2.14 for different models.

Based on the results of different 2-D analyses of Clements Bridge, following are the observed nonlinear response behavior in longitudinal direction under 0.18g PGA.

1) The maximum demand for plastic rotation, shear and moment forces at the pier columns tends to decrease with softer soils. Figure 7-8 shows the shear time history of pier #1 for different soil shear moduli. As it appears from the graph, for very soft soil (G-soil = .4 ksi) the maximum shear response has decreased about 40% compared to the stiffer soils (G=40 and 4 ksi). Softer soil also causes a larger gap opening/closure and bridge longitudinal displacements. Figure 7-9 shows the gap width of abutment #2 for different soil stiffnesses and as seen, a larger gap opening/closure has occurred in very soft soils with G=0.4 ksi.
2) A lower frictional coefficient at failed bearings does not always result in a lower demand on the pier columns. This can be seen in Figure 7-10, which shows the shear time histories of pier #2 for different frictional coefficients at the bearings.
3) Impact forces are higher for softer soils.
4) Higher impact forces occur with higher frictional coefficients at failed bearings.
5) In most cases the impact force between abutment and the end-span deck is much higher than the shear capacity of the top portion of the abutments. This requires consideration of backwall failure in modeling the bridge.
6) Stiffer soil causes higher seismic demand in the abutments backfill soil.
7) At abutment #1 impact forces and the number of impacts are small. This abutment has almost no effect on the response of the bridge. At abutment #2, where the number and level of impact forces are higher, a larger frictional coefficient at failed bearings will cause higher abutment forces.
8) The influence of the abutment modeling parameters including mass, back fill soil stiffness and yield limits on the response of the bridge tends to decrease with stiffer soils. This observation can be seen by considering Figure 7-11, which shows the gap opening over abutment #2 for three different abutment models with two different soil conditions.

9) The influence of the abutment parameters on the rest of the bridge tends to decrease as the soil stiffness increases. This can be seen by comparing Figures 7-12a and 7-12b, which show the gap opening over abutment #2 for three different abutment models and two different soil types.
10) For points farther from abutments the effect of abutment modeling parameters tends to decrease. Figure 7-12 shows the time histories of pier#1 top displacement for different abutment conditions for a very soft soil (G=0.4 ksi), which a negligible effect from abutments can be seen.
11) Lower frictional coefficients at failed bearings cause higher deck sliding.

2-D Response of Alexander Bridge Under PGA of 0.18g

The maximum displacements, plastic rotations and shear forces at selected locations are presented in Tables 7-8, 7-9, and 7-10, respectively. Considering C/D ratios, the most critical values belong to deck relative displacement over the abutments. Table 7-11 presents C/D ratios for different bridge components. The most critical C/D ratio belongs to deck relative displacement over abutment #1, which for very soft soils (G = 0.4 ksi) reaches its minimum value of 1.1 under the Parkfield earthquake.

Based on the results of different 2-D analyses performed for Alexander Bridge, following are the observed nonlinear response behavior in longitudinal direction under 0.18g PGA.

1) Regarding the overall bridge response, softer soils cause larger displacements (Figure 7-13), larger gaps opening over the pier and abutments (Figure 7-14), less moment and shear force demands for pier columns, and more impact between the decks and also between the abutments and end spans.
2) No plastic rotation at pier columns has occurred and stiffer soils result in larger shear and moment demands.
3) A lower frictional coefficient at failed bearings does not always result in lower demand on pier columns. This can be seen in Figure 7-15, where it shows the shear time histories of the central pier for different frictional coefficients at failed bearings.
4) Impact forces are higher for softer soils.

5) Higher impact forces occur with higher frictional coefficients at failed bearings.
6) Stiffer soil causes higher seismic demand in the abutments.
7) The influence of the abutment modeling on the rest of the bridge tends to decrease as the soil stiffness increases. This can be seen by comparing Figures 7-16a and 7-16b, which show the gap opening over abutment #1 for three different abutment models and two different soil conditions.
8) As a 2-span bridge, abutments parameters show considerable influence on the overall bridge responses. Figure 7-17 shows the influence of different abutment models on the top displacement response of the pier. As it can be seen, the responses (amplitude and frequency contents) are considerably different for different abutment models.
9) A lower frictional coefficient at failed bearing along with stiffer soils cause higher sliding at fixed bearings (upon their failure).

2-D Response of Bridge-5 Under PGA of 0.18g

The maximum displacements, plastic rotations and shear forces at selected locations are presented in Tables 7-12, 7-13 and 7-14 respectively. Table 7-15 shows different C/D ratios for different bridge components. As it is seen, the most critical values belong to deck relative displacements. This ratio could be as low as 1.2 for very soft soils.

Based on the results of different 2-D analyses performed for Bridge-5, following are the observed nonlinear response behavior in longitudinal direction under 0.18g PGA.

1) Regarding the overall bridge response, softer soils cause larger displacements, larger gap opening/closure over piers and abutments (Figure 7-18), less force and plastic rotation demands for pier columns (Figure 7-19), and more impact between decks and also between abutments and the end spans.
2) A higher frictional coefficient at failed bearings causes larger plastic rotation (if there is any occurrence), shear, and moment demands at the base of pier columns. This can be seen in Figure 7-20, which shows the shear time histories of column type 3 at pier #1 for different frictional coefficients at failed bearings.

3) Abutment #1 with expansion bearing support has higher back fill soil force for stiffer soil. However, abutment #2, which has fixed bearing support, has higher back fill soil pressure for softer soil.
4) The influence of the abutment modeling parameters on the rest of the bridge tends to decrease for stiffer soils and for points farther from the abutments. Figure 7-21 shows the time histories of the top displacement of pier #2 for three different abutment models and two different soil types. As it appears from this figure, different abutment models have negligible influence on pier #2 (at center of the bridge). Figure 7-22 shows the top displacement time histories for pier #1 (adjacent to abutment #1), which is more affected by types of abutment models than pier #2.
5) Lower frictional coefficient at failed bearing causes higher sliding at fixed bearings (upon their failure).

7-4) Conclusions

Based on a comprehensive study on three actual multi-span simply supported bridges the following conclusions can be made with regard to their 2-D seismic response in the longitudinal direction:

- Seismic response of MSSS bridges is complicated by the impact between adjacent spans,
- Generally the impact reduces displacements, however, it significantly increases the level of forces in the bearings,
- Due to impact forces, bearing failure and backwall damage are quite possible even under low levels of peak ground accelerations,
- Except for fixed bearings failure and marginal C/D ratios for deck sliding in very soft soils, other components of the bridges have enough capacity to withstand the demands of earthquakes with PGA of 0.18g. Thus, it is unlikely for an earthquake with 0.18g PGA to cause bridge collapse. This is the maximum acceleration coefficient for New Jersey required by AASHTO specifications,

- Plastic rotation demand is affected by soil-structure interaction. Under earthquakes strong enough to involve free standing abutments in the bridge dynamic response (here, PGA 0.4g), the demand is higher for medium soil than softer or stiffer soils. For low intensity earthquakes (here, PGA 0.18g) this demand is less for softer soils,
- Abutment strength has more effect on longitudinal seismic response than stiffness and mass,
- Soil-structure interaction has a detrimental effect on seismic response in the longitudinal direction and dynamic analysis of this class of bridge system should explicitly consider the SSI.

As specifications go more toward performance based seismic design of structural systems, including bridges, it is important to develop a realistic response spectrum that reflect the actual level of equivalent damping. To this end, in order to be able to quantify the effect of soil-structure interaction in a “design” format, consideration should be given to detailed study of nonlinear systems with stiffening load-deformation characteristics.

Table 7-1 Clements Bridge maximum deck displacements for different SSI models. (2-D model, Parkfield record, PGA=0.4g)

Abutment Model	**G-soil (ksi)**		
	0.4	**4.0**	**40**
Intact	9.7”	7.3”	6.7”
Damaged	13.5”	10.8”	9.4”

Table 7-2 Clements Bridge pier column plastic rotation (rad) for different SSI models. (2-D model, Parkfield record, PGA=0.4g)

Abutment Model	**G-soil (ksi)**		
	0.4	**4.0**	**40**
Intact	0.00	0.015	0.014
Damaged	0.015	0.021	0.016

Table 7-3 Clements Bridge maximum displacements (2-D model, PGA=0.18g)

Location	Displacement (inch)	Model Description
Top of pier #1	4.63	G=.4 ksi, Elastic bearings, PF EQ
	-4.42	G=0.4 ksi, μ=0.6 or elastic bearings, PF EQ, Damaged-abut.
Top of pier #2	5.00	G=0.4 ksi, μ=0.2, PF EQ, Damaged-abut.
	-6.16	G=.4 ksi, μ=.6, EC EQ
Gap width over pier #1	+.0045	G=.4 ksi, Elastic bearings, PF EQ
	-6.75	G=0.4 ksi, μ=0.6, PF EQ, Damaged-abut.
Gap width over pier #2	+.0025	G=.4 ksi, μ=.6 , EC EQ
	-1.27	G=.4 ksi, Elastic bearings, EC EQ
Gap width over abut. #1	+.0061	G=.4 ksi, Elastic bearings, PF EQ
	-8.21	
Gap width over abut. #2	+.0067	G=.4 ksi, μ=.6 , PF EQ
	-10.70	G=.4 ksi, μ=.2 , PF EQ
Abutment #1	+1.00	G=.4 ksi, Elastic bearings, EC EQ
	-1.43	G=0.4 ksi, μ=.6 or elastic bearings, PF EQ, Damaged-abut.
Abutment #2	+1.69	G=.4 ksi, μ=.2, .6 & Elastic bearings, PF EQ
	-2.00	

Notes:

1) PF=Parkfield, EC= El-Centro
2) Positive gap width is for gap closure.

Table 7-4 Clements Bridge maximum plastic rotation demand at the base of pier columns. (2-D model, PGA=0.18g)

Location	Plastic Rotation (rad)	2-D Model Description
Base of pier #1	+0.00287 -0.0	G=40 ksi, Elastic bearings, PF EQ, Whole or Damaged abut. All models
Base of pier #2	+0.00480 -0.00264	G=40 ksi, μ =.2 , PF EQ G=40 ksi, μ = .2 , PF EQ, Whole or Damaged abut.

Note: PF=Parkfield

Table 7-5 Clements Bridge maximum shear force at pier columns (2-D model, PGA=0.18g)

Location	Shear Force (kips)	2D Model Description
Column of pier #1	238.3/2 = 119.2	G=40 ksi, Elastic bearings, PF EQ, Whole or Damaged abut.
Column of pier #2	194.1/2 = 97.1	G=40 ksi, μ = .2 , PF EQ, Whole or Damaged abut.

Note: PF=Parkfield

Table 7-6 Clements Bridge minimum Capacity/Demand ratios
(2-D model, PGA=0.18g)

Response	Demand	Capacity	C/D Ratio
Plastic Rotation, θ_p (rad) at the base of pier #1 at the base of pier #2	 0.00287 0.00264	 0.015 0.0173	 5.2 6.6
Curvature Ductility , $\mu_\phi = \phi_u/\phi_y = 1+\phi_p/\phi_y$ (1 / inch) at the base of pier #1 at the base of pier #2	 1 + .00009/.00008 = 2.12 1 + .000072/.00008 = 1.90	 .00055/.00008 = 6.88 .00055/.00008 = 6.88	 3.2 3.6
Shear (kips) at the base of pier #1 at the base of pier #2	 238.3/2 = 119.2 194.1/2 = 97.1	 315-.12*91=304 315	 2.6 3.2
Deck Relative Displacement (inch) over pier #1 over pier #2 over abutment #1 over abutment #2	 (6.75-1.75) ±1.02= 5 ±1.02 1.27 8.21-3 = 5.21 10.70-3 = 7.70	 10 10 8 8	 2.5-1.7 7.9 1.5 1.04

Notes:

1) Deck relative displacement is obtained from link element deformation.
2) C/D ratio of the deck relative displacement over pier #1 is given in a range. This range is calculated by considering the fixed bearing maximum displacement and gap opening over the pier.
3) The maximum fixed bearing displacements are equal to 1.02” and 1.27” at pier #1 and pier #2, respectively.

Table 7-7 Clements Bridge Capacity/Demand ratios for deck relative displacement over abutment #2 under Parkfield earthquake. (2-D model, PGA=0.18g.)

2-D Model Description	Demand	Capacity/Demand
At bearings μ=0.6, G-soil=.4 ksi, Damaged abutment	8.52-3 = 5.52	8/5.52=1.45
At bearings μ=0.6, G-soil=.4 ksi	10.54-3 = 7.54	1.06
At bearings μ=0.6, G-soil=4 ksi	7.51-3 = 4.51	1.77
At bearings μ=0.6, G-soil=40 ksi	7.04-3 = 4.04	1.98
At bearings μ=0.6, G-soil=40 ksi, Damaged abutment	7.04-3 = 4.04	1.98
At bearings μ=0.2, G-soil=.4 ksi, Damaged abutment	8.78-3 = 5.78	1.38
At bearings μ=0.2, G-soil=.4 ksi	10.70-3 = 7.70	1.04
At bearings μ=0.2, G-soil=4 ksi	8.13-3 = 5.13	1.56
At bearings μ=0.2, G-soil=40 ksi	7.96-3 = 4.96	1.61
At bearings μ=0.2, G-soil=40 ksi, Damaged abutment	7.96-3 = 4.96	1.61
Elastic bearings, G-soil=.4 ksi, Damaged abutment	8.49-3 = 5.49	1.46
Elastic bearings, G-soil=.4 ksi	9.71-3 = 6.71	1.19
Elastic bearings, G-soil=4 ksi	7.29-3 = 4.29	1.86
Elastic bearings, G-soil=40 ksi	6.74-3 = 3.74	2.14
Elastic bearings, G-soil=40 ksi, Damaged abutment	6.74-3 = 3.74	2.14

Table 7-8 Alexander Bridge maximum displacements (2-D model, PGA=0.18g)

Location	Displacement (inch)	2-D Model Description
Top of pier #1	4.73	G=.4 ksi, μ=.6, PF EQ, Damaged-abut.
	-4.69	G=.4 ksi, Elastic bearings, PF EQ, Damaged abutment
Gap width over pier #1	+.0042	G=4 ksi, μ=.6 at Bearings, PF EQ
	-1.011	G=.4 ksi, Elastic bearings, PF EQ
Gap width over abut. #1	+.0082	G=.4 ksi, μ=.6 at Bearings, EC EQ
	-8.90	G=.4 ksi, μ=.6, PF EQ, Damaged-abut.
Gap width over abut. #2	+.0129	G=.4 ksi, Elastic bearings, PF EQ
	-7.95	G=.4 ksi, μ=.2, PF EQ, Damaged-abut.
Abutment #1	+2.51	G=.4 ksi, Elastic bearings, PF EQ
	-2.06	G=.4 ksi, Elastic bearings, PF EQ, Damaged abutment
Abutment #2	+2.47	G=.4 ksi, μ=.6 at Bearings, PF EQ
	-2.09	G=.4 ksi, μ=.6, PF EQ, Damaged abutment

Notes:

1) PF = Parkfield, EC = El-Centro
2) Positive gap width is for gap closure.

Table 7-9 Alexander Bridge maximum plastic rotation demand at the base of pier columns (2-D model, PGA=0.18g)

Location	Plastic Rotation (rad)	2-D Model Description
Base of pier #1	0.0	All Models

Table 7-10 Alexander Bridge maximum shear force demand at the pier columns (2-D model, PGA=0.18g)

Location	Shear Force (kips)	2-D Model Description
Column of pier #1	652.0/10=65.2	G=4 ksi, μ=.6 at bearings, PF EQ

Note: PF = Parkfield

Table 7-11 Alexander Bridge Capacity/Demand ratios
(2-D model, PGA=0.18g)

Response	Demand	Capacity	C/D Ratio
Plastic Rotation, θ_p (rad) at the base of the pier	0.00	0.126	No Demand
Curvature Ductility **$\mu_\phi = \phi_u/\phi_y = 1+\phi_p/\phi_y$** (1 / inch) at the base of the pier	~1	.0045/.0001=45	45
Shear (kips) at the base of the pier	65.2	442.1	6.8
Deck Relative Displacement (inch) over the pier over abutment #1 over abutment #2	2.64 8.896-2.625=6.3 7.952-2.625=5.3	7 7 7	2.7 1.1 1.3

Notes:

1) At abutments the deck relative displacement is obtained from the link deformation.
2) The maximum fixed bearing displacement over the pier is equal to 2.64".

Table 7-12 Bridge-5 maximum displacements
(2-D model, PGA=0.18g)

Location	Displacement (inch)	2-D Model Description
Top of pier #1	+2.93	G=.4 ksi, μ=.6 at Bearings, PF EQ
	-1.96	G=.4 ksi, μ=.2 , EC EQ
Top of pier #2	+4.82	G=.4 ksi, Elastic bearings, PF EQ, Damaged abutment
	-4.15	G=.4 ksi, μ=.2 , PF EQ, Damaged abutment
Top of pier #3	+3.53	G=.4 ksi, Elastic bearings, PF EQ
	-3.37	
Gap width over pier #1	+.0035	G=.4 ksi, Elastic bearings, PF EQ, Damaged abutment
	-7.42	G=.4 ksi, μ=.6 , PF EQ, Damaged abutment
Gap width pier #2	+.0084	G=.4 ksi, Elastic bearings, PF EQ
	-6.51	G=.4 ksi, Elastic bearings, EC EQ.
Gap width over pier #3	+.0056	G=.4 ksi, Elastic bearings, PF EQ
	-6.23	
Gap width over abut. #1	+.0049	G=.4 ksi, Elastic bearings, PF EQ
	-4.82	G=.4 ksi, μ=.2 , PF EQ.
Gap width over abut. #2	+.0075	G=.4 ksi, μ=.6 , PF EQ
	-6.82	G=.4 ksi, μ=.2 , PF EQ.
Abutment #1	+.72	G=.4 ksi, μ=.6 , EC EQ
	-1.12	G=.4 ksi, μ=.2 , PF EQ.
Abutment #2	+3.59	G=.4 ksi, μ=.2 , PF EQ, Damaged-abut.
	-3.06	G=.4 ksi, Elastic bearings, PF EQ.

Notes:

1) PF = Parkfield, EC = El-Centro
3) Positive gap width is for gap closure.

Table 7-13 Bridge-5 maximum pier column plastic rotation
(2-D model, PGA=0.18g)

Location	Plastic Rotation (rad)	2-D Model Description
Base of pier #1	col. Type 1 +.00015	G=40 ksi, Elastic bearings, EC EQ, Damaged-abut.
	-0.0	All Models
	col. Type 3 +0.0 -0.0	All Models
Base of pier #2	col. Type 1 +.0012	G=4 ksi, μ=.6, EC EQ.
	-0.0017	G=40 ksi, Elastic bearings, EC EQ, Damaged-abut.
	col. Type 2 +0.0017	G=4 ksi, μ=.6, EC EQ.
	-0.0022	G=40 ksi, Elastic bearings, EC EQ, Damaged-abut.
Base of pier #3	col. Type 1 +.0011	G=40 ksi, Elastic bearings, EC EQ, Damaged-abut.
	-0.0038	G=40 ksi, μ=.6 , PF EQ, Damaged-abut.
	col. Type 4 +0.0017	G=40 ksi, Elastic bearings, EC EQ, Damaged-abut.
	-0.0044	G=40 ksi, μ=.6 , PF EQ, Damaged-abut.

Note:
PF = Parkfield, EC = El-Centro

Table 7-14 Bridge-5 maximum pier column shear force.
(2-D model, PGA=0.18g)

Location	Shear Force (kips)	2-D Model Description
Columns of pier #1	col. Type 1 54.8 col. Type 3 72.6	G=40 ksi, Elastic bearings, EC EQ, Whole or Damaged abutment. G=40 ksi, Elastic bearings, EC EQ, Damaged-abut.
Columns of pier #2	col. Type 1 78.8 col. Type 2 58.0	G=40 ksi, μ=.6 , EC EQ, Whole or Damaged abutment. G=40 ksi, μ=.6 , EC EQ.
Columns of pier #3	col. Type 1 124.0 col. Type 4 71.7	G=40 ksi, Elastic bearings, PF EQ, Damaged-abut. G=40 ksi, μ=.6 , PF EQ, Damaged-abut.

Table 7-15 Bridge-5 Capacity/Demand ratios (2-D model, PGA=0.18g).

Response	Demand	Capacity	C/D Ratio
Plastic Rotation, θ_p (rad)			
at the base of pier #1			
col. type-1	0.000152	0.124	815.8
col. type-3	0.00	0.124	ND
at the base of pier #2			
col. type-1	0.00220	0.124	56.4
col. type-2	0.00167	0.124	74.3
at the base of pier #3			
col. type-1	0.00441	0.098	22.2
col. type-4	0.00382	0.098	25.7
Curvature Ductility $\mu_\phi = \phi_u/\phi_y = 1+\phi_p/\phi_y$ (1 / inch)			
at the base of pier #1			
col. type-1	1+ .0000048/.00006=1.08	.004/.00006=66.7	61.8
col. type-3	~1	66.7	66.7
at the base of pier #2			
col. type-1	1+.00007/.00006=2.16	66.7	30.9
col. type-2	1+.000053/.00006=1.88	66.7	35.5
at the base of pier #3			
col. type-1	1+.000178/.00006=3.96	66.7	16.8
col. type-4	1+.000154/.00006=3.57	66.7	18.7
Shear (kips)			
at the base of pier #1			
col. type-1			
col. type-3	72.6	421.8	5.8
at the base of pier #2	54.8	421.8	7.7
col. type-1			
col. type-2	78.8	421.8-.16*69.8=410.6	5.2
at the base of pier #3	58.0	421.8	7.3
col. type-1			
col. type-4	124.0	421.8-1.96*69.8=285.0	2.3
	71.7	421.8-1.57*69.8=312.2	4.4
Deck Relative Displacement (inch)			
over pier #1	3.47 to (7.42-3) + 3.47=7.42	9.3	2.7 - 1.3
over pier #2	(6.51-3) ± 1.32=3.51 ± 1.32	9.5	4.3 - 2.0
over pier #3	3.59 to (6.23-1.5) + 3.59 = 8.3	10.2	2.8 - 1.2
over abutment #1	4.82-1=3.82	9.3	2.4
over abutment #2	6.82-1=5.82	9.3	1.6

Notes:

1) At abutments and piers the deck relative displacements are obtained from link element deformation.
2) Capacity/Demand ratios for the deck relative displacements of piers are given in a range. This range is calculated by considering the fixed bearing maximum displacement and gap opening over the piers.
3) The maximum displacements at fixed bearings are 3.47" at pier#1, 1.32" at pier #2, and 3.59" at pier#3.
4) ND = No Demand

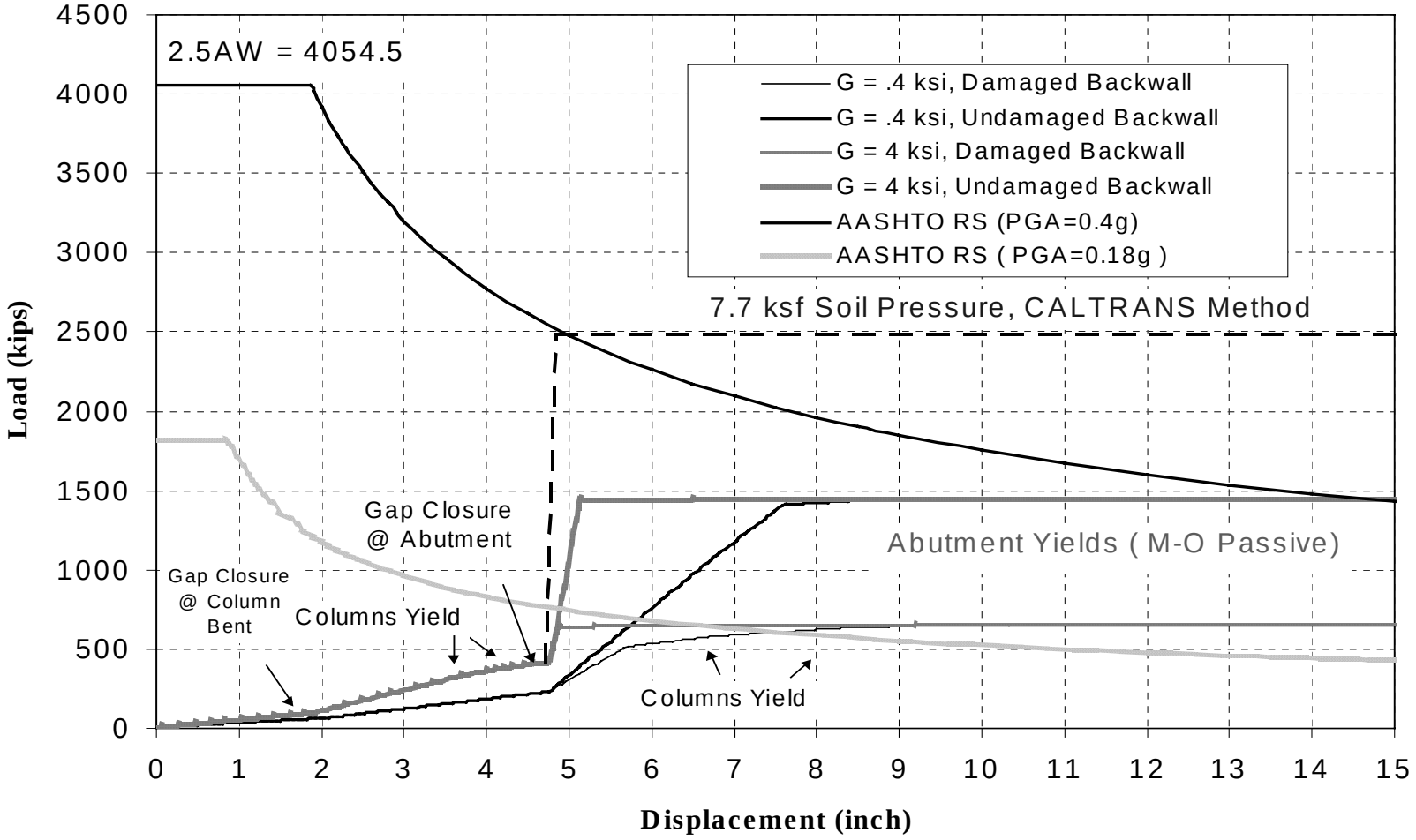

Figure 7-1 Pushover analysis of Clements Bridge (2-D model)

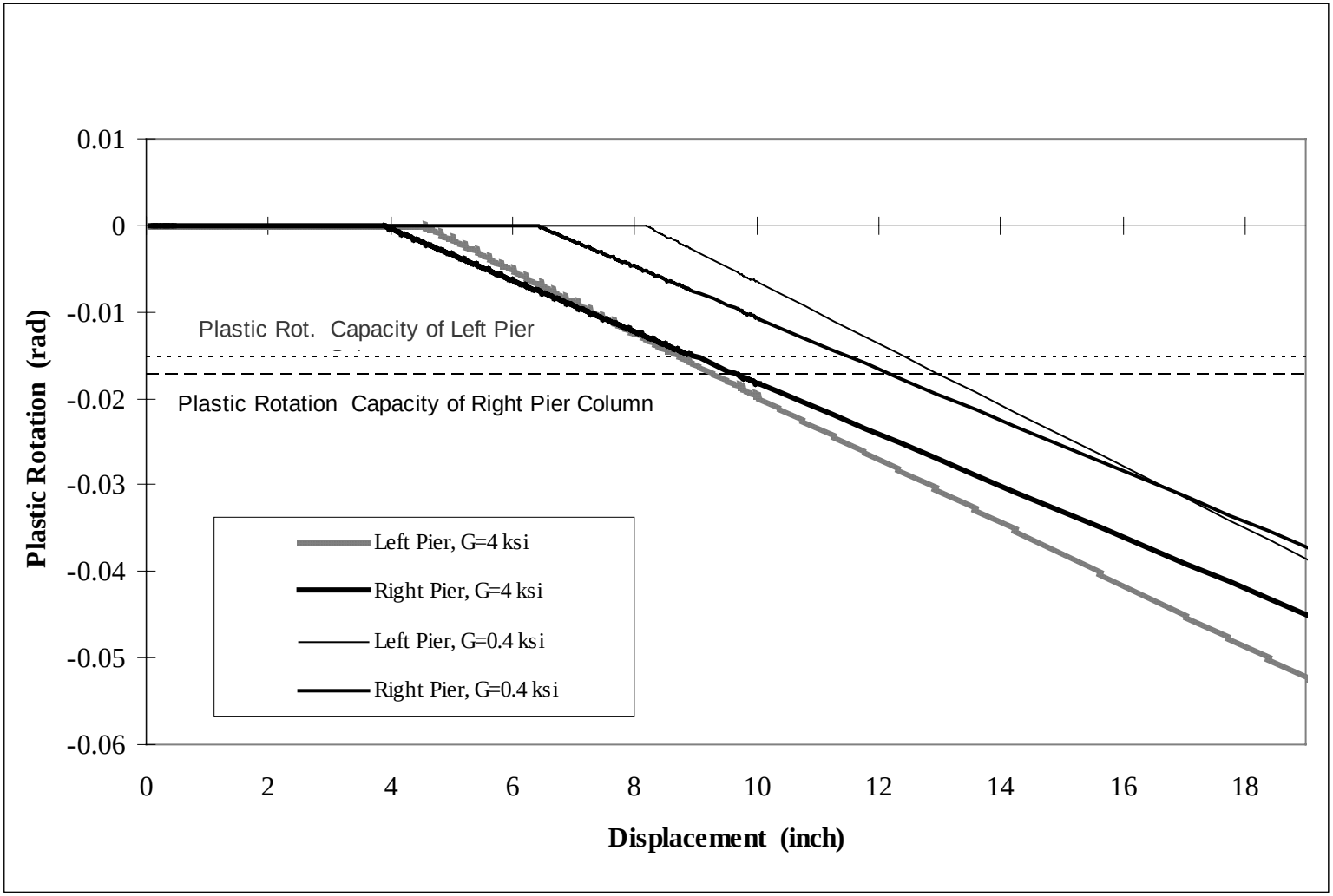

Figure 7-2 Plastic rotation at the base of Clements Bridge pier columns from 2-D pushover analysis.

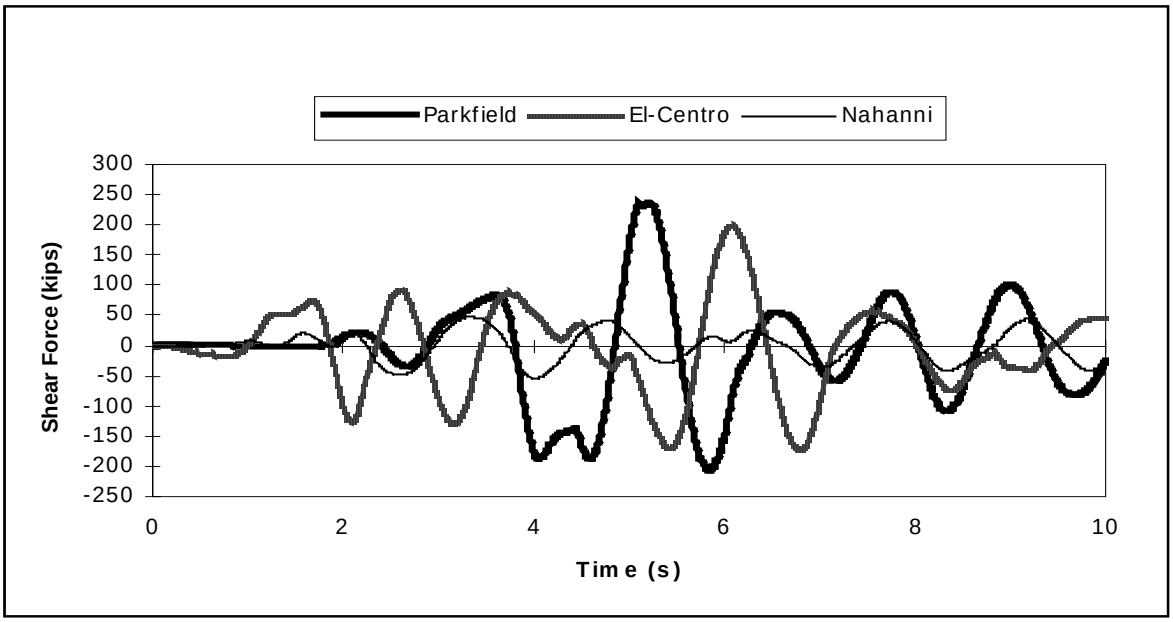

Figure 7-3 Clements Bridge shear force time histories of Pier #1 columns (2 columns) for three earthquake records with PGA of 0.18g (2-D model, μ=0.6 at bearings, Gsoil=4 ksi).

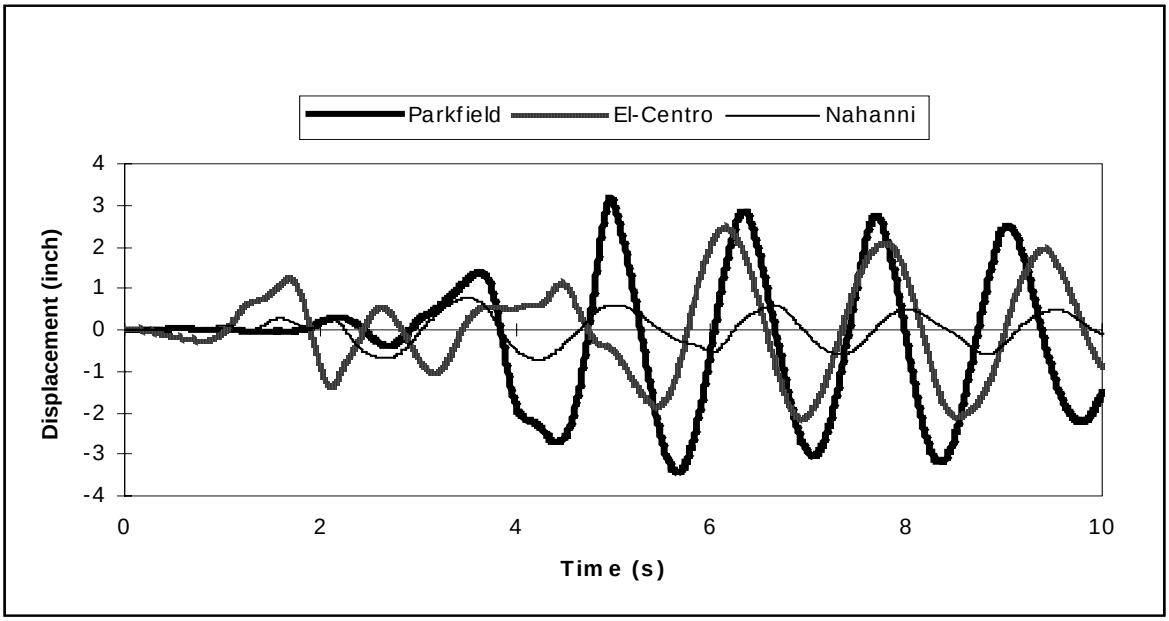

Figure 7-4 Alexander Bridge pier top displacement time histories for three earthquake records with PGA of 0.18g (2-D model, μ=0.6 at bearings, G-soil=4 ksi).

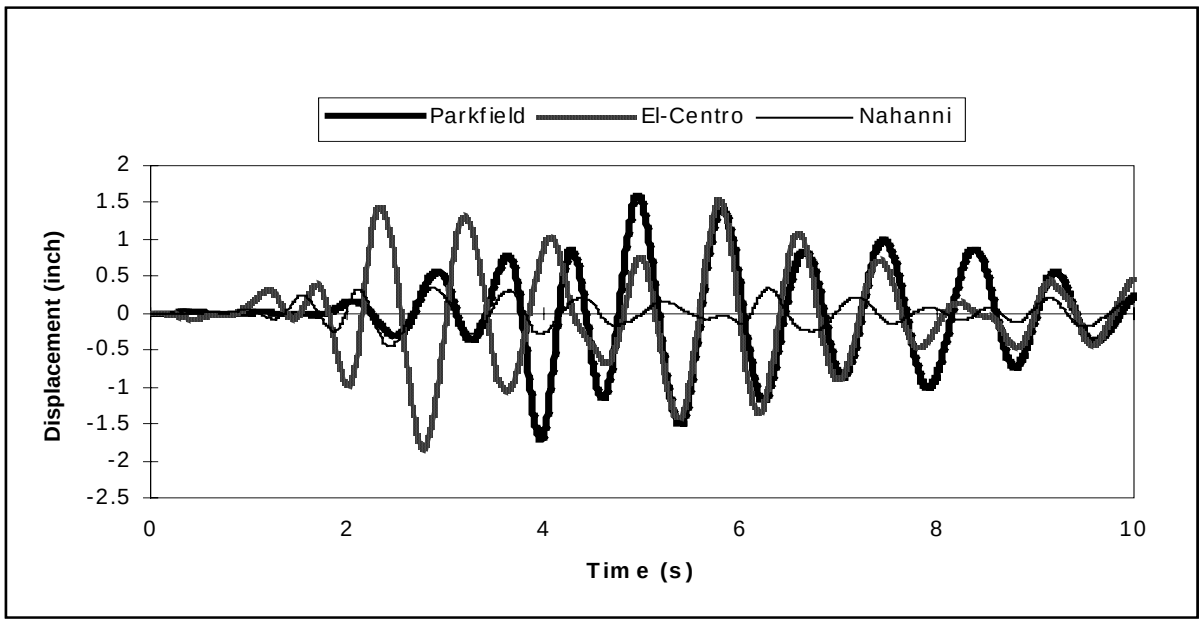

Figure 7-5 Bridge-5 top displacement time histories of Pier#3 for three earthquake records with PGA of 0.18g (2-D model, μ=0.6 at bearings, G-soil=4 ksi).

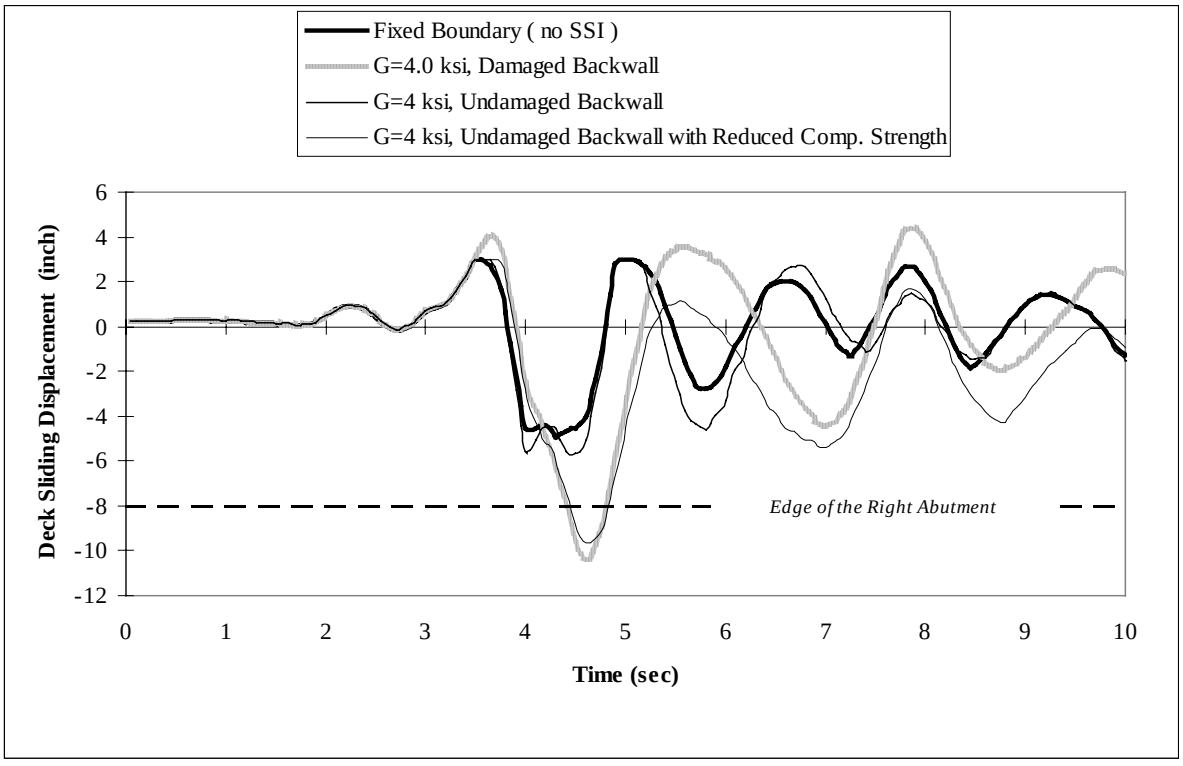

Figure 7-6 Time histories of deck sliding at Clements Bridge abut. #2 for various SSI models under Parkfield record scaled to 0.4g PGA
(2-D model, elastic bearings)

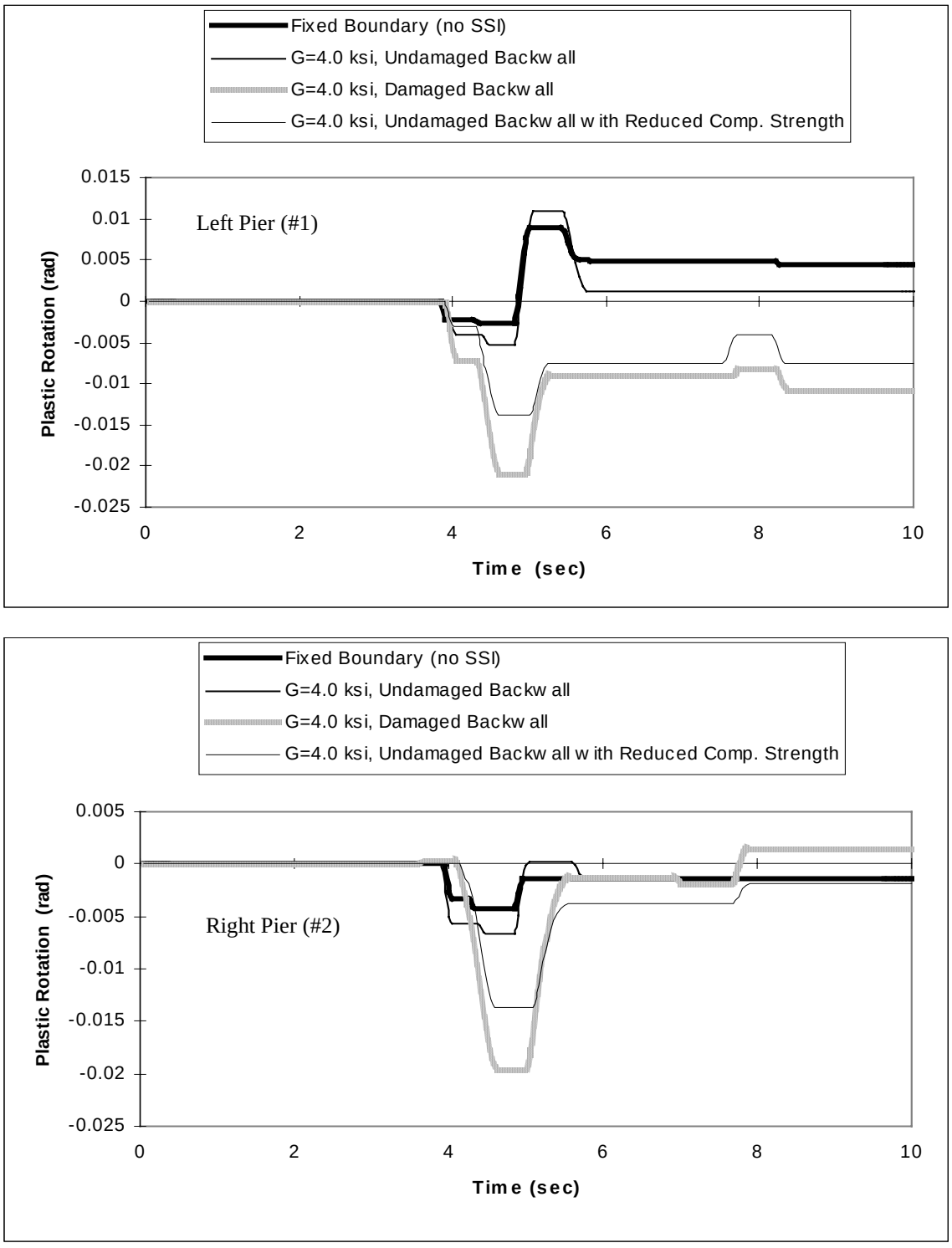

Figure 7-7 Time histories of plastic rotation at the base of pier columns in Clements Bridge abutment for various SSI models under Parkfield record scaled to 0.4g PGA (2-D model, elastic bearings)

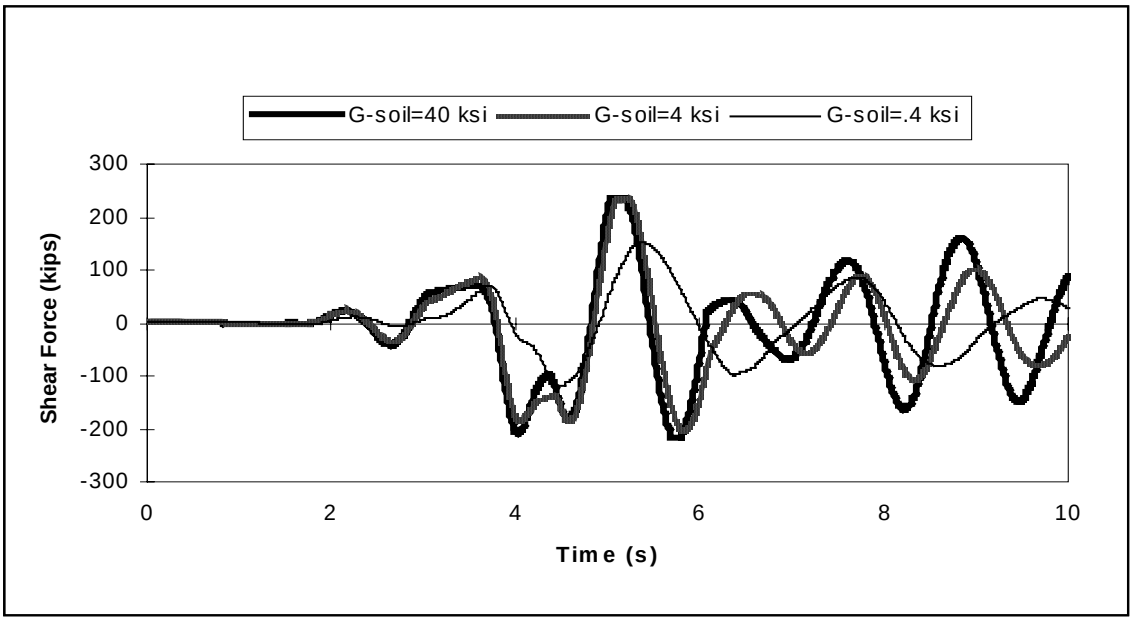

Figure 7-8 Shear force time histories for Clements Bridge, pier #1. Different soil shear moduli under Parkfield earthquake. (2-D model, μ=0.6 at bearings, PGA=0.18g.).

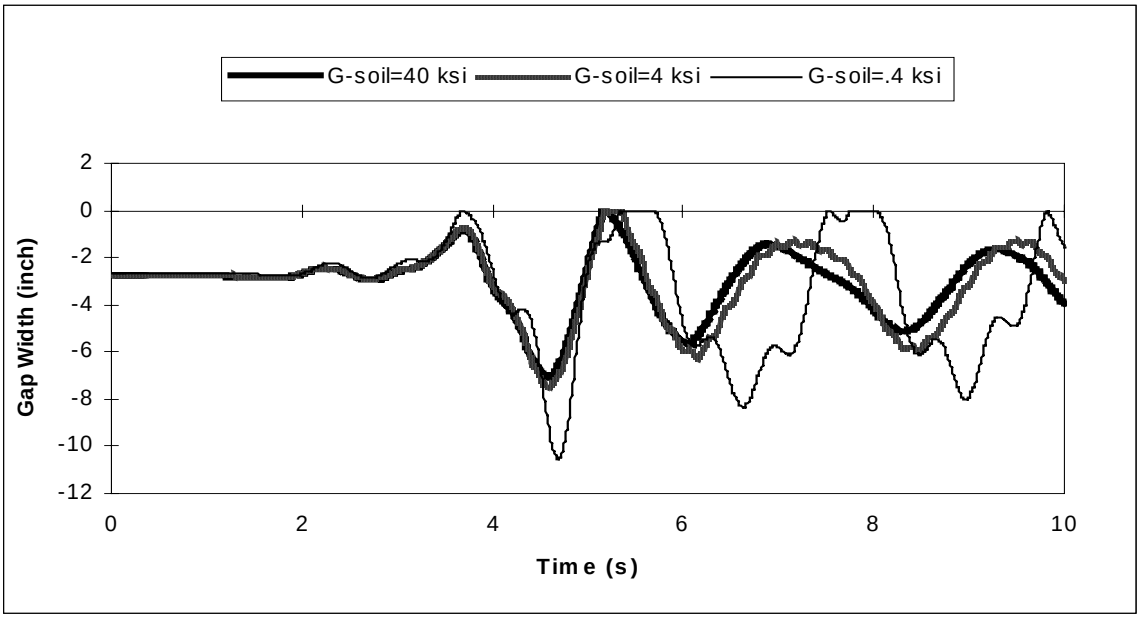

Figure 7-9 Gap width time histories for Clements Bridge, abutment #2. Different soil shear moduli under Parkfield earthquake (2-D model, μ=0.6 at bearings, PGA=0.18g).

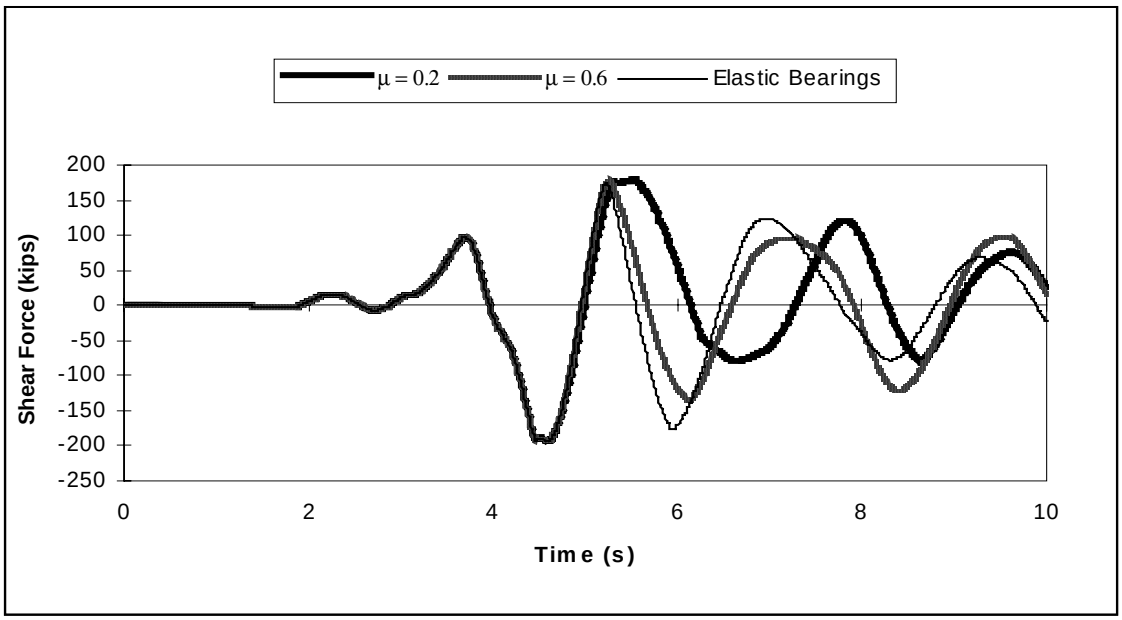

Figure 7-10 Shear time histories for Clements Bridge, pier #2.
Different bearing frictional coefficients under Parkfield earthquake.
(2-D model, G-soil=4 ksi, PGA=0.18g).

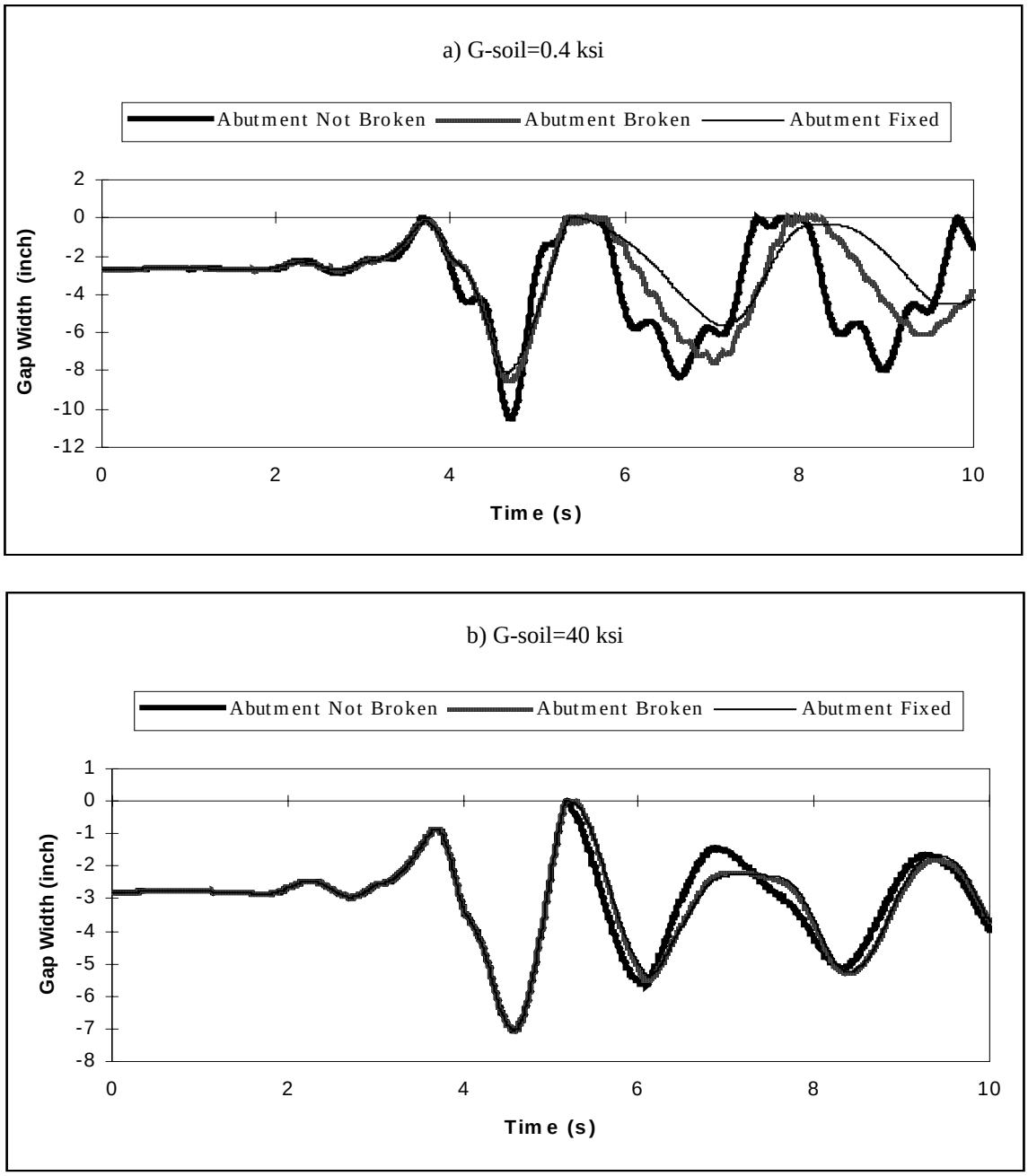

Figure 7-11 Gap width time histories for Clements Bridge abutment #2. Different SSI models under Parkfield earthquake (2-D model, μ=0.6 at bearings, PGA=0.18g).

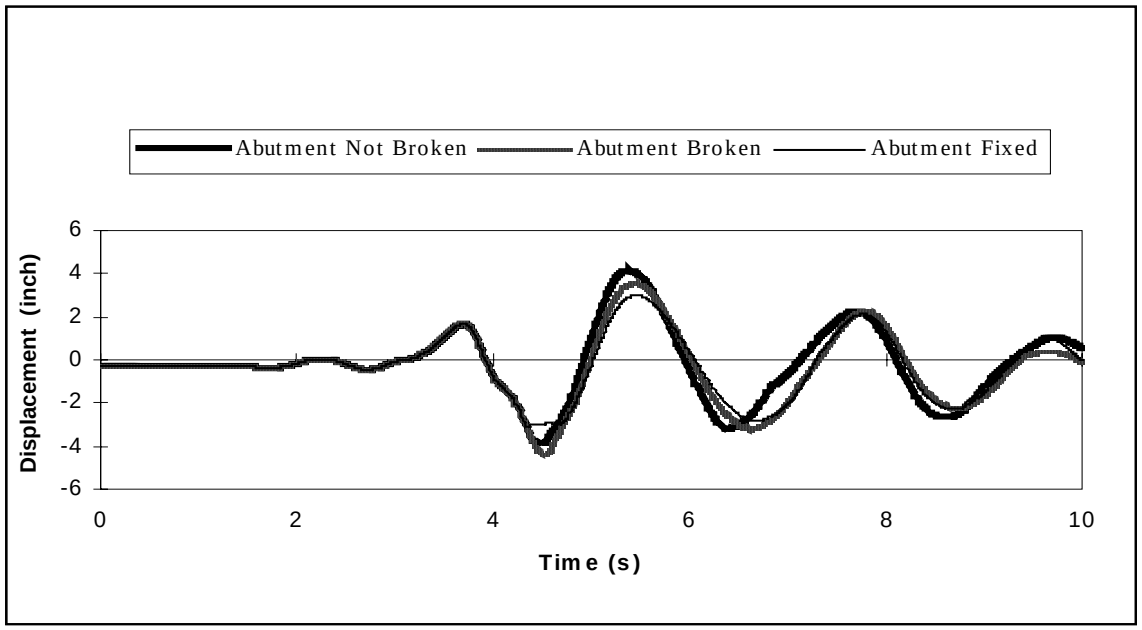

Figure 7-12 Top displacement time histories for Clements Bridge, pier #1.
Different abutment models under Parkfield earthquake.
(2-D model, μ=0.6 at bearings, G-soil = 0.4 ksi, PGA=0.18g).

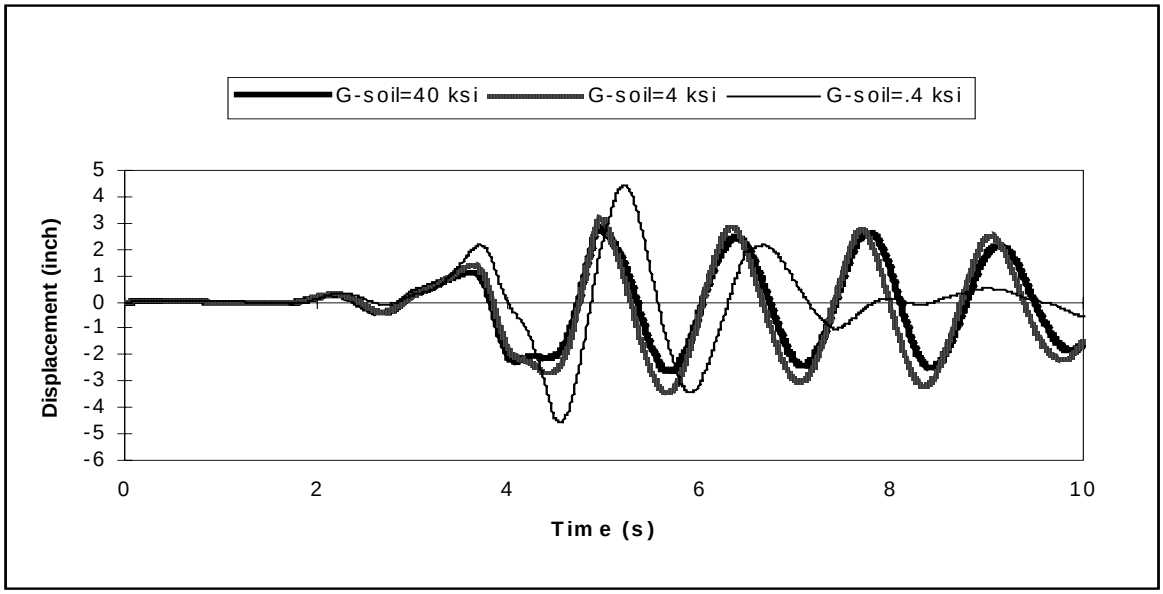

Figure 7-13 Top displacement time histories for Alexander Bridge pier.
Different soil shear moduli under Parkfield earthquake.
(2-D model, μ=0.6 at bearings, PGA=0.18g).

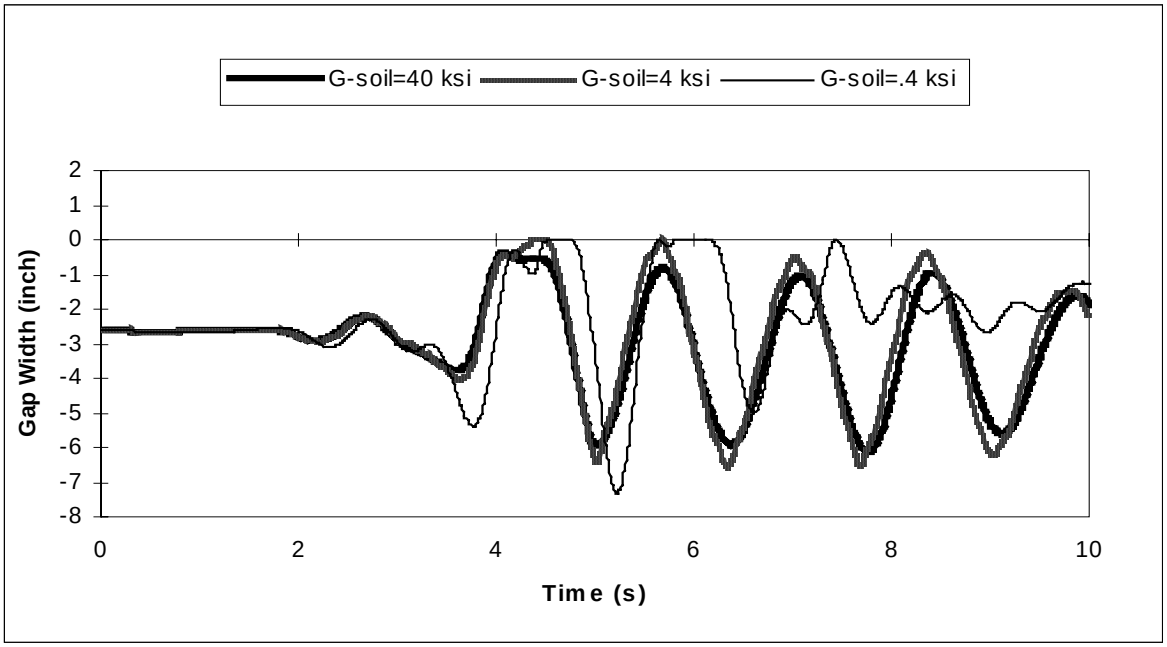

Figure 7-14 Gap width time histories for Alexander Bridge, abutment #1. Different soil shear moduli under Parkfield earthquake. (2-D model, μ=0.6 at bearings, PGA=0.18g).

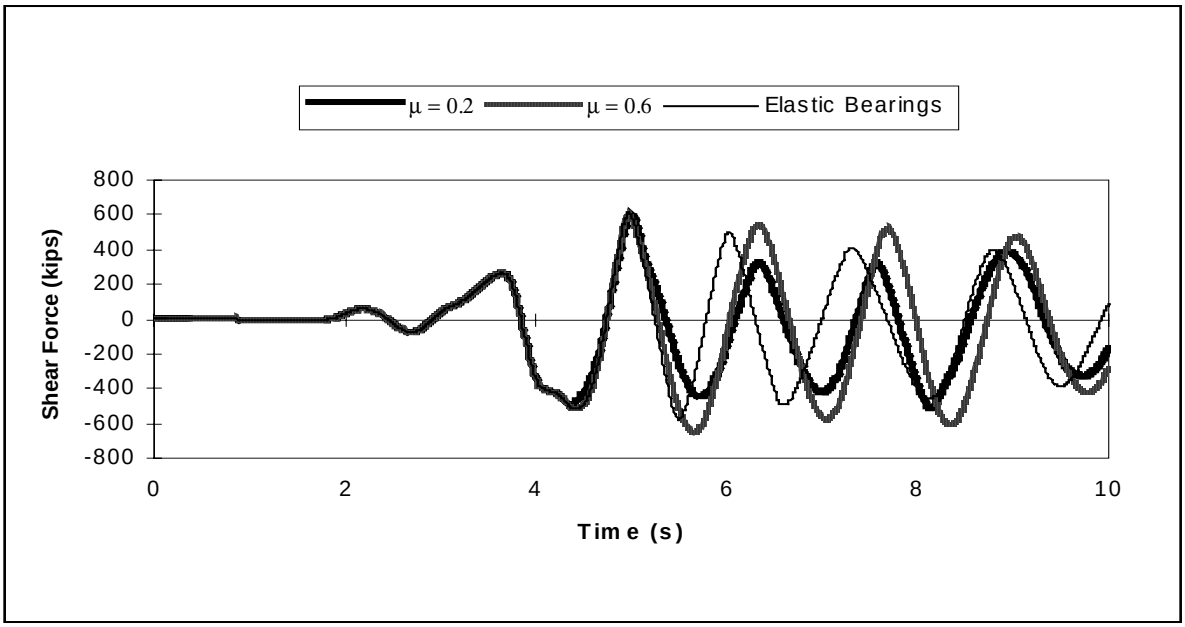

Figure 7-15 Shear force time histories for Alexander Bridge pier. Different bearing frictional coefficients under Parkfield earthquake. (2-D model, G-soil=4 ksi, PGA=0.18g)

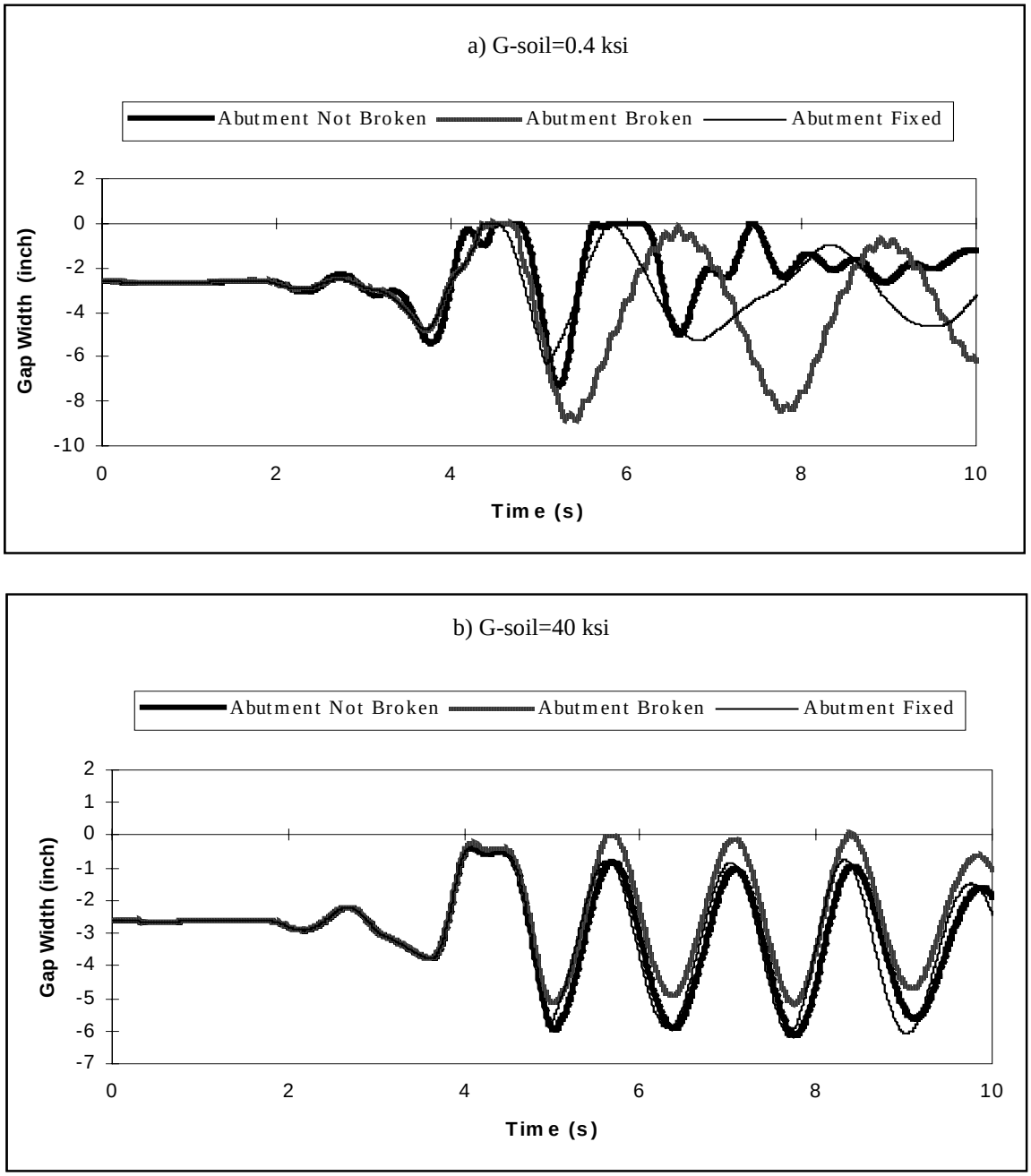

Figure 7-16 Gap width time histories for Alexander Bridge, abutment #2. Different SSI models under Parkfield earthquake (2-D model, μ=0.6 at bearings, PGA=0.18g).

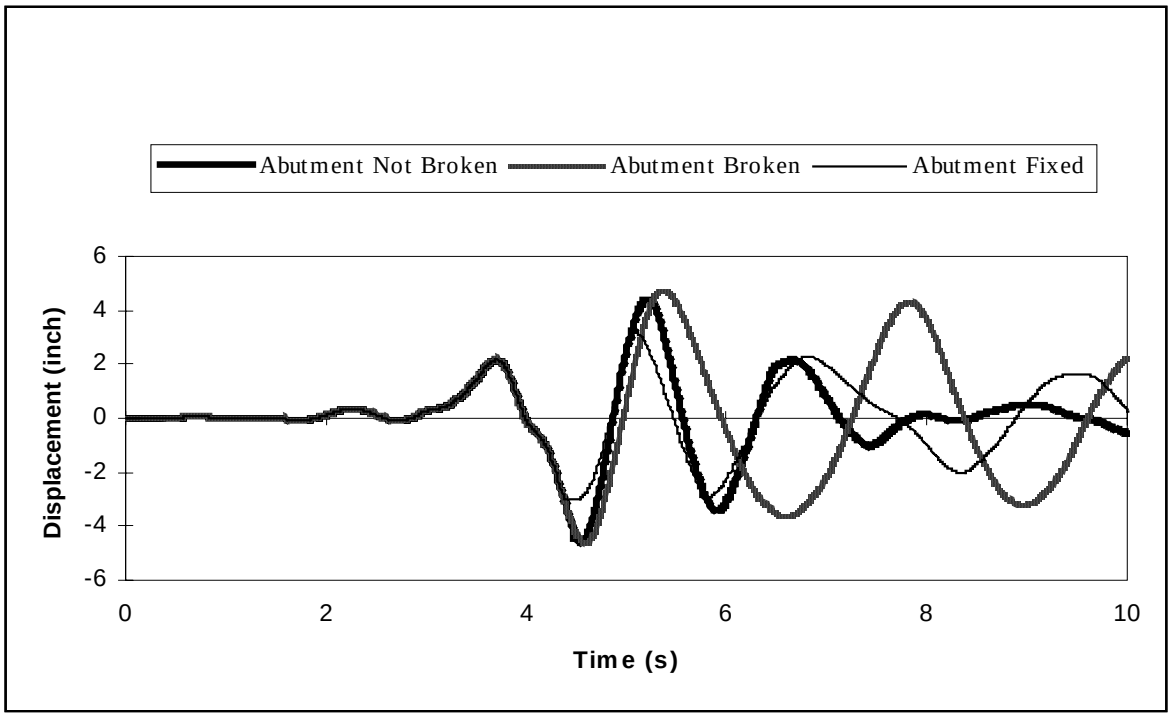

Figure 7-17 Top displacement time histories for Alexander Bridge pier.
Different abutment models under Parkfield earthquake.
(2-D model, μ=0.6 at bearings, G-soil = 0.4 ksi, PGA=0.18g)

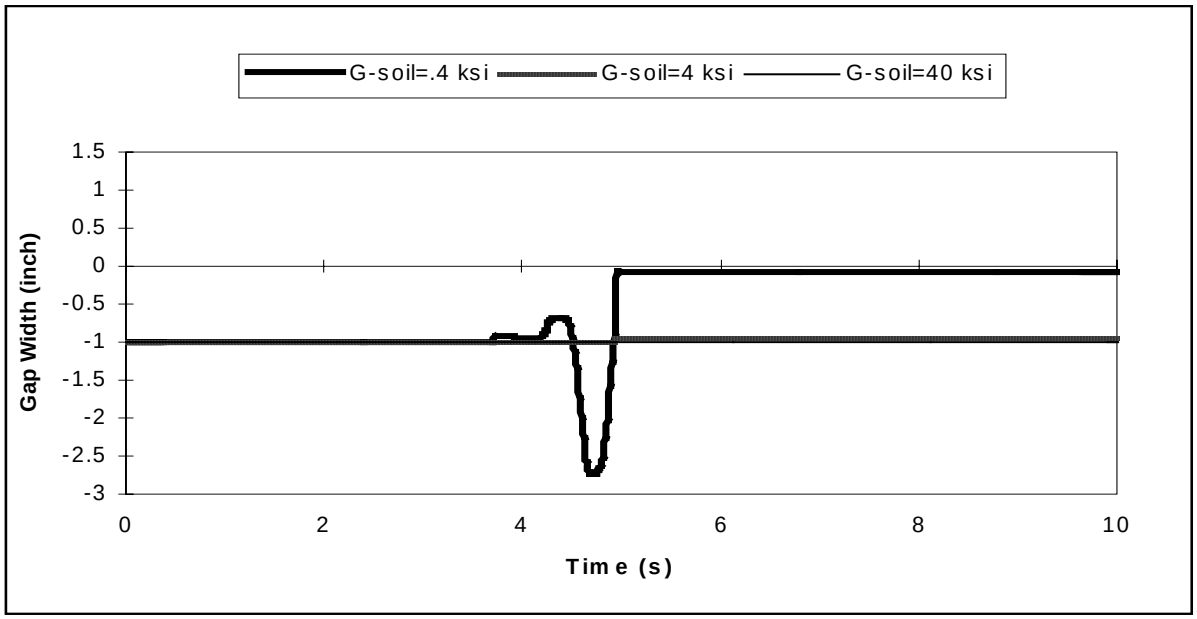

Figure 7-18 Gap width time histories for Bridge-5, abutment #2.
Different soil shear moduli under Parkfield earthquake.
(2-D model, μ=0.6 at bearings, PGA=0.18g)

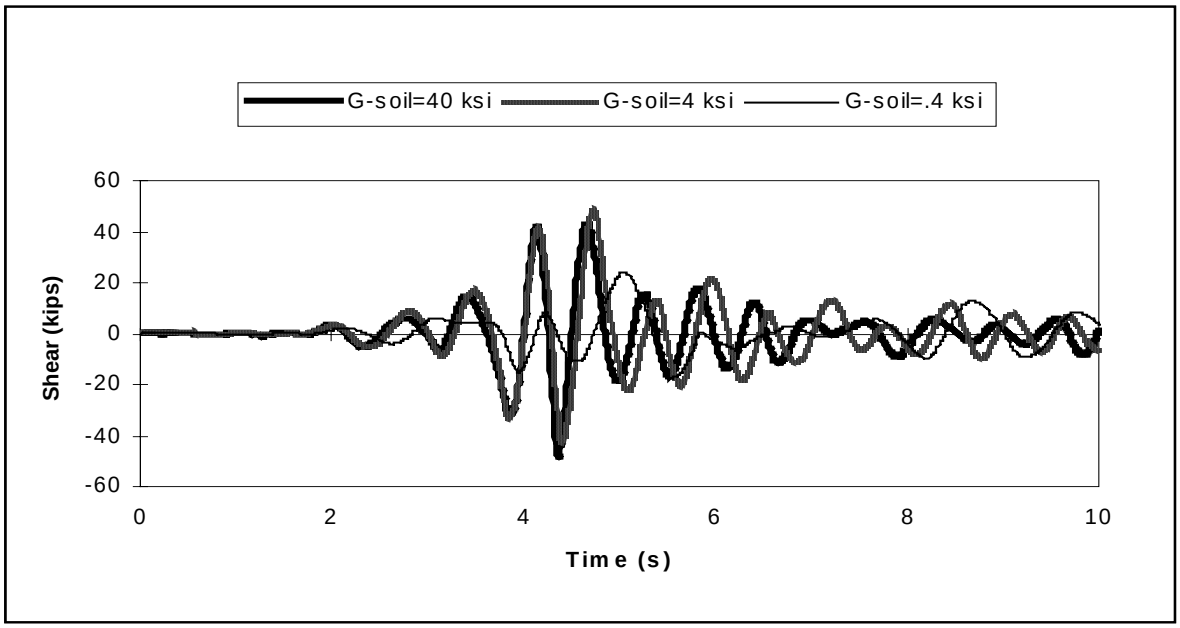

Figure 7-19 Bridge-5 shear time histories for pier #1, column type-1.
Different soil shear moduli under Parkfield earthquake.
(2-D model, μ=0.6 at bearings, PGA=0.18g).

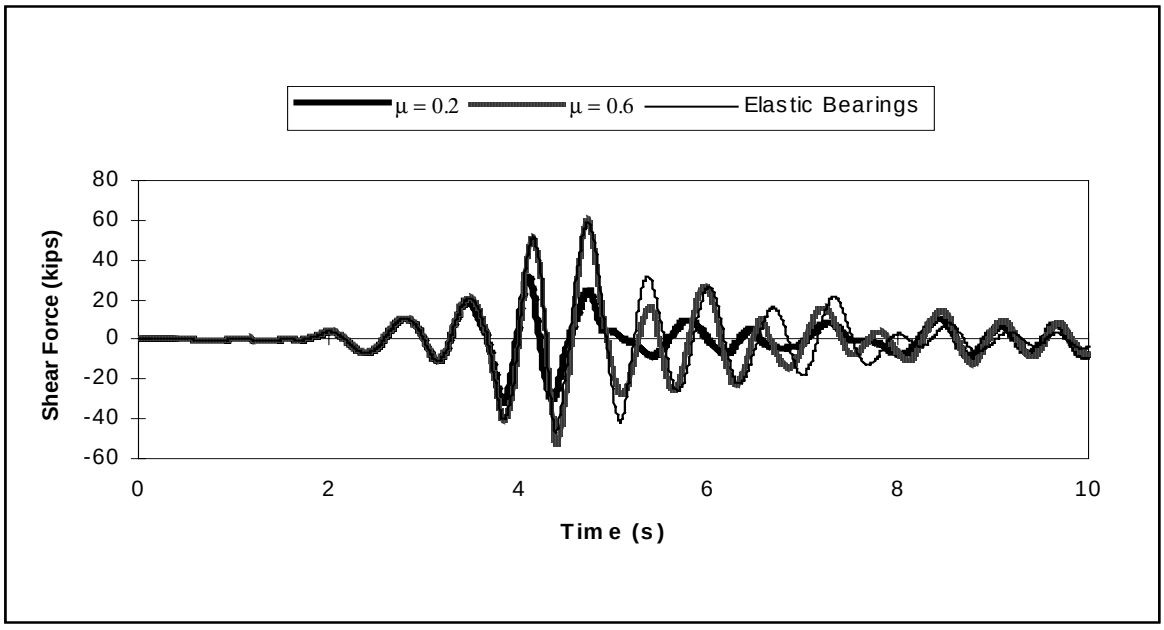

Figure 7-20 Bridge-5 shear force time histories for pier #1, column type-3.
Different bearing frictional coefficients under Parkfield earthquake.
(2-D model, G-soil=4 ksi, PGA=0.18g)

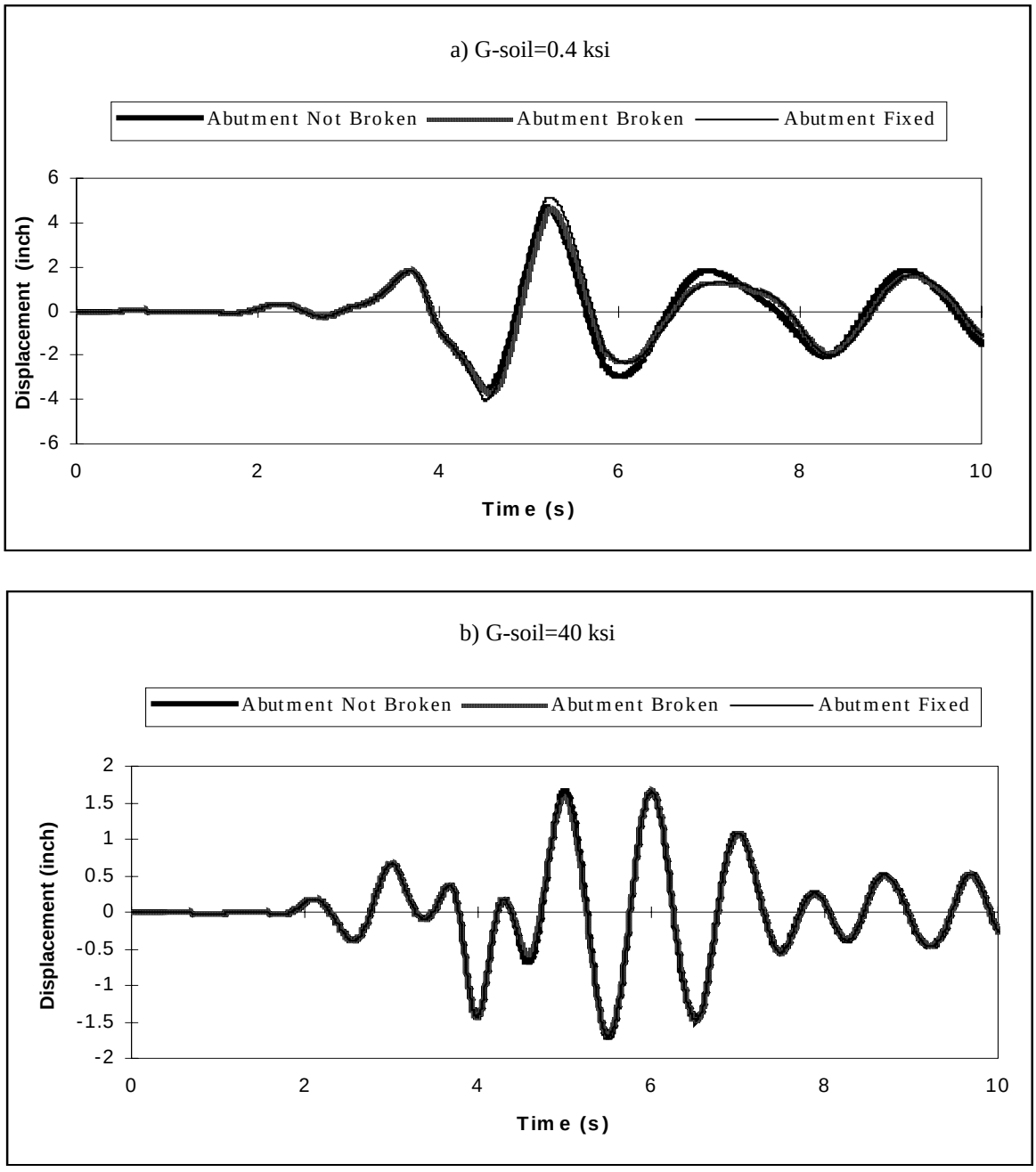

Figure 7-21 Top displacement time histories for Bridge-5, pier #2.
Different SSI models under Parkfield earthquake.
(2-D model, μ=0.6 at bearings, PGA=0.18g)

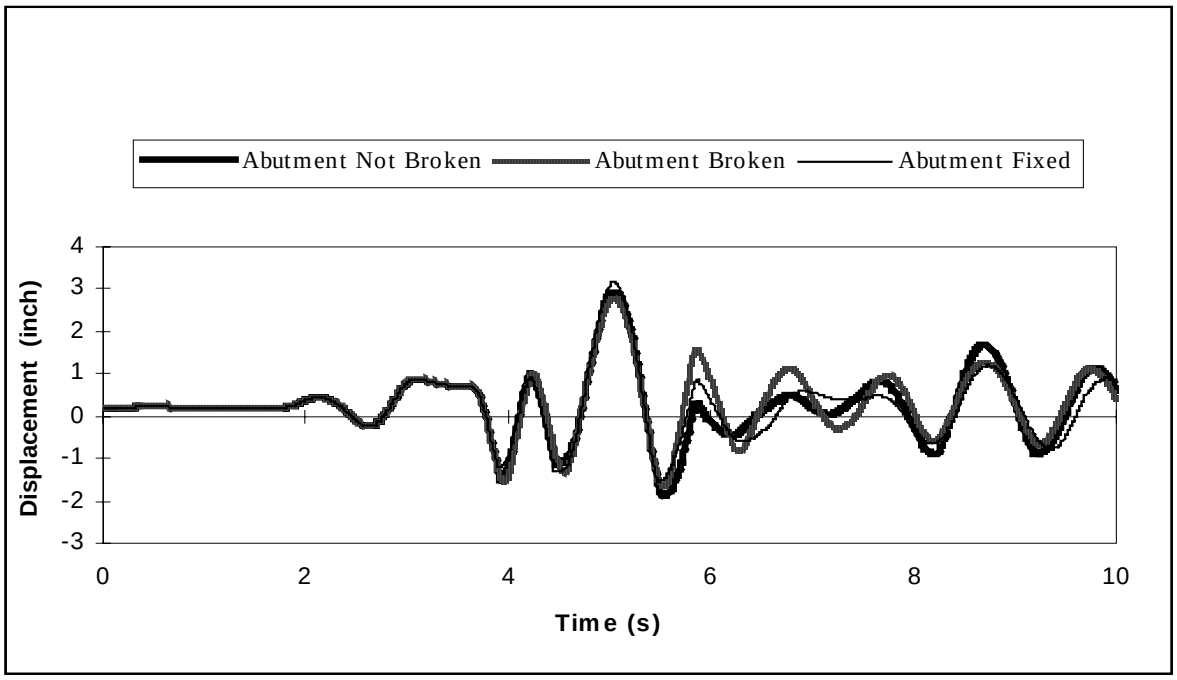

Figure 7-22 Top displacement time histories for Bridge-5, pier #1.
Different abutment models under Parkfield earthquake
(2-D model, μ=0.6 at bearings, G-soil=0.4 ksi, PGA=0.18g).

SECTION 8

3-D ANALYSES AND THE RESULTS COMPARISON

8-1) General

In this section first the results of nonlinear 3-D time history analyses are presented. These analyses are performed under two sets of earthquake records (Parkfield and El Centro) with PGAs of 0.18g and 0.4g. Later in this section, the results of 3-D analyses are compared to those for 2-D models and AASHTO specifications.

8-2) Results of 3-D Nonlinear Time History Analyses

Three-dimensional modeling makes it possible to model the skewness of the bridges. This will significantly affect the bridge dynamic behavior, including reduction in vibrating periods and coupling of mode shapes in three major directions (i.e., longitudinal, transverse and vertical). As a result of the skewness, pier columns show axial load variations under longitudinal earthquake excitation, which in turn affects the nonlinear behavior of the columns at plastic hinge locations.

Generally, detailed distribution of seismic forces among various components of the abutment is complex and will require 3-D finite element analysis, which was not within the scope of this study. Impact forces are resisted by the approach slab, the backfill soil, and friction at the base of the abutment footings. Therefore, actual value of shear at the juncture of the backwall and breast wall, which determines backwall failure, can not be determined based on the frame models used. However, it is clear that the higher the level of impact forces the higher the shear demand at this critical section. For example in the 2-D analyses impact forces reached as high as 20 times the back wall shear capacity (under low intensity earthquakes of 0.18g PGA). This necessitated the need to model backwall failure in the 2-D analyses, and as it was shown in the previous section the case of failed backwall resulted in the most critical performance in terms of low C/D ratios.

An advantage of 3-D model is a better representation of impact between bridge components. The reason is that in 3-D models impact forces are distributed over the

width of decks and are considerably less than those obtained from 2-D models. In a distributed model the impact is less sudden (i.e., rather than one intense impulse there are several impulses of lower intensity). Furthermore, for the 3-D models even under higher input PGAs the damaged abutment did not show a significant effect on the bridge responses. That is, unlike the 2-D case, bridge response did not increase for damaged abutments. This can be seen in Table 8-1, which shows selected responses of Clements Bridge and Bridge-5 for two abutment-modeling conditions under Parkfield earthquake scaled to PGA of 0.4g. As is seen, the damaged abutment condition does not have a significant effect on increasing the bridge responses and even in some cases shows a decreasing effect (e.g., plastic rotation demands of the Clements Bridge pier columns). The reason for this is coupling between the responses in the transverse and longitudinal directions. Therefore, in the 3-D study only a few cases of damaged abutment condition were considered, and for most cases the abutment is assumed intact.

The complete list of the maximum responses at selected locations and corresponding demand / capacity ratios, which are calculated by a special computer program developed for this study, are presented in Appendix II. Following is a brief description of the analysis results for each bridge investigated (i.e., Clements Bridge and Bridge-5).

3-D Response of Clements Bridge

Skewness and low lateral concrete confinement of the pier columns are among the special characteristics of this bridge. Under PGA of 0.18g, Clements Bridge has C/D ratios larger than 1.0 for most cases. The only condition that leads to pier column failure is a model with elastic bearings (i.e., no failure at bearings). In an actual situation, it is very likely that the fixed bearings will fail under impact forces, even at a PGA as low as 0.18g. This is because of the low shear capacity of the connecting bolts. Consequently, the post-failure behavior of the bearings will be defined by Coulomb-friction between the decks and their supports. This will cause dissipation of energy through friction/damping. Figure 8-1 shows the time histories of the resultant shear force demand in pier columns of Clements Bridge considering both elastic bearings and μ=0.6 at the bearings. It can be seen that the maximum shear force demand for pier columns is higher in the case of

elastic bearings than the cases of failed bearing (μ= 0.6 and 0.2). This can also be observed in Table 8-2, which shows the minimum C/D ratios for Clements Bridge under earthquakes scaled to PGA of 0.18g. As it is seen, pier column force and plastic rotation demands decrease significantly by for failed bearings.

To investigate the effect of higher ground motion acceleration, cases of 0.4g PGA were also considered. The summary of the minimum C/D ratios for this value of PGA is shown in Table 8-3, where it is seen that the columns' shear demands greatly exceed the shear capacities. This mode of failure (i.e., shear) has occurred for almost all of the assumed bearings conditions (i.e., elastic and failed) and input earthquake records (i.e., Parkfield and El Centro).

3-D Response of Bridge-5

Because this bridge has well-confined concrete pier columns and relatively large number of columns at each pier bent, good seismic performance is expected for low intensity earthquakes. Therefore, this bridge was first analyzed under PGA of 0.4g, and then for critical cases analyses were performed for the lower PGA of 0.18g. As mentioned before, 0.18g is the maximum seismic coefficient for New Jersey per AASHTO's seismic design guidelines.

Table 8-4 shows the minimum C/D ratios for Bridge-5 components under earthquakes scaled to PGA of 0.4g. Also, Table 8-5 shows the C/D ratios under 0.18g earthquakes for critical cases.

The observed damage (besides bearing failure) under PGA of 0.4g was shear failure of pier columns. Although plastic rotation demand for pier columns was as low as 10% of the capacity, the ductility demand at this level of plastic rotation was enough to induce shear failure. The reason for this is substantial decrease in the concrete shear capacity for curvature ductilities larger than 4. Therefore, in retrofit of bridges, or design of new ones, care must be exercised to develop an optimal balance between the lateral reinforcement and concrete area (or cross-sectional size). For example, in the case of Bridge-5, it

appears that a larger cross-section even with lower lateral reinforcement would have better performance.

Under 0.4g PGA most column shear failures occur at moderately stiff soils (G-soil=4 ksi) and except for a few cases of column shear failure no damage is observed with other types of soils (G-soil=0.4 and 40 ksi). This can be explained by considering the effect of soil structure interaction as it was explained before under the discussions of 2-D results (section 7).

In very stiff soils there are less impact instances and abutments exert more restraint on both the bridge displacements and the column curvature ductility demands. Because of the fixed bearings over the right abutment (abutment #2), the abutments show more restraining effect over the bridge displacements. This is the reason for having the maximum demands in models with the lowest frictional coefficient at failed bearings (μ=0.2) where lower frictional resistance at the bearings compromises the abutments limiting effects on the response of the superstructure.

8-3) Comparison Between 3-D and 2-D Models

As it was mentioned before, 3-D modeling has the additional capabilities of modeling skewness, distribution of impact forces within the deck width, and exact mean of combining longitudinal and transverse earthquake forces in bridge components. Following are the description of these features.

1) In any skewed bridge, skewness significantly affects the dynamic characteristics and nonlinear responses of the bridges. Mode shapes in three major directions are coupled, in other word the bridge longitudinal and transverse responses are not separable. Table 8-6 shows periods of the Clements Bridge for 2-D (longitudinal) and 3-D models for G-soil=4 ksi. As is seen as a result of coupled mode shapes shorter periods were obtained for 3-D models. Also as a result of the skewness, axial loads at

pier columns show significant variation. This is shown in Figure 8-2 and is seen that this variation was not captured in 2-D models

2) The level of impact force in 3-D models is considerably less than the impact level for 2-D models. Impact force is the reason for the backwall failure at the abutment. Table 8-7 presents the impact forces on the Clements Bridge abutments for one of the modeling cases. As is seen, the total impact force at abutment #2 in 3-D model is reduced to the one-third of the 2-D model.

3) There is more abutment interaction with the superstructure response in 3-D models. This is because in the transverse direction the roller bearing are also fixed, causing the abutments to be an integrated part of the bridge even when the gaps are open. For skewed bridges the 3-D response is further coupled in longitudinal and transverse directions.

4) Based on 3-D analyses for skewed bridges the effect of backwall failure is not as significant as it is for the 2-D case. This is due to the coupling mentioned above. For example, consider tables 8-1, and 8-8, where the effects of backwall failure for 3-D and 2-D cases are shown, respectively. As seen, in Table 8-8 for the 2-D model there is an increase, as high as 100%, for plastic rotation demands for damaged backwall case, while in the 3-D model (Table 8-1) plastic rotation demands have even decreased for the case of damaged backwall.

5) The pier column flexural deformation in the plane of the pier bent is double curvature, therefore, higher plastic shear force is associated with the pier bent plastic hinge sway mechanism (i.e., Vp=2*Mp/h rather than Mp/h for single curvature bending). In columns with low lateral reinforcements (e.g., Clements Bridge) the shear failure would be a potential hazard if curvature ductility demand exceeds 4. At this level of curvature demand there is a substantial decrease in concrete shear capacity (section 4-2). Table 8-9 demonstrates a comparison between shear capacities and demands, which were obtained from 3-D and 2-D (longitudinal) models. It should

be noted that in current AASHTO codes effect of curvature ductility demand on shear capacity is not recognized.

8-4) Comparison of the 3-D Analysis Results and AASHTO's Single Mode Method

For comparison purposes it is instructive to evaluate the response of MSSS bridges assuming that there won't be closure of any gap. This assumption is needed so that the response under uniformly distributed load, per Single-Mode Spectral Method, is independent of the intensity of the load. Employing a model of Clements Bridge with G-soil=4 ksi, the seismic forces using this method are determined for both longitudinal and transverse directions. The calculated periods and base shear coefficients are shown in Table 8-10. Periods in both directions obtained based on this method are in good agreement with those from 3-D computer model.

The equivalent static seismic forces determined based on the Single-Mode-Spectral method are then applied to the 3-D model of the Clement Bridge based on the distribution specified for this method in AASHTO. The resultant force for each pier is a combination of longitudinal and transverse forces as described in the codes (100% + 30% of maximum responses in two perpendicular directions). Figure 8-3 shows the Clements Bridge piers shear demand based on this combination rule along with the results of time history analyses. Based on AASHTO to obtain the design forces the elastic forces are divided by the member response modification factor (R). This is a simplified and approximate way for considering the nonlinear response of the bridge. Based on AASHTO-LRFD specifications [11] the modification factor for multi-column bents varies from 1.5 to 5 depending on the bridge importance category. Referring to Figure 8-3, where to simplify comparison R is assumed equal to unity, it is apparent that the AASHTO design force for the left pier would be much smaller than the demand obtained by 3-D analysis. With R equal to one the two are comparable, thus, the design force when R is applied would be smaller by this factor. One reason for this is that dominant modes of response have periods between 0.3 to 0.8 seconds where the AASHTO response spectrum (RS) yields lower forces than the earthquake records used in the 3-D analyses (Figure 6-6). Another

reason is incompatibility in application of an elastic spectrum (along with R factor to account for nonlinear action) to a nonlinear stiffening system. That is, current design guidelines use elastic spectrum and account for nonlinear behavior through response modification factor R, which are based on studies of nonlinear SDOF systems with elastic-plastic load-deformation characteristic. The response of MSSS bridges is initially stiffening due to closure of gaps.

Another important point to consider is that in design of new bridges due to application of response modification factor, the seismic displacement demand would be larger. This in turn will cause more abutment interaction in the bridge responses.

The pushover analysis is a graphically useful method in calculating the demands for bridge elements. Figure 8-4 shows the pushover analyses of Clements Bridge in longitudinal and transverse directions. By comparing the AASHTO RS (0.18g) with the pushover curves displacement and force demands for the entire bridge can be determined. The total displacement demands in longitudinal and transverse directions for PGA of 0.18g, as seen in Figure 8-4, are about 4.9” and 2.2”, respectively. These displacements are in the range of those obtained from 3-D analyses (e.g., 3.2” and 2.8” under El Centro earthquake and elastic bearings). But for higher PGA of 0.4g this agreement of the results does not hold. As seen in Figure 8-4 displacement demands in longitudinal and transverse directions are about 10” and 6”, respectively. These displacements are not in the range of the computed displacements by 3-D analyses (e.g., for Parkfield earthquake and elastic bearings these displacements are 5.8 and 3.4, respectively, which are about half of those obtained by pushover analysis). This shows that the obtained results from pushover analyses are not always in good agreement with the results obtained by nonlinear time history analyses. The difference becomes more when there is more nonlinearity involved in the bridge responses as a result of stronger earthquakes.

8-5) Conclusions

Based on a comprehensive 3-D study on two actual multi-span simply supported bridges the following conclusions can be made with regard to their 3-D seismic response:

- Under PGA of 0.18g, except in the case of elastic bearings (i.e., no failure at the bearings), no damage is observed for Clements Bridge by C/D ratio less than one. Bolts connecting steel bearings to the girder or concrete seat are expected to fail even under low intensity earthquakes due to low shear capacity. This failure acts like a fuse and will reduce the demands on the rest of the bridge. In Clements Bridge the most critical C/D ratio belongs to the pier column shear and the deck sliding.

- Clements Bridge pier columns under PGA of 0.4g have shown shear failure with C/D ratio as low as 0.2. This was mostly due to low lateral reinforcements in the pier columns.

- Bridge-5 has shown high C/D ratios for earthquakes scaled to 0.18g PGA, and no damage was observed even when the bearings are assumed to remain elastic. In reality it is except at that the bearings will fail due to low shear capacity at the connecting bolts. The main reasons for better performance of this bridge are that the concrete columns are well confined and that several columns are each pier bent.

- Despite better confinement, Bridge-5 in moderate soil (G = 4ksi) will also sustain failure under 0.4g PGA due to shear failure in the columns.

- Very stiff soils enhance the restraining action of the abutments in limiting bridge displacements, which may lead to no impact between decks. On the other end, very soft soils have less rotational restraining at the base of pier columns causing low curvature ductility demand and less damage. The most critical cases generally occur for models with moderately stiff soils. Note that this is the case only when there is high input acceleration (e.g., 0.4g PGA). For lower PGA, since abutment interaction is minimal, stiffer soil causes higher demand at pier columns.

- Geometric and response characteristics, such as skewness and distributed impact, have a significant effect on dynamic response and can only be represented by employing a 3-D model. Therefore, for seismic evaluation of MSSS bridges even under low PGA the use of 3-D models are more appropriate.

- The response spectrum used in AASHTO specifications may result in unconservative demands for bridge elements. Among the reasons for this, following can be mentioned; a) Contribution of periods between 0.3 to 0.8 seconds, where the AASHTO response spectrum (RS) yields the lower forces than the employed earthquake records. b) Stiffening dynamic behavior of the bridge due to gap closure has different characteristics that are not considered in development of AASHTO response spectrum. Therefore, use of nonlinear time history analysis should be considered for critical bridges.

- Pushover analysis is an efficient tool for estimating displacement demands but the obtained results are not always in good agreement with those obtained from nonlinear dynamic analyses. This lack of agreement becomes more significant especially for strong earthquake motions where the response becomes more nonlinear.

The beneficial effect of bearing failure must be emphasized. As the time history results show, the most critical situation arises when the bearings are assumed to remain elastic (e.g., consider Table 8-2). Obviously, this beneficial effect of bearing failure is due to consequent energy dissipation through friction at the bearings. The advantage and critical importance of this mechanism of behavior (i.e. bearings acting like a fuse) warrants experimental investigation to validate. It is important to ensure that the pull out of bearing seat on the abutments and cap beams are prevented. That is, bearing failure must occur rather than concrete seat failure.

Table 8-1 Selected responses of the 3-D bridge models under Parkfield earthquake (alt-1) for two different abutment modeling conditions. (G-soil=4 ksi and elastic bearings)

Bridge Name	**PGA**	**Location**	**Displacement (inch)**		**Plastic Rotation (rad)**	
			Whole Abut.	Damaged Abut.	Whole Abut.	Damaged Abut.
Clements	0.18g	Pier#1	X 3.07 Y 1.25	X 2.50 Y 1.78	0.012	0.001
		Pier#2	X 4.34 Y 1.22	X 4.23 Y 2.06	0.004	0.002
	0.40g	Pier#1	X 4.10 Y 3.25	X 5.17 Y 3.10	0.017	0.013
		Pier#2	X 5.60 Y 2.60	X 6.30 Y 3.07	0.013	0.009
Bridge-5	0.40g	Pier#1	X 1.07 Y 0.69	X 1.17 Y 0.73	~0	0.010
		Pier#2	X 4.98 Y 2.30	X 3.94 Y 2.54	0.021	0.022
		Pier#3	X 2.05 Y 1.35	X 2.07 Y 1.57	0.018	0.014

Notes:
1) Displacements are for the middle of the pier bents.
2) Plastic rotations are at the pier column ends.

Table 8-2 The minimum C/D ratios for Clements Bridge under PGA of 0.18g (3-D Model)

G-soil (ksi)	C/D ratios for		
	Pier col. Shear (y-y, z-z)	**Plastic Rot. (y-y, z-z)**	**Deck Sliding (longitudinal)**
0.4	(0.8,1.3) EL-2, μ = NY Above ratios change to (2.0,3.3) for μ =0.6	(1.3,1.3) EL-2, μ = NY Almost zero demand for μ =0.6	1.1 PF-1, μ = NY
4.0	(0.4,1.3) EL-1, μ = NY Above ratios change to (1.3,2.5) for μ =0.6	(2.5,1.3) PF-1, μ = NY Almost zero demand for μ =0.6	1.6 PF-1, μ = 0.6
40.0	(0.4,1.7) EL-1, μ = NY Above ratios change to (1.3,2.5) for μ =0.6	(1.4,1.4) EL-2, μ = NY almost zero demand for μ =0.6	1.8 PF-1, μ = 0.2

Notes:

1) Shades in the above table mark failure by C/D ratios less than one for either at least one direction or resultant of two directions.
2) EL and PF indicate El Centro and Parkfield earthquakes. 1 and 2 refer to alternatives one and two of earthquake component sets.
3) μ is the frictional coefficient at failed bearings.
4) Deck sliding C/D ratios are obtained from the gap opening responses over pier columns and abutments.

Table 8-3 The minimum C/D ratios for Clements Bridge under PGA of 0.4g (3-D Model)

G-soil (ksi)	C/D ratios for		
	Pier col. Shear (y-y, z-z)	**Plastic Rot. (y-y, z-z)**	**Deck Sliding (longitudinal)**
0.4	(0.4,1.0) EL-2, μ = NY (0.4,0.9) EL-2, μ = 0.6 (0.6,1.3) EL-2, μ = 0.2	(3.3,0.9) EL-2, μ = NY *Above ratios change to (1.7,1.4) for μ =0.6*	1.0 EL-2, μ = 0.2
4.0	(0.2,0.8) PF-1, μ = NY (0.3,1.1) EL-2, μ = 0.6 (0.5,0.8) EL-1, μ = 0.2	(3.3,0.9) PF-1, μ = NY *Above ratios change to (1.7,3.3) for μ =0.6*	1.2 EL-2, μ = 0.2
40.0	(0.3,1.3) EL-1, μ = NY (0.4,0.8) EL-1, μ = 0.6 (0.5,1.0) EL-1, μ = 0.2	(5.0,0.8) EL-1, μ = NY *Above ratios change to (5.0,1.4) for μ =0.6*	1.3 EL-2, μ = 0.2 & 0.6

Notes:

1) Shades in the above table mark failure by C/D ratios less than one for either at least one direction or resultant of two directions.
2) EL and PF indicate El Centro and Parkfield earthquakes. 1 and 2 refer to alternatives one and two of earthquake component sets.
1) μ is the frictional coefficient at failed bearings.
4) Deck sliding C/D ratios are obtained from the gap opening responses over pier columns and abutments.

Table 8-4 The minimum C/D ratios for Bridge-5 under PGA of 0.4g (3-D Model)

G-soil (ksi)	C/D ratios		
	Pier col. Shear (y-y, z-z)	**Plastic Rot. (y-y, z-z)**	**Deck Sliding (longitudinal)**
0.4	(1.7,2.0) EL-1, μ = NY (1.1,1.4) EL-1, μ = 0.6 (0.83,1.0) EL-1, μ = 0.2	(5,5) EL-2, μ=0.2 ~(10,10) for most cases	1.3 EL-2, μ = 0.2
4.0	(0.9,1.0) EL-1, μ = NY (1.0,1.1) EL-1, μ = 0.6 (0.9,0.9) EL-1, μ = 0.2	(5,10) EL-2, μ = NY ~(10,10) for most cases	1.6 PF-1, μ = NY
40.0	(1.4,1.7) PF-1, μ = NY (2.0,1.7) EL-1, μ = 0.6 (1.4,1.3) PF-1, μ = 0.2	(24.7,10) PF-1, μ = 0.2 Demand is very small at all cases	2.9 EL-1, μ = 0.2

Notes:

1) Shades in the above table mark failure by C/D ratios less than one for either at least one direction or resultant of two directions.
2) EL and PF indicate El Centro and Parkfield earthquakes. 1 and 2 refer to alternatives one and two of earthquake component sets.
3) μ refers to frictional coefficient at bearings.
4) Deck sliding C/D ratios are obtained from the gap opening responses over pier columns and abutments.

Table 8-5 The C/D ratios for Bridge-5 under PGA of 0.18g for selected cases. (3-D Model)

Selected case	C/D ratios for		
	Pier col. Shear (y-y, z-z)	**Plastic Rot. (y-y, z-z)**	**Deck Sliding (longitudinal)**
G-soil=0.4 ksi EL-1, μ = 0.2	(10,10)	~0.0	3.7
G-soil=4 ksi EL-1, μ = 0.2	(2.5,2.5)	~0.0	6.7
G-soil=40 ksi PF-1, μ = 0.2	(3.3,5)	~0.0	7.7

Notes:
1) EL and PF indicate El Centro and Parkfield earthquakes. 1 and 2 refer to alternatives one and two of earthquake component sets.
2) μ refers to frictional coefficient at bearings.
3) Deck sliding C/D ratios are obtained from the gap opening responses over pier columns and abutments.

Table 8-6 Clements Bridge periods obtained by 3-D and 2-D models (G-soil=4 ksi)

Model	**Longitudinal**		**Transverse**
	Pier #1	**Pier #2**	
3-D	1.10	1.67	0.52
2-D (Longitudinal)	1.40	2.26	N/A

Note:
In 3-D models the mode shapes are coupled and presented periods are for the dominant mode shapes in longitudinal and transverse directions

Table 8-7 Comparison of the impact forces on the Clements Bridge abutment backwalls obtained from 2-D and 3-D models.
(Elastic bearings, G-soil=4 ksi, Parkfield record (alt-1), PGA=0.18g)

Abutment No.	2-D Model	3-D Model	Backwall Shear Capacity
1	0	0+3002+597=3,599	2*1675=3,350
2	23,299	852+5964+694=7,510	

Notes:
1) Since the approach slab supports the abutment back wall, two shear surfaces are considered for capacity calculations.
2) For 3-D models, the total impact force is equal to the summation of the links envelope responses.

Table 8-8 Selected responses of the 2-D bridge models under Parkfield earthquake for two different abutment modeling conditions.
(G-soil=4 ksi and elastic bearings)

Bridge Name	PGA	Location	Displacement (inch)		Plastic Rotation (rad)	
			Whole Abut.	Damaged Abut.	Whole Abut.	Damaged Abut.
Clements	0.18g	Pier#1	X 3.1	X 3.1	0.0013	0.0013
		Pier#2	X 4.2	X 4.2	0.001	0.001
	0.40g	Pier#1	X 5.8	X 8.6	0.011	0.021
		Pier#2	X 6.07	X 10.4	0.0067	0.0195
Bridge-5	0.40g	Pier#1	X 2.2	X 2.1	~0	~0
		Pier#2	X 4.3	X 4.3	0.0088	0.0088
		Pier#3	X 4.7	X 7.0	0.0067	0.0254

Table 8-9 Comparison of the shear C/D ratios obtained from 3-D and 2-D (longitudinal) models in Clements Bridge pier columns.
(G-soil=4 ksi, Elastic bearings, Parkfield EQ (alt-1), PGA=0.18g.)

Model	Curvature ductility demand	Shear		Shear C/D
		Demand	Capacity	
3-D	6.5	269	133	0.5
2-D	1.5	119	315	2.7

Table 8-10 Clements Bridge periods and base shear coefficients obtained by the AASHTO single mode method
(PGA=0.18g, S=1.2, G-soil=4 ksi, Open Gaps)

	T (sec)	**Cs**
Long. Pier #1	1.15	0.24
Long. Pier #2	1.71	0.18
Transverse	0.61	0.36

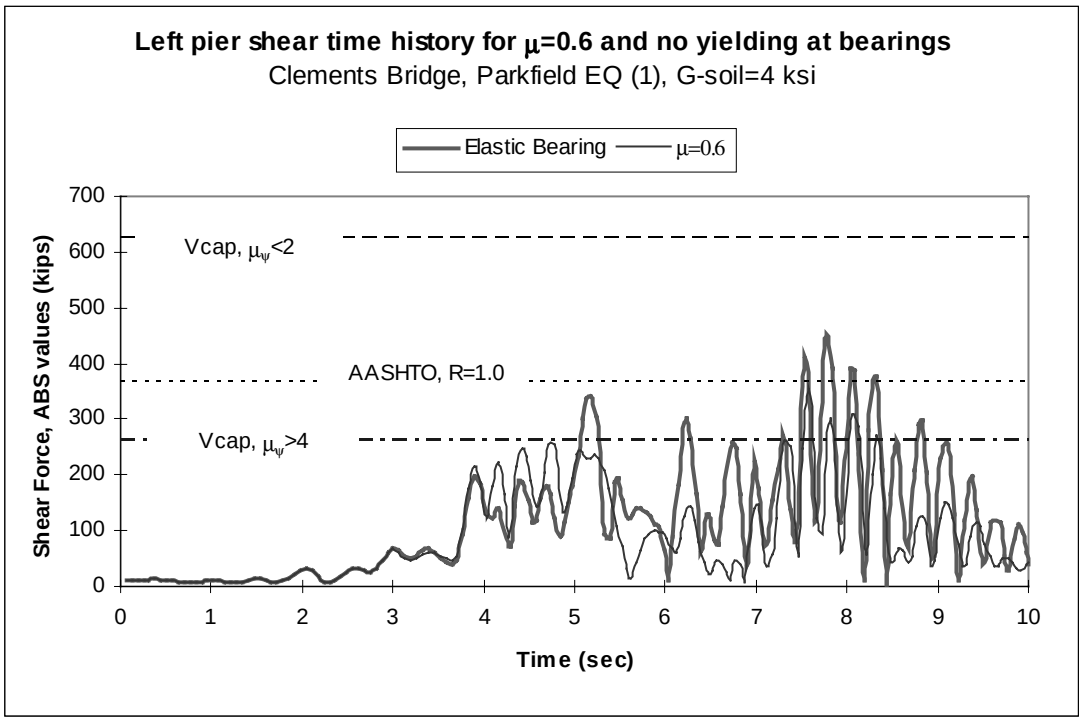

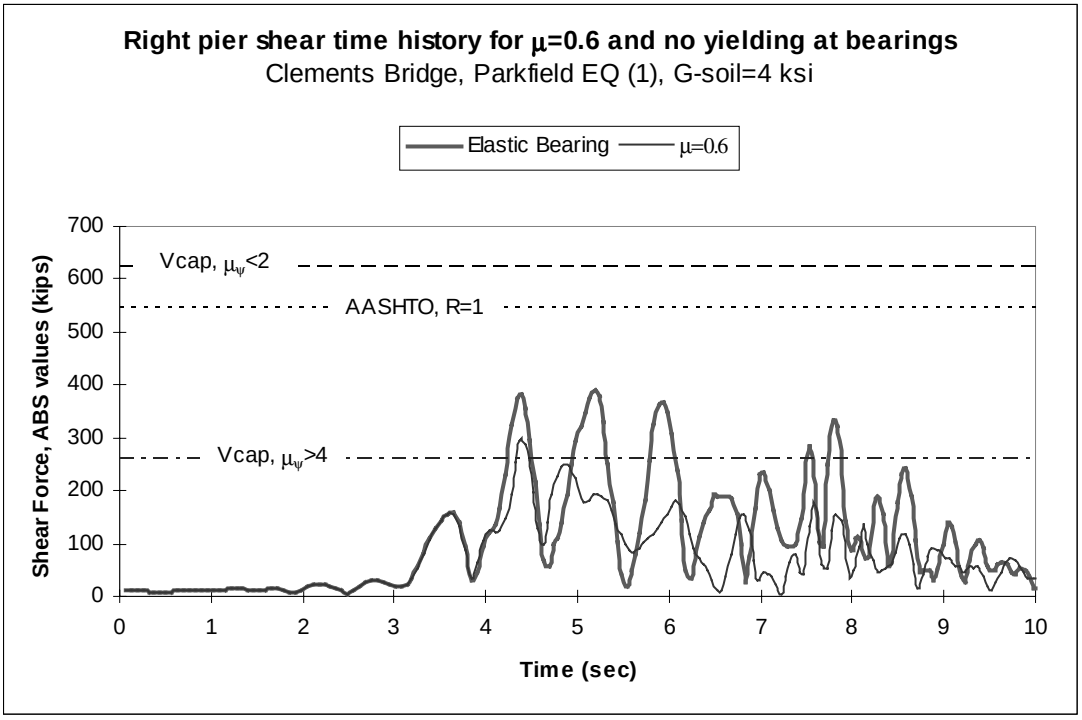

Figure 8-1 Clements Bridge time histories of resultant shear force demand at pier columns

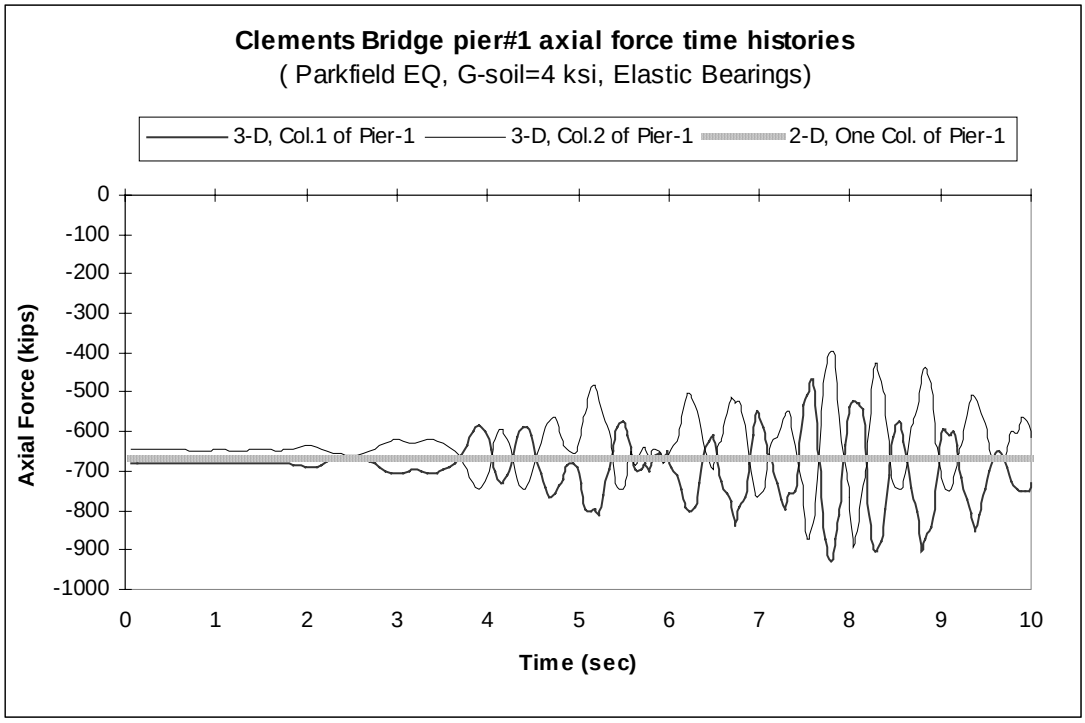

Figure 8-2 Axial force time histories of the Clements Bridge pier#1 columns for 2-D and 3-D models.
(G-soil=4 ksi, Parkfield Record (alt-1), Elastic Bearings)

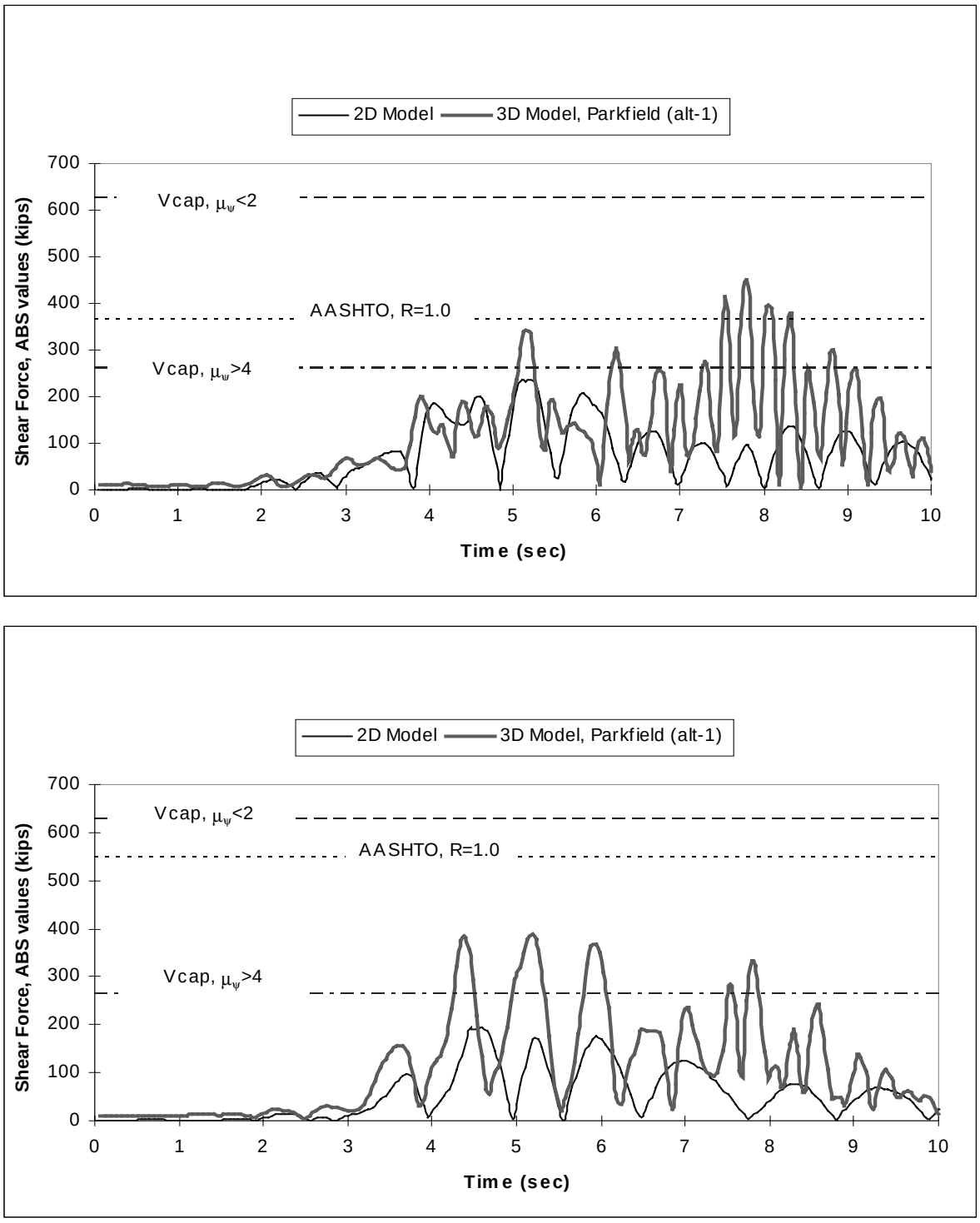

Figure 8-3 Pier column shear time history comparison of Clements Bridge for 2-D and 3-D models
(Parkfield (alt-1) record, G-soil=4 ksi, Elastic bearings)

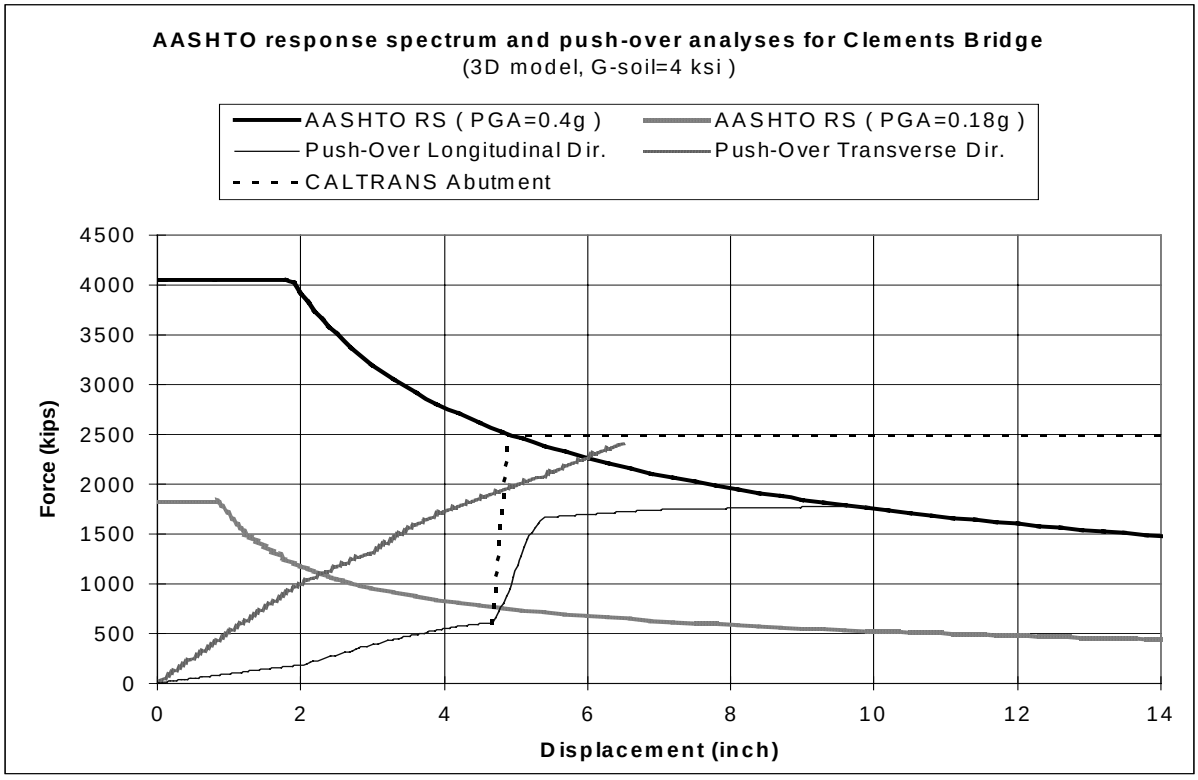

Figure 8-4 Push over analyses for Clements Bridge
(3-D model, G-soil=4 ksi)

SECTION 9

CONCLUSIONS AND RECOMMENDATIONS

9-1) Conclusions

Based on the results of both phases of this comprehensive analytical study, which included numerous computer simulations, the following specific conclusions can be made:

- Steel bearings will most likely fail even under low level of earthquake ground accelerations because of development of high level of impact forces during the dynamic response of MSSS bridges.
- Assuming stable post-failure behavior at the bearings, the failure at the bearing will act like a fuse and will limit further response of the bridge. This will lower the shear demand in the columns and the abutments. Therefore, due to dissipation of seismic energy through friction, the collapse of the bridge under 0.18g PGA will most likely be prevented.
- Friction coefficient at failed bearing affects the response. Efforts should be made to quantify its actual value and/or sensitivity analysis must be performed on a case-by-case basis to determine the most critical value.
- Seismic response of MSSS bridges is sensitive to soil-structure interaction and it should be considered in dynamic analysis of this class of bridges.
- Three-dimensional models must be used in nonlinear time history analyses, especially for skewed bridges.
- Under earthquakes with 0.4g PGA most bridges will sustain damage in the form of shear failure in the columns. This will most likely cause the collapse of the bridge. However, this level of ground acceleration is higher (in many locations much higher) than AASHTO's seismic coefficient for New Jersey. It is more typical for high seismic regions or it maybe considered as an event with significantly higher return period for New Jersey.

9-2) Recommendations

In light of the observations made during this research investigation and the above conclusions, the following recommendations are made with regard to retrofit and design of bridges in New Jersey:

- Although current seat length for the bridges considered are marginally adequate, consideration should be given to increasing the seat lengths of existing bridges. Current AASHTO's requirements for seat length will be adequate for the design of new bridges.
- Bearing seats must be regularly inspected to ensure their integrity so that in the event of an earthquake bearing failure will occur rather than pullout of the concrete seat.
- Retrofit of columns, if considered, should include considerations to increasing both confinement and cross-sectional size. Both of these two factors should be considered in order to obtain an optimal balance between higher flexural ductility and higher shear capacity.
- Analysis of new and existing bridges should employ nonlinear time history analysis using 3-D models.

9-3) Future work

As it can be seen from the results and discussions of this study, the bridges studied will not collapse under a ground motion with PGA of 0.18g given the post-failure behavior at the bearings is stable. Guaranteeing such performance is central to survival of bridges in New Jersey under AASHTO's specified PGA. Furthermore, this study relied solely on analytical studies. Therefore, the following tasks maybe considered for further investigation:

- Analytical evaluation of the pullout capacity of the concrete seat using three-dimensional finite element models. The first phase of this study indicated the adequacy of the concrete seat, however, that study employed 2-D FE models. In light of the importance of this factor a 3-D analysis, which can accurately model stress concentrations is warranted.

- Experimental study of model bearings to validate the load transfer mechanisms and the weak link per analytical results.
- Experimental study of post-bearing behavior to determine frictional characteristics.
- Full-scale tests of actual bridges in longitudinal and transverse directions.
- Parametric analyses of nonlinear stiffening SDOF systems to determine their ductility demand and energy dissipation capacity. Development of design guidelines (response spectrum, pushover methodology) that consider stiffening load-deformation characteristic.

SECTION 10

REFERENCES

1. Saadeghvaziri, M. Ala, S. Rashidi, “Seismic Retrofitting and Design of Highway Bridges in New Jersey,” Phase-I Final Report, NJIT, July, 1997.
2. Saadeghvaziri, M. Ala, S. Rashidi, "Seismic Retrofit and Design Issues for Bridges in New Jersey," Transportation Research Records, No. 1594, TRB, Nov., 1997.
3. Rashidi, S., and M. Ala Saadeghvaziri, “Modeling and Effect of Impact on Seismic Response of Multi-Span Bridges,” Computers and Structures, Vol. 64, No. 5/6, 1997.
4. Saadeghvaziri, M. Ala, and S. Rashidi, “Effect of Steel Bearings on Seismic Response of Bridges in Eastern United States,” Proceedings, 6th U.S. National Conference on Earthquake Engineering, Seattle, June, 1998.
5. *Seismic Design of Highway Bridge Foundations Vol. II*: Design Procedures and Guidelines, Report No. FHWA/RD-86/102, Federal Highway Administration, June 1986.
6. AASHTO *Standard Specifications for Highway Bridges,* 15th Edition, 1992, published by the AASHTO, Washington, D.C. 20001.
7. CALTRANS, *Bridge Design Aids 14-1,* California Department of Transportation, Sacremento, CA, October, 1989.
8. Goel, Rakesh K., and A. K. Chopra, “Evaluation of Bridge Abutment Capacity and Stiffness during Earthquakes,” Earthquake Spectra, Volume 13, No. 1, pp. 1-23, February, 1997.
9. Siddharthan Raj V., M. El-Gamal, E. A. Maragakis, “Stiffnesses of abutments on spread footings with cohesionless backfill,” Canadian Geotechnical Journal, Vol. 34, pp. 686-697, 1997.
10. Wilson, John, and B. S. Tan, “Bridge Abutments: Formulation of Simple Model for Earthquake Response Analysis,” Journal of Engineering Mechanics, ASCE, Vol. 116, No. 8, pp. 1828-1837, August, 1990.

11. AASHTO LRFD *Bridge Design Specifications,* Customary U.S. Units, 1st Edition 1994, published by the AASHTO, Washington, D.C. 20001.
12. *Seismic Retrofitting Manual for Highway Bridges*, Publication No. FHWA-RD-94-052, May 1995
13. Hognestad, E., "A Study of Combined Bending and Axial Load in Reinforced Concrete," University of Illinois Experiment Station, Bull. Series No. 339, November 1952.
14. Mander, J. B., M.J.N. Priestly, and R. Park, "Theoretical Stress-Strain Model for Confined Concrete," ASCE Journal of Structural Engineering, Vol. 114, No. 8, Aug., 1988.
15. *DRAIN-2DX Preliminary Element User Guide*, by: V. Prakash, G.H. Powell, D.D. Campbell, F.C. Filippou. Structural Engineering, Mechanics and Material, Department of Civil Engineering, University of Berkeley, California, December 1992.
16. *DRAIN-3DX Element Description and User Guide*, by: G.H. Powell and S. Campbell. Structural Engineering, Mechanics and Material, Department of Civil Engineering, University of Berkeley, California, Report No. UCB/SEMM-94/08, December 1994.
17. Maroney, B., B. Kutter, K. Romstad, Y. H. Chai, and E. Vanderbilt, "Interpretation of large scale bridge abutment test results," Proceedings, 3rd Annual Seismic Research Workshop, California Department of transportation, Sacramento, Calif., 1994.
18. Zimmerman, R. M., and R. D. Brittain, Seismic response of multi-simple span highway bridges. In: Proceedings of the 3rd Canadian Conference on Earthquake Engineering, Montreal, 1979. Pp. 1091-1120